Images of Early Continental Breakup in and around the Gulf of California and the Role of Basal Shear in Producing Wide Plate Boundaries

Thesis by

Patricia Persaud

In Partial Fulfillment of the Requirements

for the Degree of

Doctor of Philosophy

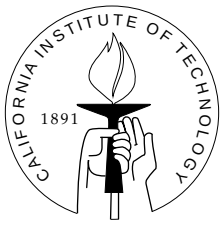

California Institute of Technology

Pasadena, California

2003

(Submitted October, 2003)

© 2003

Patricia Persaud

All Rights Reserved

I dedicate this thesis to
my husband, Holger Fortnagel, whose
love and help deserved better.

Acknowledgements

I cannot help but feel that much of what I have focused on in the last 5 years has little value when compared to the essential things, the things that matter in the world. Without the knowledge that there were people who cared about my work and even more who cared about me, on days when I worked alone, I may have become convinced that it was all useless. I've therefore relied heavily on that handful or so of colleagues, friends and family who have nurtured me, kept me sane and grounded while I built this thesis.

For accompanying me in this process, for listening to and encouraging the development of own thoughts and freely sharing his ideas and knowledge with me, I thank Michael S. Steckler[1]. I will never forget the fact that you cared. Thanks for the many many conversations on rifting and deformation of the lithosphere. Thanks also for thoroughly reviewing all of my papers, those long phone conversations helping me to get finished, making your facilities available to me when I visited LDEO, lending me your car and making me feel fully at home there. I also thank Luc Lavier[2] who came to Caltech as a postdoc during my 3rd year. I've learnt so much from you; thanks for the discussions on tectonics at all types of plate boundaries, all types of lithospheric deformation; for teaching me about numerical modeling and for being proactive about my graduate training and almost always taking the opposite side. Most of all thanks for being confident that I would succeed. Mike and Luc, you should be credited with playing a major role in developing the solid contributions in this thesis, because you encouraged me to come forward with my ideas and helped me build intuition.

Every single word matters, when the words are few. I'd also like to acknowledge Vincent Courtillot[3] for sharing his enthusiasm, knowledge about Afar and endless curiosity for rifting and asking: what do you think? I thank Brian Taylor[4] for his gen-

[1]LDEO, Columbia University
[2]University of Texas, Austin
[3]IPG Paris
[4]SOEST, University of Hawaii

erous nature and constant inquiry; Bruce Rosendahl[5] for lending me his eyes through which I could see the deep structure of the lithosphere. Thanks to Vicki Langenheim[6] for her tremendous generosity in sharing her data and work on the Peninsular Ranges batholith. I've benefited from interacting with Reginald DesRoches[7]; thanks for encouraging me to stay in academia and seeking out opportunities on my behalf.

In five super-intensive weeks of summer 1999, just before my oral exams, Joyce Alsop[1] taught me how to process the seismic reflection data at LDEO and later helped me survive over one year of data processing back at Caltech. Joyce, working with you was pleasant and kept both me and the project going, thanks! I'd also like to thank John Diebold[1] for updating the *jdseis* interface so that I could use it at Caltech for picking velocities and also for processing and teaching me the basics about sonobuoy refraction data. Thanks to Arturo Martin-Barajas[8] for his positive attitude, support and encouragement. Thanks to Greg Mountain[1] for all of his loud cheering over the years, getting his hands dirty with the interpretation of the data, career advice, thesis advice and those wonderful New Jersey margin stories that made a zillion unconformities seem trivial. I'm grateful to the captain and the crew of CICESE's research vessel, the *B/O Francisco de Ulloa*, Sergio Paz[8] and Jose Luis Garcia Puga[8] for making the data collection process in May-June, 1999 successful; as well as Peter Buhl[1] for giving me all types of tasks and keeping me busy on the cruise, and finally Erich Scholz[1] and John Diebold for allowing me to learn about the technical side of seismic data collection.

I wholeheartedly acknowledge the hard work of Bill Haxby[1] on the MapApp Java application to house the data collected during our cruise. Thanks for making this rich dataset available for others in such an easy-to-use format.

I started working with Xyoli Pérez-Campos at the end of 2002 on the receiver function study around the Gulf of California. Xyoli, thanks for welcoming me to a project that you had already started and working so hard with me to get it done. It was a huge pleasure to work with you and a very different experience for me to be

[5]University of Miami
[6]USGS, Menlo Park
[7]Georgia Institute of Technology
[8]CICESE

able to rely on someone who wasn't hundreds of miles away.

I am most grateful to Vadim Levin[1] for his generosity and willingness to teach me about interpreting receiver functions, for an unofficial review of Chapter 3, which provided significant improvement and giving me a quick course on anisotropy (if such a thing can be done, he did it). Without your help, I'm sure it would have taken me many months to come up to speed.

I thank my thesis advisors, Rob Clayton[9] and Joann Stock[9], for giving me their full support and the unique opportunity to carve my own course as a graduate student. Even though the steps were difficult, the process was enormously empowering. Thanks for not giving me a recipe and for allowing me to work towards a better support system for minorities. I'd also like to thank the other members of my thesis committee: Don Anderson[9], for his positive words, Jean-Philippe Avouac[9] for his numerous questions and enthusiasm, and Tom Heaton[9] for his support. I also thank the Luce Boothe Fellowship and James Irvine Diversity Fellowship for their financial support during the first 4 years of my Ph.D. This work was also supported by US National Science Foundations grants EAR-0111650, OCE-0221522 and OCE-9730790 to Caltech, and OCE-9730569 to LDEO; and by CONACYT grant 26669-T to CICESE. Landmark Graphics Corporation provided the software used to interpret and analyze the reflection seismic data in the Gulf of California.

I acknowledge the support of the staff of the Seismological Lab. I'm grateful to the Geology Department at the Pasadena City College for giving me the invaluable experience of teaching, which helped place my own research in perspective.

I thank the friends I've gained over the last 5 years, Gustavo Correa[1], Francesca DiLuccio[10], Jane Dmochowski[9] and Ann Shen for their conversation and caring and the time we spent together.

By far the most important aspect of my life and often the only source of sustenance over the last 5 years was my close relationship with my sister, Gita Persaud; my mom, Lyn Persaud, and my husband, Holger Fortnagel. I want to thank you all for giving my life a sense of reality that kept me human and grounded. Without you, I would

[9]Seismological Lab., Caltech
[10]Instituto Nazionale di Geofisica e Vulcanologia, Rome, Italy

have never started this and never would have believed I was capable of ending it. I give my oldest brother, Matah Sookul Persaud, a big hug for always tormenting me and asking when I would be done. Gita, you inspire me to make things better. Holger, there are no words to thank you for the sacrifice you were willing to endure on my behalf, no words to explain the strength it took to finish this, and that I could not have done it without you.

Abstract

Active faulting in the northern Gulf of California occurs over a broad zone, 70 × 200 km, affecting two-thirds of the width of new crust that has formed there starting at 6 Ma. This is an unusually wide plate boundary zone with a high density of faults and no evidence for the formation of normal oceanic crust. Over 3000 km of high-resolution, multichannel seismic data were used to map out this zone of distributed faulting and identify multiple basins within the broad rift zone. Previously, numerical models have shown that deformation shifts from one place to another by various mechanisms of strengthening of the active rift zone relative to adjacent regions. Models are presented here that for the first time, show the development of multiple active faults across the width of the plate boundary. These models do not rely on strengthening or weakening effects; rather they assume that shear at the base of the brittle crust is distributed and explore the effects of distributed shear on the style of deformation. Additionally, the effect of obliquity on the style of deformation is studied and the styles of faulting produced in the models represent a wide range of geological structures, ranging from half-graben to flower structures. The style of faulting in the northern Gulf of California is produced in a model with distributed shear using the published obliquity for this region.

One mechanism for distributing shear at the base of the brittle crust is lower crustal flow. If a significant amount of lower continental crust exists within the Gulf, it may have flowed in the past. A study of the crustal thickness variations in the continental margins of the Gulf is presented here, that shows thinner crust in a ∼50 km wide zone close to the Gulf, along the entire eastern Baja California peninsula. This thinned crust is associated with the eastern Peninsular Ranges batholith. In contrast, the western part of the batholith has a fairly uniform thickness of 35-40 km. It is possible that at the time of breakup, the lower crust was still behaving ductilely and that some of the lower continental crust from the margins now exists within the Gulf.

Contents

List of Tables

List of Figures

Introduction

Continental splitting is an integral part of the Wilson cycle and essential for the formation of new ocean basins. Continental crust tends to break up much more than oceanic crust and extensional plate boundaries often take a continental path even when an oceanic route would seem geometrically easier. Examples are the Pacific-North America plate boundary severing the 1400 km long Baja California peninsula from North America [Vink et al., 1984] and the Carlsberg Ridge circumventing the oceanic Somali basin in the Indian Ocean over a total distance of 750 km, then breaking into East Africa [Steckler and ten Brink, 1986]. Although rifts just cover 2% of the surface area of continents [Rosendahl, 1987], at least 18,000,000 words on 60,000 pages in 4,200 papers have been written on the subject of continental rifting. In spite of this, studies of rifting are still being plagued by the lack of consensus on how continents break up.

This thesis deals with the broad problem of continental breakup from the perspective of geophysical studies in the Gulf of California, an incipient ocean basin. It is divided up into three chronological parts and represents a culmination of thought on the processes of continental breakup and ocean basin formation. In **Chapter 1**, observations of distributed deformation, i.e., multiple active faults, in the Gulf of California are outlined. **Chapter 2** presents dynamic numerical models with distributed shear at the base of the brittle crust to explain the distributed deformation. Finally, **Chapter 3** outlines observations in the continental margins of the Gulf of California to explore the validity of the deformation mechanism proposed by the models. The conclusions are not all directly applicable to the early stages of continental breakup in every type of tectonic setting, but rather they open up a space of reasoning outside of classical plate tectonics and lend support to theories of semi-rigid, semi-organized plate tectonics.

The Gulf of California is one of only a few newly forming ocean basins; the Woodlark basin, Dead Sea – Gulf of Aqaba/Elat, and Gulf of Suez are similar settings,

with only the Gulf of Aqaba being loosely analogous to the Gulf of California. All of these have different styles of deformation, which are manifested in the width of the deforming zone, progression from continental rifting to seafloor spreading and the style of faulting. The main point here is that no two rifts are alike. It is therefore rare that generalizations on continental breakup hold in the real world, but in this chapter, I broaden the scope of this thesis in order to set up a framework.

It has long been recognized that the forces needed to split the continents exceed the normal plate driving forces (or are on the order of the plate driving forces), which led many workers to introduce heat from below in the form of hotspots [Bott, 1982] as a mechanism for rifting. Additionally, the amount of subsidence observed at some margins, such as the Gulf of Lion/Lyon, was found to be larger than predicted by the McKenzie [1978] stretching models [Steckler and Watts, 1980], prompting workers on that basis to find mechanisms by which heat is added to the rift zone. Studies of the East African rift zone both advanced and complicated the search for rifting mechanisms, since they confirmed some of the predictions of the McKenzie models by providing evidence for uplift and doming before the onset of rifting. The idea of anomalous heat sources in the mantle beneath rifts was therefore accepted as the norm. It is, however, now known that rifting is not always associated with thermal anomalies. This later led to the classification of active rifts, such as the East African rifts, and passive rifts, such as the Rhine Graben (Figure 1), where no anomalous heating of the lithosphere has been documented.

Studies of lithospheric deformation and crustal dynamics were born in era of the stretching models because it was also noted that little equality exists amongst rifts. They come in all forms: wide ones like the Basin and Range and narrow ones like the Rio Grande Rift. Under what conditions do, for example, large-offset, low-angle normal faults versus multiple faults form? Studies of the verticality of rifting in terms of uplift and subsidence based on stretching models evolved into studies focusing on the horizontal dimension of rifts determined from observations of upper crustal deformation. Rheological layering in numerical and analog models pitted the strength and hence brittle, plastic, or ductile behavior of the upper crust, lower crust and mantle against each other. The geotherm and strain rate determine the

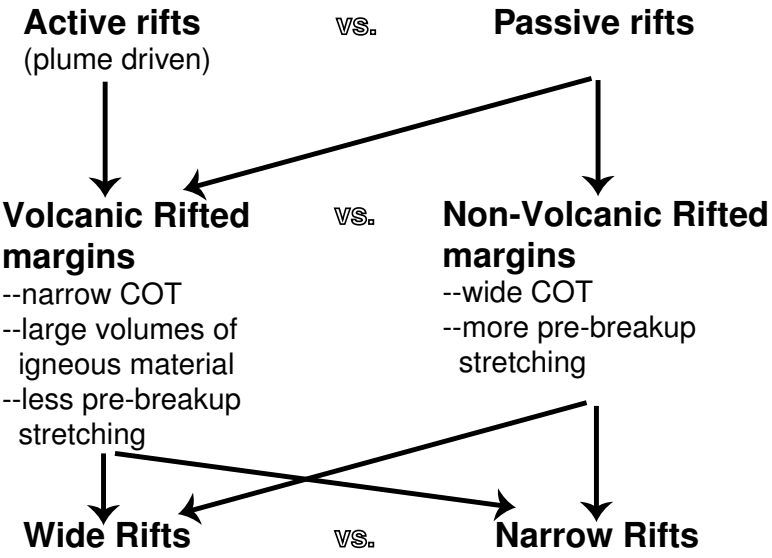

Figure 1: Flow Diagram showing the three major classification of rifts: active vs. passive rifts, volcanic vs. non-volcanic margins, and wide vs. narrow rifts.

thermo-mechanical behavior of rocks through the choice of rheology. Additionally, the integrated strength of the lithosphere varies strongly with the thickness of its weakest part, the crust. At a constant strain rate, thick hot crust is weaker relative to thin cold crust. It was found that a wide rift can be constructed *over time*, by strengthening the rift zone, thus, causing deformation to shift to a new location [e.g., recent synthesis in Buck et al., 1999]. The lower crust could in some cases be weak enough to flow and could be thought of as a conveyor belt for distributing deformation to adjacent areas and decoupling the upper crust and lower mantle. The uniform pure shear approach to deforming the lithosphere was now accompanied by the simple shear models of deformation, whereby deep-seated rocks could be exhumed along "detachment" faults to the Earth's surface, even without very large extensional strains. Differential thinning of the lithosphere as a mechanism for the formation of large-offset low-angle normal faults and lower crustal flow as a mechanism for smoothing out extension-related Moho topography are now widely accepted.

We, however, now know that there are other ways of detaching the upper and lower lithospheric layers and exhuming even deeper-seated mantle rocks to the Earth's surface. It has been noted that some margins, such as the West Iberia margin, are magma-poor and have a broad ocean-continent transition made up mainly of

serpentinized peridotites [Pérez-Gussinyé et al., 2001]. These margins are termed non-volcanic rifted margins. In the West Iberia margin,"detachment" have developed along the crust-mantle boundary due to serpentinization of this surface, causing it to be a weak zone and act as a décollement. This is a very different type of "detachment" compared to those found in the Basin and Range and Aegean Sea where initially thick, hot crust was deformed. Again this points to yet another divergence in the many types of rifts and styles of rifting.

In contrast to non-volcanic margins, volcanic rifted margins, e.g., the southern Red Sea, characteristically have upper mantle temperatures 100–200° above "normal" asthenosphere [Menzies et al., 2000]. They generally have an abrupt ocean-continent transition characterized mainly by magmatic material accreted to the base of the crust during rifting [Minshull, 2002]. The evolution of volcanic and non-volcanic margins are quite different, e.g., the amount of stretching needed before final breakup is more in non-volcanic margins, the type of "detachment fault" that develops is not the same as the classical detachment fault in the Basin and Range and the ocean-continent transition in non-volcanic rifted margins is broad relative to volcanic rifted margins. Again, the classification of rifts and dominant mechanisms in the rifting process bifurcates.

The interplay of magmatism and focused deformation presents a chicken-and-egg problem. For example, in the central Atlantic, there is evidence that volcanism postdated rifting by 30 m.y. in some locations, but was synchronous with rifting in others. Historically, however, magmatism and deformation have been dealt with separately. Recently, analog models have shown that magma emplacement promotes strain localization and reduces strain partitioning; at the same time, deformation focuses magma emplacement [Corti et al., 2001].

With all of this in mind, the Gulf of California should have focused deformation, some melt accreted to the base of the crust, a sharp ocean-continent transition, no serpentinized peridotites and large-offset low-angle normal faults. This is, however, not the case. As is shown in **Chapter 1** of this thesis, the northern Gulf of California is a broad zone of distributed deformation as evidenced in recent high-resolution multichannel seismic data. **Chapter 2** presents numerical models of distributed de-

formation, which lend support to a basal drag mechanism for distributed deformation. Finally, **Chapter 3** presents a study of the continental margin of the Gulf aimed at helping us to better understand what lies at the base of the upper brittle crust in the Gulf. This final chapter also highlights the difference in structure between the eastern and western Peninsular Ranges batholith and points to the need for future work on Pressure-Temperature-time constraints in this region.

References

M. H. P. Bott. The Mechanism of Continental Splitting. *Tectonophysics*, 81:301–309, 1982.

W. R. Buck, Luc L. Lavier, and Alexei N. B. Poliakov. How to make a rift wide. *Philosophical Transactions of the Royal Society of London A*, 357:671–693, 1999.

Giacomo Corti, Marco Bonini, Fabrizio Innocenti, Piero Manetti, and Genene Mulugeta. Centrifuge models simulating magma emplacement during oblique rifting. *Journal of Geodynamics*, 31:557–576, 2001.

Dan McKenzie. Some Remarks on the Development of Sedimentary Basins. *Earth and Planetary Science Letters*, 40:25–32, 1978.

M. A. Menzies, C. Ebinger, and S. Klemperer (conveners). Penrose Conference Report; Volcanic Rifted Margins. *GSA Today*, pages 8–11, 2000.

T. A. Minshull. The break–up of continents and the formation of new ocean basins. *Philosophical Transactions of the Royal Society of London A*, 360:2839–2852, 2002.

M. Pérez-Gussinyé, T. J. Reston, and J. Phipps Morgan. Serpentinization and magmatism during extension at non-volcanic margins: the effect of initial lithospheric structure. In R. C. L. Wilson, R. B. Whitmarsh, B. Taylor, and N. Froitzheim, editors, *Non-Volcanic Rifting of Continental Margins: A Comparision of Evidence from Land and Sea*, volume 187 of *Geological Society Special Publications*, pages 551–576. 2001.

B. R. Rosendahl. Architecture of continental rifts with special reference to East Africa. *Annual Review of Earth and Planetary Science*, 15:445–503, 1987.

Michael S. Steckler and Uri S. ten Brink. Lithospheric strength variations as a control on new plate boundaries: examples from the northern Red Sea region. *Earth and Planetary Science Letters*, 79:120–132, 1986.

Michael S. Steckler and A. B. Watts. The Gulf of Lion: subsidence of a young continental margin. *Nature*, 287:425–429, 1980.

Gregory E. Vink, W. Jason Morgan, and Wu-Ling Zhao. Preferential Rifting of Continents: A Source of Displaced Terranes. *Journal of Geophysical Research*, 89 (B12):10072–10076, 1984.

Chapter 1 Active deformation and shallow structure of the Wagner, Consag and Delfín Basins, northern Gulf of California, Mexico

Published by Persaud, P., J. M. Stock, M. S. Steckler, A. Martín-Barajas, J. B. Diebold, A. González-Fernández, and G. S. Mountain, Active deformation and shallow structure of the Wagner, Consag, and Delfín Basins, northern Gulf of California, Mexico, *J. Geophys. Res.*, 108(B7), 2355, doi:10.1029/2002JB001937,2003.

Abstract

Oblique rifting began synchronously along the length of the Gulf of California at 6 Ma, yet there is no evidence for the existence of oceanic crust or a spreading-transform fault system in the N. Gulf. Instead, multichannel seismic data show a broad shallow depression, ∼70 x 200 km, marked by active distributed deformation and six ∼10-km-wide segmented basins lacking well-defined transform faults. We present detailed images of faulting and magmatism based on the high resolution and quality of these data. The N. Gulf crust contains a dense (up to 18 faults in 5 km) complex network of mainly oblique-normal faults, with small offsets, dips of 60–80° and strikes of N-N30°E. Faults with seafloor offsets of tens of meters bound the Lower and two Upper Delfín basins. These subparallel basins developed along splays from a transtensional zone at the NW end of the Ballenas Transform Fault. Twelve volcanic knolls were identified and are associated with the strands or horsetails from this zone. A structural connection between the two Upper Delfín basins is evident in the switching of the center of extension along axis. Sonobuoy refraction data suggest the basement consists of mixed igneous-sedimentary material, atypical of mid-ocean ridges. Based on the near-surface manifestations of active faulting and magmatism, seafloor spreading will likely first occur in the Lower Delfín basin. We suggest the transition to seafloor-spreading is delayed by the lack of strain-partitioned and focused deformation as a consequence of shear in a broad zone beneath a thick sediment cover.

1.1 Introduction

Our current understanding of the process of continental rifting and break up comes from three main sources. The first source is geophysical and geological observations in passive margins, intracontinental rift systems, and mature rifts; examples of these are the Galicia margin [Boillot et al., 1989; Manatschal and Bernoulli, 1999], Australia margin [Driscoll and Karner, 1998]), Okinawa Trough [Herman et al., 1979], Bransfield Strait [Barker, 1998], Andaman Sea [Curray et al., 1979]), interior Sudan rifts [McHargue et al., 1992] and Gulf of Suez [Steckler et al., 1988]. Secondly, evidence on the rifting process is available from studies in areas that are actively undergoing continental break up, such as the Woodlark basin, Papua New Guinea [e.g., Taylor et al., 1995, 1999]; Red Sea [e.g., Cochran and Martinez, 1988]; Asal Rift in the Gulf of Aden [e.g., Manighetti et al., 1998]; Central Gulf of California, Mexico [e.g., Saunders et al., 1982; Einsele, 1986] and Salton Trough, California [e.g., Fuis and Kohler, 1984; Lonsdale, 1989]. A third source of information is numerical and analog experimentation [e.g., Clifton et al., 2000; Lavier et al., 2000]. Observations in passive margins, intracontinental rift zones and mature rifts provide useful insight into pre- and post-breakup kinematics and the timing, extent and style of rifting, but they provide limited information on the processes active during breakup. Areas that are actively extending and thinning, enough to generate new crustal area, are few and poorly understood. In principle, numerical and analog experiments can provide information about the forces and different deformation paths of extending areas. However, in many cases the results are only valid for small strains, and experiments either cannot deal with the complex rheology of earth materials, or they introduce non-realistic boundary conditions.

The Pacific-North American plate boundary in the N. Gulf of California is an area of active continental breakup. Unlike the mouth of the Gulf where seafloor spreading began at $\sim$3.5 Ma [Bischoff and Henyey, 1974; DeMets, 1995; Lonsdale, 1989], the N. Gulf still lacks seafloor spreading, despite at least 255 $\pm$ 10 km of separation between the rifted margins that would have required formation of considerable new crustal area [Oskin et al., 2001]. The oceanic plate boundary of the southern and central

Gulf comprises narrower zones of deformation, e.g., the Guaymas basin and Ballenas Transform fault zone (Figure 1.1a). The N. Gulf, in contrast, contains a broader zone of diffuse deformation akin to the continental domain of southern California. It is expected that a plate boundary should narrow as it passes from a continental regime, such as S. California, to an oceanic regime, such as the S. Gulf of California [Molnar, 1988]. Along a transcurrent boundary, this localization process may differ because of differences in the rheology of the lithosphere, the heat flow, tectonic style and the amount and type of new crust being produced. Based on the high sedimentation rates and lack of evidence of seafloor spreading, the N. Gulf crust is expected to be similar to the transitional crust identified in drill samples in the central Gulf of California [Saunders et al., 1982] and interpreted from seismic velocities in the Salton Trough [Nicolas, 1985]. This active transcurrent plate boundary, thus, presents an excellent opportunity for studying the influence of obliquity and transitional crust on the style of deformation and the progression from continental breakup to seafloor spreading.

In this paper, we identify the N. Gulf of California as the region of the Gulf north of latitude 28.5° (Figure 1.1). The major transform faults and extensional basins of the N. Gulf of California include, from north to south, the Cerro Prieto fault (southernmost fault of the San Andreas fault system), the Wagner Basin, the Delfín Basins and the Ballenas Transform fault system (Figure 1.1b). These active segments of the plate boundary have been identified from seismicity and seafloor morphology. Details of the tectonic and sedimentary history of the N. Gulf of California have, however, been obscured by high sedimentation rates and a low rate of large earthquakes.

The most detailed interpretation of the tectonics of the N. Gulf to date is based on single channel seismic reflection data acquired in 1970 [Henyey and Bischoff, 1973]. From these data, Henyey and Bischoff [1973] developed a fault map of the N. Gulf; their interpretations of the seismic data were, however, limited by inter-bed multiples and reverberations derived from the source signal. Several deeper multichannel seismic (MCS) reflection profiles were collected during the 1996 cruise of the Spanish ship *Hespérides* in the Gulf of California. Within our survey area, one seismic line ran across the Delfín basin (Figure 1.1b)[González-Fernández et al., 1999] showing distributed faulting with many active and inactive faults. Another seismic profile across

the Lower Delfín basin and Ballenas-Salsipuedes channel (Figure 1.1b) found evidence for intense magmatism in the Salsipuedes basin which decreased northward into the Lower Delfín basin [Paz-López, 2000]. A representative industry seismic line across the N. Gulf, showing steeply dipping, sinuous faults that cut the entire sedimentary column, was also published by Pérez-Cruz [1980], but this line did not image the near surface strata with high resolution, nor result in an integrated fault map showing the active kinematics of the region. Thus many questions about the modern fault system remain.

We have collected a grid of high-resolution MCS reflection data and sonobuoy refraction data in the N. Gulf of California. The quality of these data along with the wide spatial coverage and high-precision navigation allow us to provide an improved fault map, defining in detail the style of faulting in the area surveyed. Our study also constrains the depth to basement near the Baja California coast and maps recent volcanic features on the seafloor.

1.2 Geologic and Tectonic Background

Extension in the Gulf of California appears to have started after 12 Ma along a ∼24 - 12 Ma subduction-related volcanic arc [Gastil et al., 1979; Sawlan, 1991]. A Mid- to Late Miocene period of possibly minor extension [Karig and Jensky, 1972; Stock and Hodges, 1989] occurred at the site of the future Gulf with transform motion west of the future Baja Peninsula. At this time, a broad area east of the future Gulf, from southern Arizona and New Mexico to the Gulf Extensional Province was undergoing extension [Henry and Aranda-Gómez, 2000; Humphreys and Weldon II, 1991]. At approximately 6 Ma, the plate boundary jumped inland to the Gulf of California [Lonsdale, 1989; Oskin et al., 2001] and marine sediments were widely deposited in the N. Gulf [Helenes and Carreño, 1999]. The plate margin subsequently evolved into a series of long transform faults connected by smaller rift basins. Seafloor-spreading type magnetic anomalies are, however, only observed in the Alarcón Basin and southward (Figure 1.1a) [Klitgord et al., 1974; Larson, 1972; Lawver et al., 1973; Sánchez-Zamora et al., 1991; Ness et al., 1991].

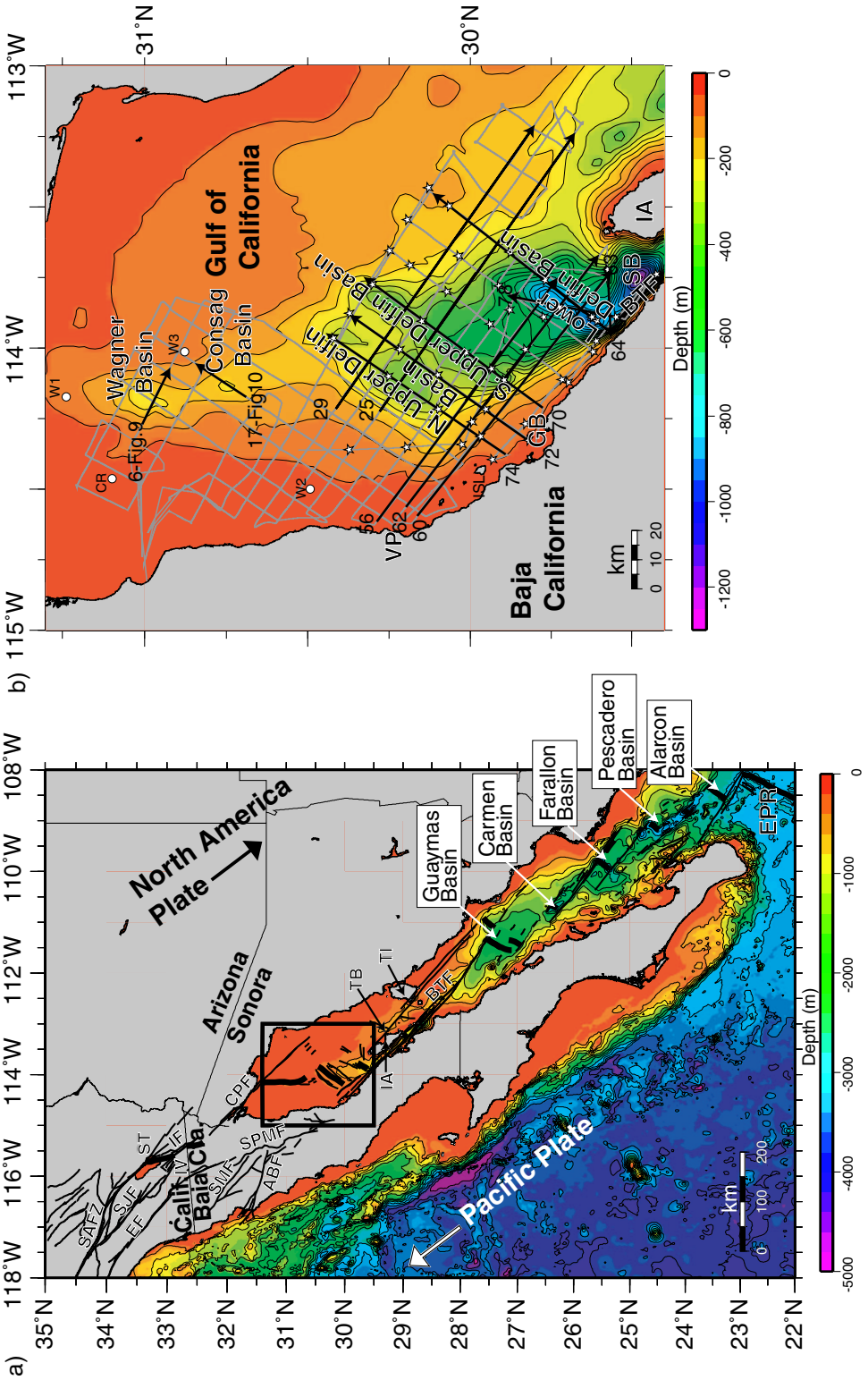
a)
b)
North America Plate
Pacific Plate
Arizona
Sonora
Baja California
Gulf of California
Guaymas Basin
Carmen Basin
Farallon Basin
Pescadero Basin
Alarcon Basin
Wagner Basin
Consag Basin
N. Upper Delfin Basin
S. Upper Delfin Basin
Lower Delfin Basin
EPR
SAFZ
SJF
EF
ST
IF
SMIF
SPMF
ABF
CPF
TB
TI
BTF
IA
SB
GB
VP
CR
W1
W2
W3
6-Fig.9
17-Fig.10
Depth (m)
km

Figure 1.1:

The centers of extension in the N. Gulf have jumped westwards in several cases, and thus lie towards the western side of the rift. Around 3.3 Ma the locus of extension in the N. Gulf jumped westward from Tiburón basin to the Upper Delfín basin, with the Wagner and southern Tiburón basins still active parts of the plate boundary [Lonsdale, 1989; Stock, 2000] (Figure 1.1a). The current structures in the N. Gulf originated after yet another westward relocation of the plate boundary sometime after 2 Ma, as spreading jumped from the southern Tiburón basin to the Lower Delfín basin and the Ballenas transform fault became the major transform fault in this region [Lonsdale, 1989; Stock, 2000] (Figure 1.1). The Wagner basin is also closer to the western side of the rift and may have jumped from a previous location to the E or SE [Aragón-Arreola et al., 2002].

The Ballenas transform fault system has well-defined en-echelon transform zones subparallel to relative plate motion. There is, however, a 10° change in strike between the Ballenas transform fault and the Cerro Prieto fault to the north [Goff et al., 1987] (Figure 1.1a). Geological data and earthquake patterns suggest that some of the slip is transferred from the northern end of the Ballenas Transform fault to the transpeninsular faults located in the continental crust of Baja California [e.g., Goff et al., 1987] (Figure 1.1a). It is estimated that between 7 and 15 mm/yr of right lateral slip is accommodated by these faults [Bennett et al., 1996; Humphreys and Weldon II, 1991; Goff et al., 1987]. There is, however, no clear evidence that the faults are physically linked [Stock and Hodges, 1989, 1990] or interact through their stress fields [Frez and González, 1991]. Seismological observations rather suggest distributed

Figure1.1 (opposite)(a) Map of the Gulf of California. Heavy box outlines the survey area, which is shown in more detail in (b). Black arrows indicate the current Pacific-North America relative plate motion direction, N37°W [Atwater and Stock, 1998]. Pacific-North America plate boundary faults and spreading centers are from Fenby and Gastil [1991]. The major rift basins in the Gulf are labeled. (b) Location of multichannel seismic lines in the N. Gulf of California collected by the *Ulloa* in 1999. Stars mark sonobuoy locations. Seismic profiles shown in this work are marked with thick black lines and labeled. Arrowheads mark the right ends of the plotted seismic data. Lines 6 and 17 are shown in figures only. The rest of the seismic profiles are shown in plates, which refer to figures for more detail. ABF=Agua Blanca Fault; BTF=Ballenas Transform Fault Zone; CPF=Cerro Prieto Fault; CR=Consag Rock; EF=Elsinore Fault; EPR=East Pacific Rise; GB=Gonzaga Bay; IA=Isla Angel de la Guarda; IF=Imperial Fault; ISL=Isla San Luis; SAFZ=San Andreas Fault Zone; SJF=San Jacinto Fault; SB=Salsipuedes Basin; SMF=San Miguel Fault; SPMF=San Pedro Mártir Fault; ST=Salton Trough; TB=Tiburón Basin; TI=Tiburón Island; VP=Volcán Prieto. W1, W2 and W3 are PEMEX proprietary wells.

deformation [Frez and González, 1991; Thatcher and Brune, 1971]. The exact way in which slip is transferred into the Gulf of California is not known.

From the Salton Trough southward, the crust thins from a minimum thickness of 21 km to 13 km and 10 km in the northern and central Gulf respectively, where the thinnest crust is found along the peninsular coast [Couch et al., 1991]. In the southern Gulf, the crust is 8 km thick and crustal thinning is symmetrical [Couch et al., 1991]. Seismic refraction studies in the N. Gulf require a crustal thickness of $\sim$ 20-25 km and a crustal structure that is similar to that found in the continental borderland of Southern California [Phillips, 1964]. More recent work also constrains crustal thickness for the N. Gulf and indicates that its seismic properties are not typical of oceanic crust. Along a profile at $\sim$ 31°N latitude, Moho depth estimates from P-to-S converted phases increase from $\sim$ 33 $\pm$ 3 km near the Pacific coast of Baja California to $\sim$ 40 $\pm$ 4 km beneath the western part of the Peninsular Ranges batholith [Lewis et al., 2001]. The crustal thickness then decreases rapidly across the eastern Peninsular Ranges and Main Gulf Escarpment to a fairly uniform thickness of $\sim$15-18 $\pm$ 2 km within and on the margins of the N. Gulf [Lewis et al., 2001]. This eastward thinning of the crust may have resulted from diffuse lower crustal extension beneath the Salton Trough and N. Gulf [Lewis et al., 2001]. In addition, from the analysis of deep seismic profiles and new gravity data, González-Fernández et al. [1999] place the bottom of the crust at $\geq$ 16-17 km in the Upper Delfín Basin and $\geq$ 18-19 km beneath Tiburón basin, to the southeast of our field area (Figure 1.1a). A structural high is interpreted between these two basins, where the crust is 21 km thick [González-Fernández et al., 1999, *González-Fernández in prep.*].

A significant part of this crust is sedimentary. Based on stratigraphic analysis of two Petróleos Mexicanos (PEMEX) wells, the up to 2 km thick sedimentary package imaged during our survey may be no older than Pleistocene in age, perhaps with some Pliocene strata at the base. The PEMEX well W2 (Figure 1.1b) shows basement consisting of a quartz-bearing diorite at a depth of 2950-3191 m [PEMEX unpublished data]. An igneous unit of altered andesite ($\sim$150 m thick) overlies the basement and has a whole rock K/Ar age of 8$\pm$1 Ma. The entire sedimentary sequence above this igneous unit is Quaternary-Pleistocene in age. Indeed, Van Andel [1964] estimates a

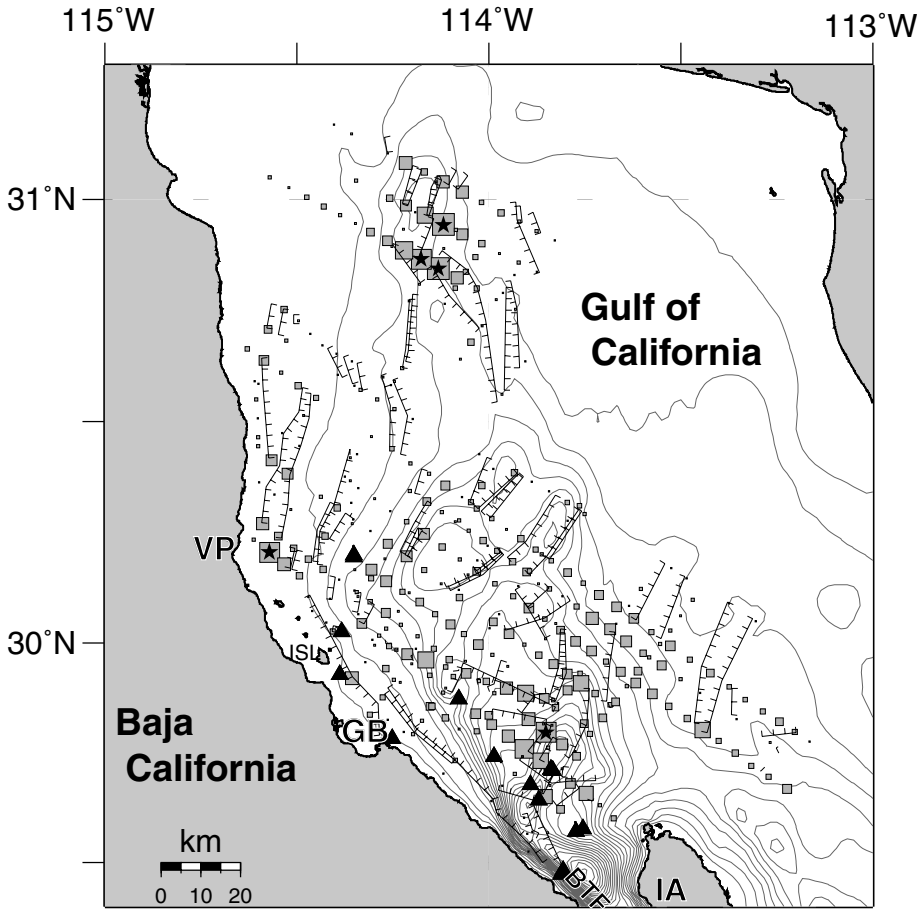

Figure 1.2: Map of faults that were interpreted on more than one seismic profile (black lines). Hachures mark the downthrown sides of faults. Gray lines are bathymetric contours every 50 m. Gray boxes indicate the fault density of all the picked faults (number of faults per 5 km along track). The largest and smallest boxes contain 20 faults and 1 fault, respectively, and the surveyed area has a mean fault density of $\sim$3 faults per 5 km. Stars mark areas with 18 or more faults per 5 km. Black triangles mark the locations of volcanic knolls identified in the seismic profiles. See figure 1.1b for place abbreviations.

sedimentation rate in the N. Gulf of 3.16 km/my. From bottom to top, the sedimentary unit consists mainly of consolidated, semi-consolidated and poorly consolidated sandy mudstones. Marine beds in the top kilometer of sediments contain abundant mollusk bioclasts. The PEMEX well W3 (Figure 1.1b) penetrated Recent-Pleistocene sediments down to 2540 m; from 2560-3000 m the ages are undetermined.

1.3 Data and Analysis

We used Lamont-Doherty Earth Observatory's high-resolution multichannel seismic (MCS) system with differential GPS navigation to obtain a 2-D grid of 3500 km of reflection data in May-June 1999 aboard CICESE's 28 m research vessel *B/O Francisco de Ulloa* (Figure 1.1b). The reflection equipment imaged to subbottom depths of up to 2 km. 48 expendable sonobuoys were also deployed during the cruise (Figure 1.1b); 43 of these returned usable records and provide velocities to greater depth. 4000 km of 12.5 and 208 kHz echosounder data were also collected. In addition, well data from PEMEX are now available to the CICESE research group and are here used to constrain the depth to basement and stratigraphy in the N. Gulf.

The seismic reflection data were acquired with a 48 channel, 600 m streamer, at a sampling interval of 1 ms (shot spacing of 12.5 or 25 m) and were recorded for 2-3 s. A Generator-Injector air gun provided a cleaner source pulse than the Bolt air gun used by Henyey and Bischoff [1973]. The processing sequence of the reflection data is as follows: (1) timing corrections, (2) trace edit, (3) velocity analysis based on semblance coefficients, (4) normal moveout and stack, (5) spherical divergence correction, (6) predictive deconvolution (with filter length of 30 ms and gap of 16 ms), (7) Stolt migration, (8) band-pass filter (30-240 Hz), and (9) time-variant gain. (The entire data set is available through the MapApp tool, which is downloadable at http://ocean-ridge.ldeo.columbia.edu/MapApp/MapAppJava.html.) We interpreted the data using the general techniques outlined by Badley [1985] and the criteria for identifying strike-slip zones given by Harding [1990]. Strikes of the major faults (black lines in figure 1.2) were determined. We used these strikes along with the apparent dips to calculate true dips of the major faults.

The sonobuoy or refraction data were first decimated and filtered. Seafloor reflection and direct arrivals were modeled to determine the source-receiver offsets. An offset-based linear time reduction was used to bring the interpretable arrivals within a convenient window for analysis. Interactive ray tracing was used to create velocity models.

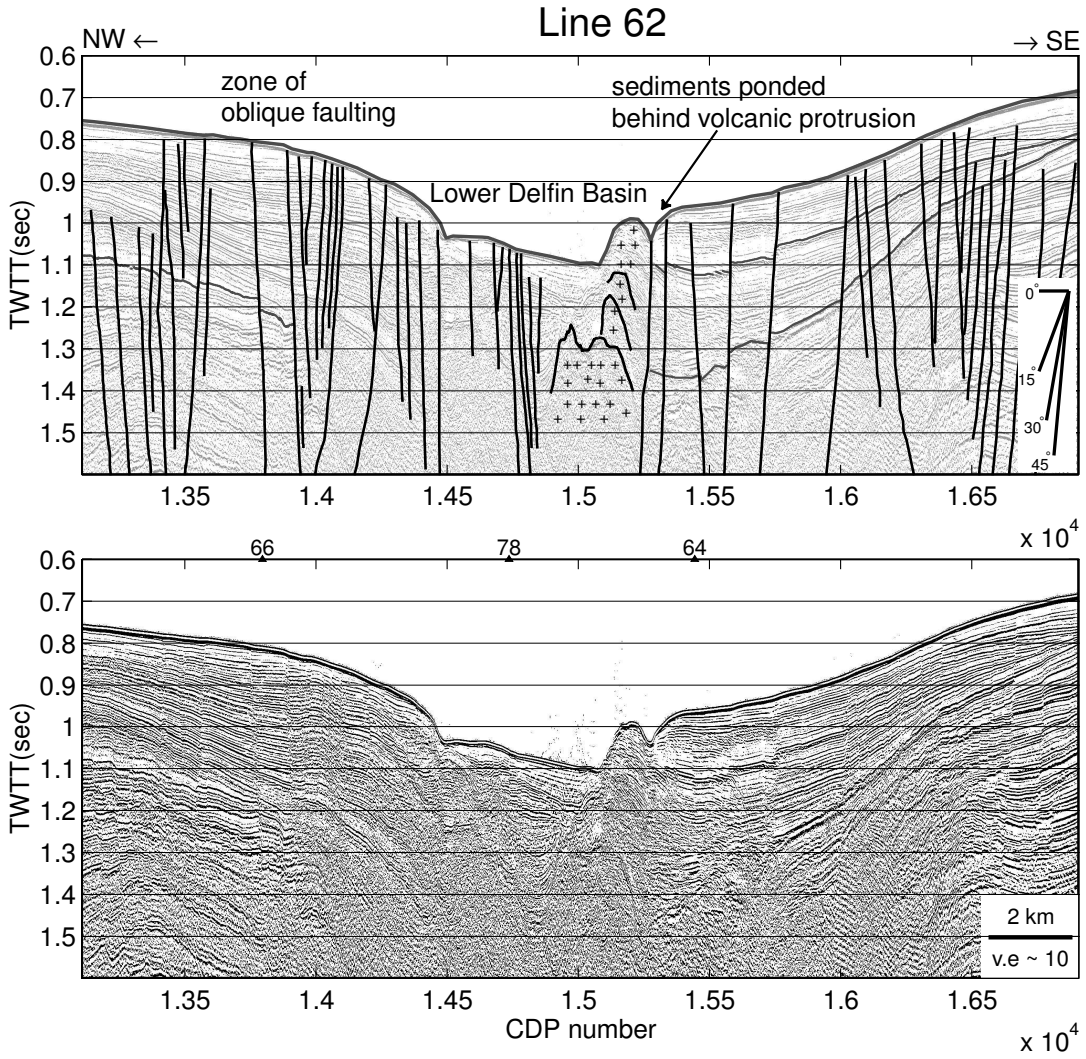

Figure 1.3: Profile perpendicular to the axis of the Lower Delfín Basin and SE of the profile shown in Figure 1.6. Isla Angel de la Guarda lies a few kilometers SE of this profile. The most prominent reflectors are highlighted. These reflectors were not traceable across the axial region of the southwestern end of the LDB (shown here), where layers are disrupted by the intrusion of magma.

Figure 1.4 Compilation of MCS profiles, (a)64, (b)78, (c)62 and (d)60, which cross the Lower Delfín Basin. Locations of the seismic profiles are shown in the map and figure 1.1b. Arrowheads mark the right end of the images. Boxes mark the location of other illustrations. The y-axis is two-way travel time (TWTT) and the x-axis is common depth point number (CDP number). Vertical exaggeration is ∼10 for all panels. The numbered black triangles along the top of the plots represent crossing lines. A dredge sample from the volcanic knoll in the southeastern flank of the SUDB, (c), was found to be rhyolite pumice [Henyey and Bischoff, 1973]. The large normal fault around CDP 10000 in (c) strikes northeastward into the SUDB. Volcanic rocks shown in (a) form a ridge across the axis of the Lower Delfín Basin, separating the NE-trending basin into two subbasins. The subbasin to the SW reaches the NW end of the Ballenas Transform Fault zone and is faulted obliquely. Oblique faults also cut across the axis of the basin in the area of the contourites (profile a). "+" = volcanic constructions, "∧"=well-resolved acoustic basement and "m"=seafloor multiple.

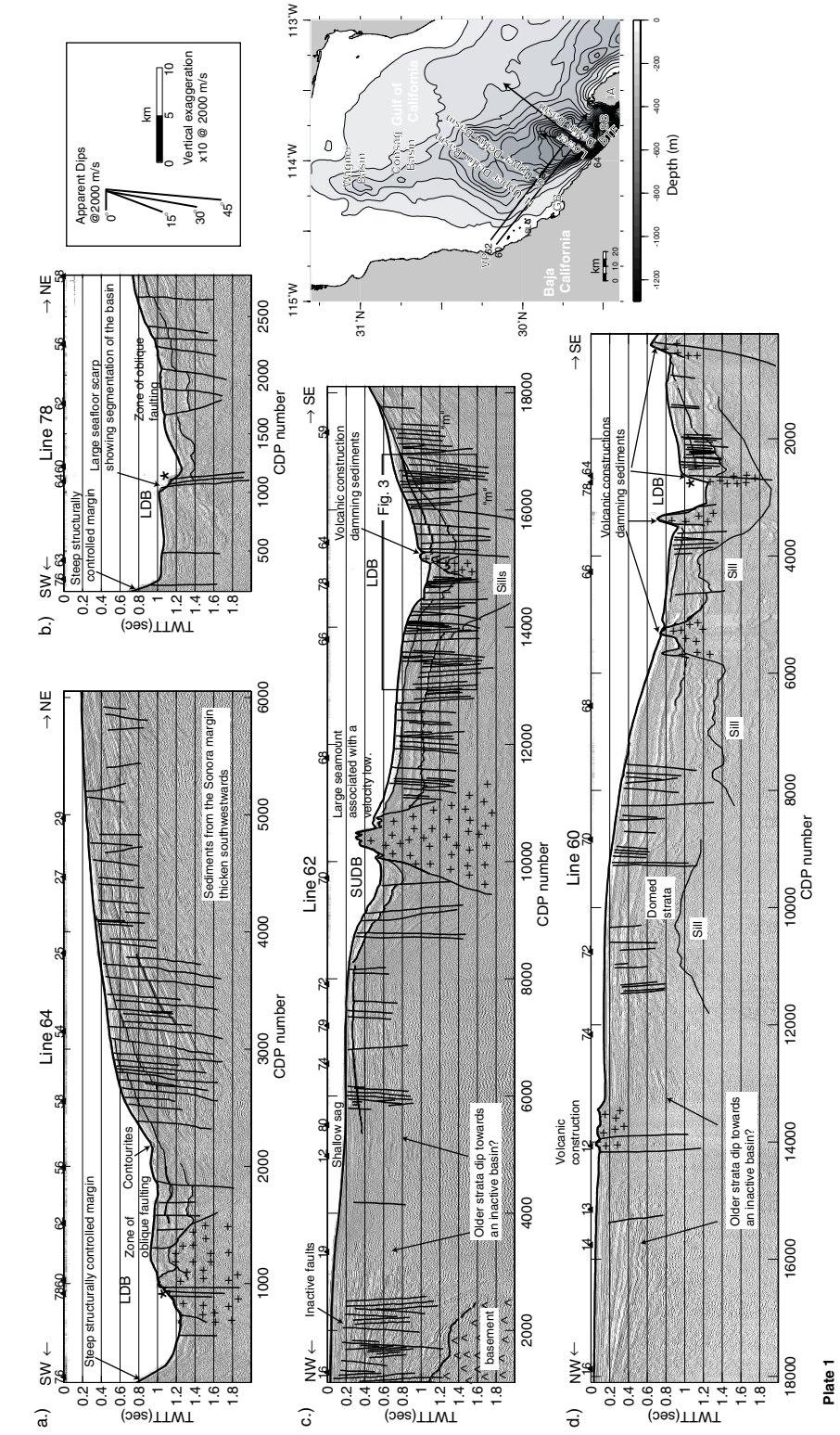

Plate 1

Figure 1.4: See previous page for caption.

1.4 Multitude and Density of Faulting

One of our most striking observations in the N. Gulf of California is the large number of faults and the broad area over which faulting occurs (Figure 1.2). Here, we describe the style of faulting with respect to the major rift basins and possible transform fault zones, i.e., the Ballenas Transform Fault (BTF). The N. Gulf of California is composed of three sets of active basins distributed within a broad shallow depression: (i) the Lower Delfín Basin (LDB) and Salsipuedes basins, (ii) the Northern Upper Delfín Basin (NUDB) and Southern Upper Delfín Basin (SUDB) and (iii) the Wagner Basin (WB) and Consag Basin (CB) (Figure 1.1b). We have grouped together basins in (i) and (ii) based on their proximity and structural similarities/connections. The WB and CB may not be structurally similar but are grouped together based on their similar orientation and shallow relief.

1.4.1 Lower Delfín and Salsipuedes Basins

Along trend, the northern half of the LDB has a higher fault density than the southern half, with $\sim$ 18 faults in 5 km in the northwest flank (stars in figure 1.2). The high density of faulting is also shown in the seismic profile in figure 1.3 where many small fault blocks are rotated and tilted basinward. Although strata in both flanks of the LDB are highly faulted, fault offsets are small, tens of meters or a few meters (at a mean seismic velocity of 2000 m/s) compared to the main normal faults that bound the basin, which have offsets of 100 m or more based on seafloor scarps (Figure 1.4a and b; lines 64 and 78). Inactive faults are uncommon in the survey area, but some were imaged 10-15 km away from the basin's axis (Figure 1.4c; line 62). Although fault dips vary significantly, most faults in the flanks of the LDB have apparent dips of $\sim 50 - 60^{\circ}$ (Figure 1.5), with opposing dips common (Figure 1.6). In general, the dip direction of faults changes across the basin's axis, with mainly east-dipping faults in the NW flank and west-dipping faults in the SE flank (Figure 1.6).

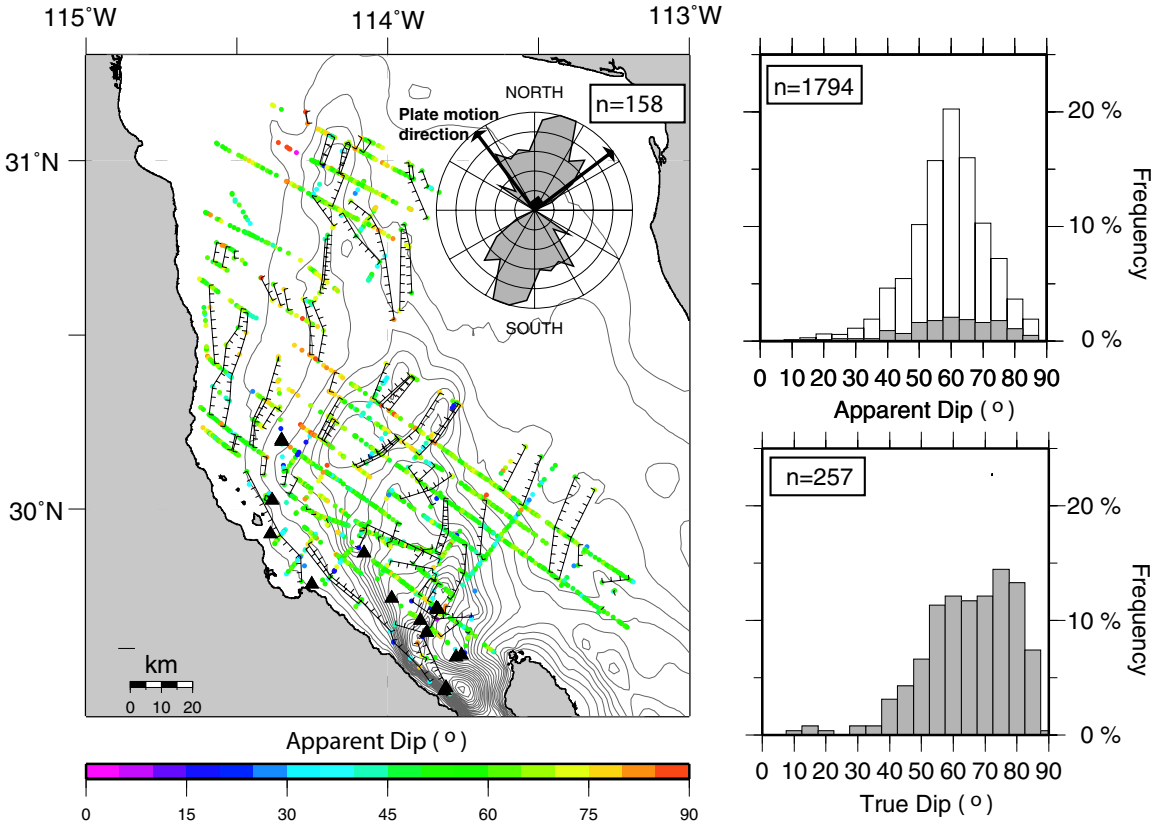

Figure 1.5: Map showing the apparent dips of all interpreted faults (total of 1794), calculated in the plane of the seismic profiles with a mean seismic velocity of 2000 m/s. Gray lines are bathymetric contours every 50 m. Strikes of all faults that were imaged on at least two seismic profiles (black lines) are shown in the inset rose diagram. This rose plot is normalized for equal area and shows a total of 158 fault segments or 112 faults with the maximum radius representing 24 fault segments. Note, the approximate trends of the major rift basins are LDB = N10°E, NUDB and SUDB = N35°E and WB = N25°E (Figure 1.14). The dominant strike of faults in the survey area is N - N30°E, which is within 5-10° of the trend of the major rift basins. The top histogram shows the apparent dips of all faults; the gray-shaded area represents the apparent dips of the faults shown by black lines in the map. The bottom histogram shows the true dip of these faults, which were calculated using the strikes.

1.4.2 Extension of the Ballenas Transform Fault?

Northwest of Isla Angel de la Guarda, oblique faults strike into the LDB (Figure 1.2). To the southwest, the LDB is faulted obliquely, by faults extending from the Ballenas Transform Fault zone northward (Figure 1.2; Figure 1.7d, line 63). These faults merge into a diffuse zone of negative flower structures, which may mark the northwestern

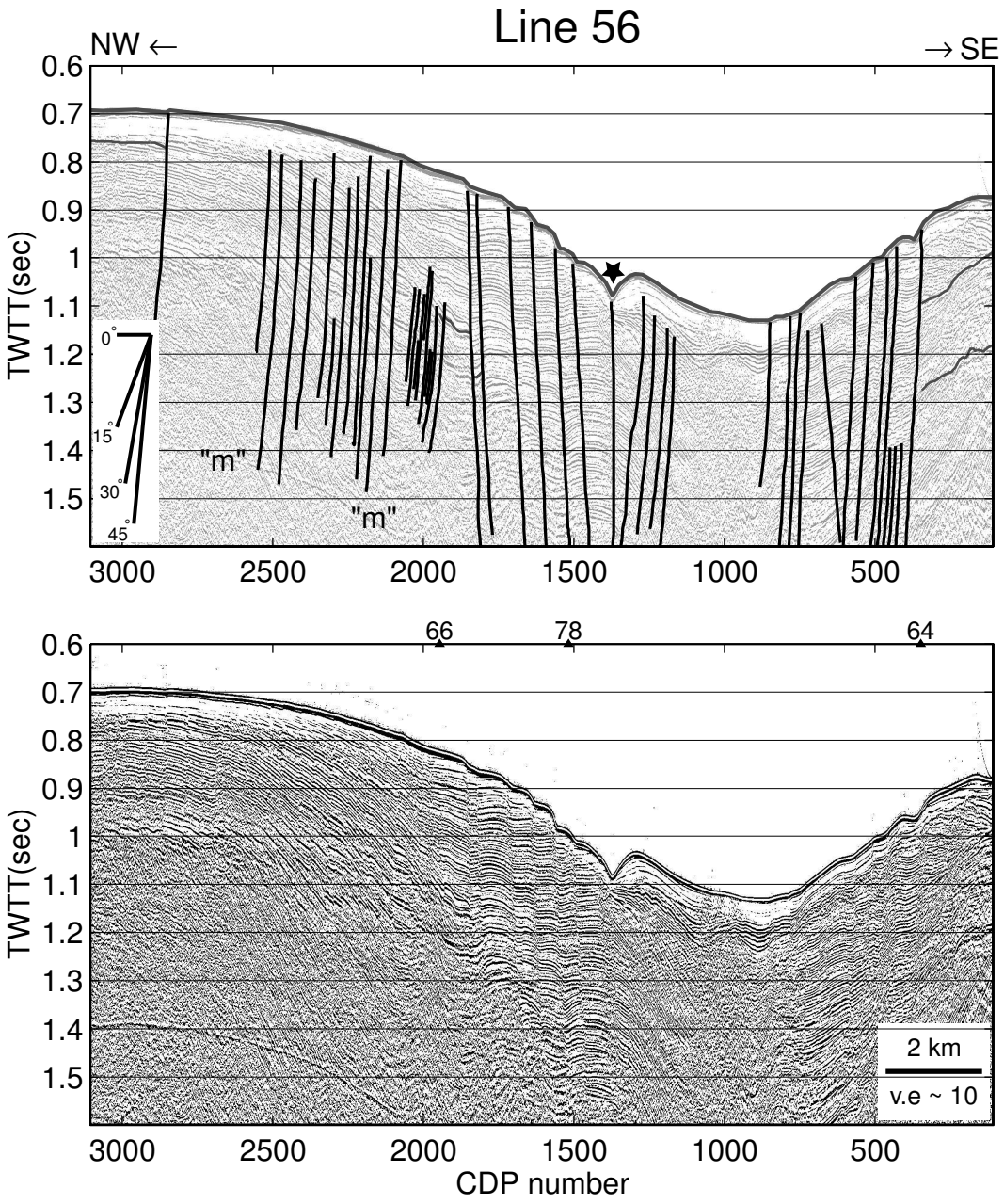

Figure 1.6: Profile perpendicular to the axis of the Lower Delfín Basin. Note the opposing dips of the faults in the northwestern flank of the basin. The large seafloor scarp around CDP 1300 (marked by the star) could be an indication of strike-slip offset. Overlapping E-W striking faults with oblique offset crosscut the Lower Delfín basin (see Figure 1.2), which may be a pull-apart basin.

end of the BTF. Negative flower structures were identified in several seismic profiles close to the Baja California coast and just north of Isla Angel de la Guarda (to the SW in figure 1.7a, b and c; lines 74, 72 and 70).

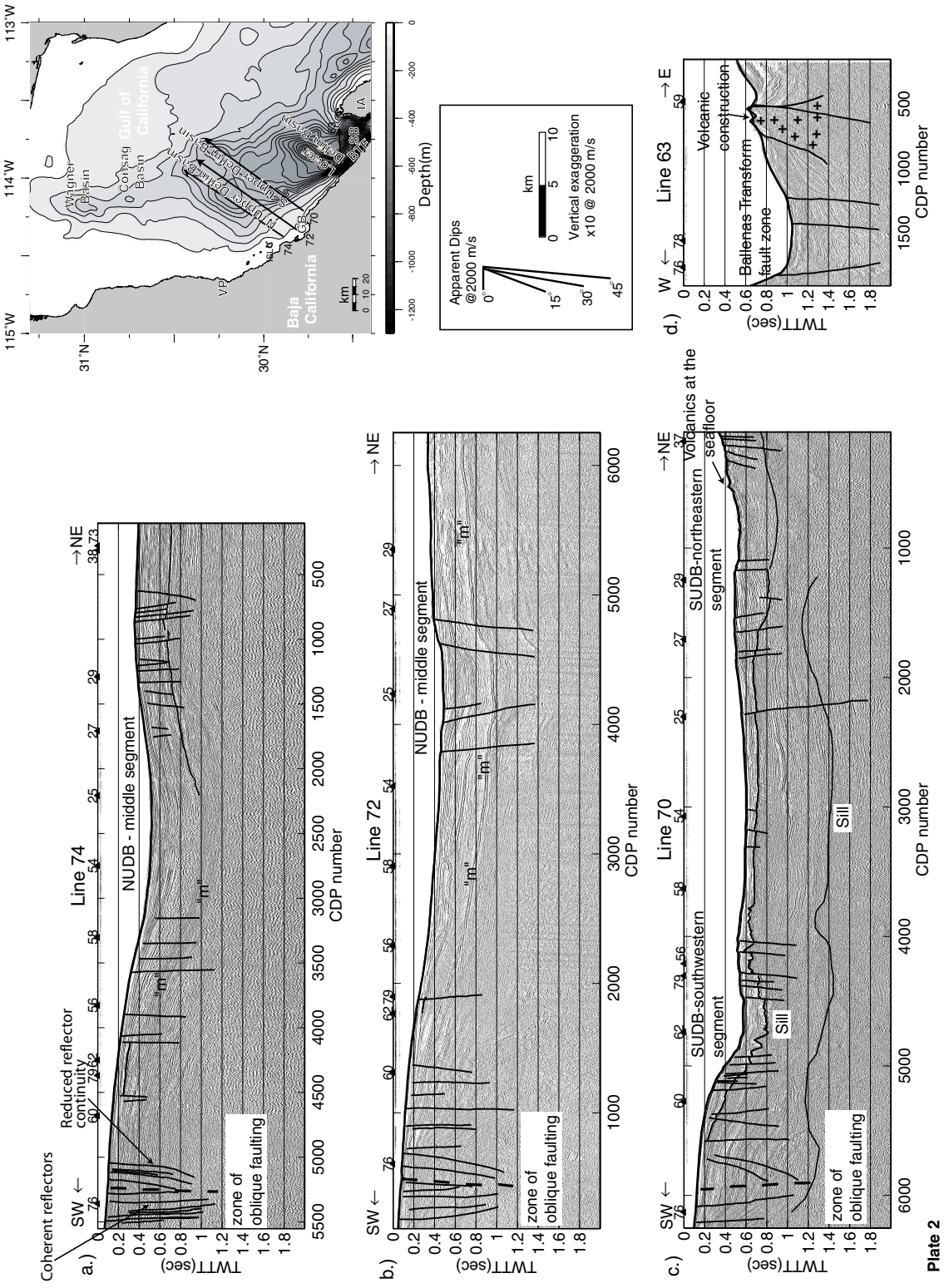

Figure 1.7: See opposite page for caption.

This discontinuous zone of oblique faulting along the Baja California coast (e.g., Figure 1.7c, line 70 around CDP 6000) extends from the southwestern end of the LDB northwestward towards Isla San Luis (Figure 1.2). The fault splays are disrupted along this zone and mostly bound blocks that are downdropped in a normal sense. The sag in the negative flower structure is evident farther north where the master fault (Figure 1.7a; $\sim$ CDP 5500, line 74) juxtaposes two distinctly different sedimentary packages. On the northeastern side of the master fault we see a series of incoherent reflectors with reduced reflector continuity, which may consist of sediments that have been baked by intrusions, or that contain gas or volcanic deposits. Across the master fault, this block is in contact with a well-layered sedimentary package indicating lateral offset. The master fault intersects basement below 1 s TWTT. The shallow depths to basement in this area are confirmed by the sonobuoy velocities.

1.4.3 N. and S. Upper Delfín Basins

These subparallel basins are divided into three segments along axis. This segmentation is expressed in the bathymetry (Figure 1.1b) and faulting. Although both basins are sites of active deformation, the center of extension switches along the axes from one basin to the next. Along seismic line 25, the seafloor scarps in the middle segment of the NUDB (Figure 1.8) are more pronounced and faults are more closely spaced than in the middle of the SUDB (Figure 1.9). Faulting in the northeast and southwest segments of these basins displays the opposite pattern, with smaller fault scarps in the NUDB than the SUDB (Figure 1.11, 1.10a and 1.10c). In a profile across the northeast segment of the Upper Delfín basins (Figure 1.10c; line 29), the seafloor scarps in the NUDB are only a few meters, whereas the scarps farther south in this basin (Figure 1.10b and 1.8) measured a few tens of meters. To the southwest in this profile (Figure 1.10c; line 29), the seafloor scarps in the SUDB are large ($\sim$ CDP 14500). In the southwest segment of the SUDB, near the volcanic protrusion in

Figure 1.7 Compilation of MCS profiles, (a) 74, (b) 72, (c) 70 and (d) 63 which cross the NW extension of the Ballenas Transform Fault Zone. The dashed line in a, b and c represents the master fault in the northward extension of the BTF. Locations of the seismic profiles are shown in the map and figure 1.1b. Arrowheads mark the right end of the images. See the caption in figure 1.4 for further details.

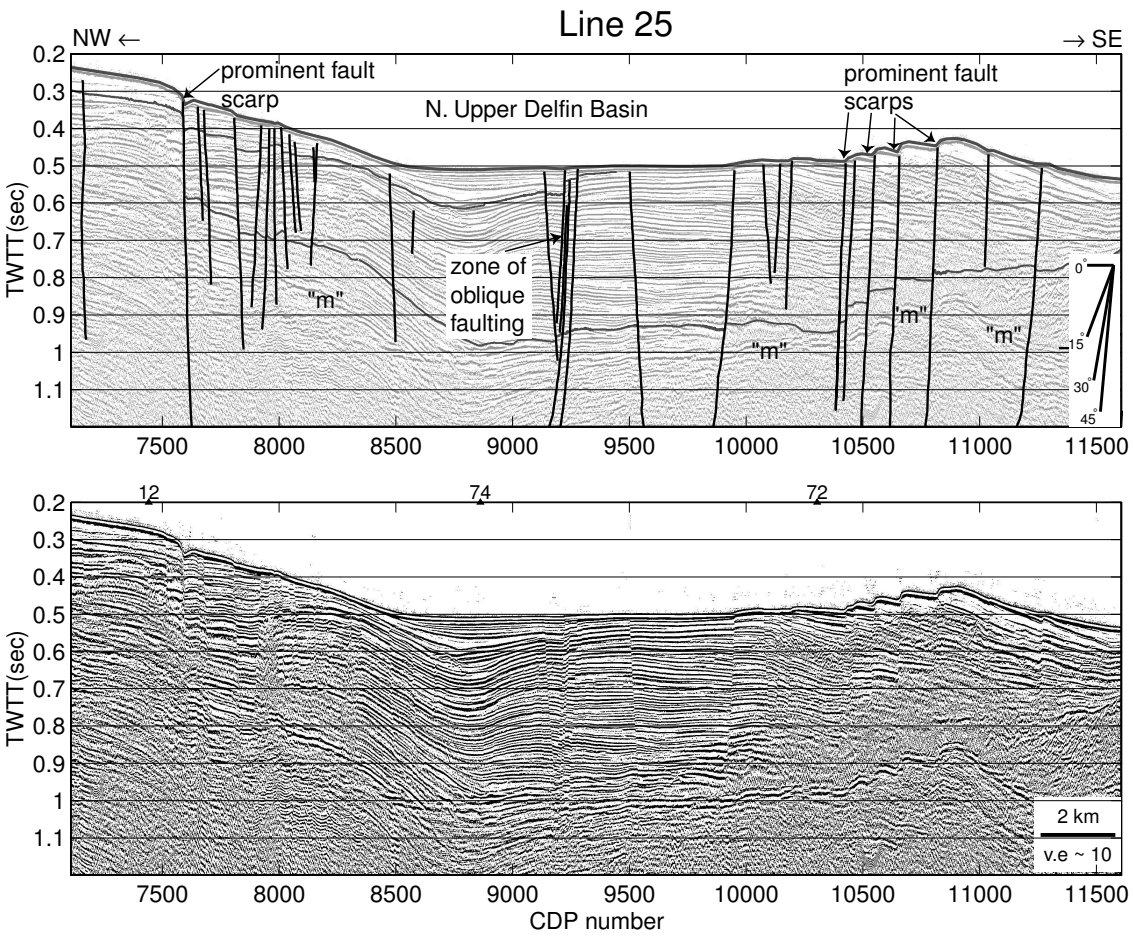

Figure 1.8: Seismic profile across the axis of the NUDB. Here the middle segment of the NUDB is more active than the middle segment of the SUDB in Figure 1.9. Note the multiple faults and the large seafloor scarps (∼25 m at water velocity = 1500 m/s).

figure 1.4c [Henyey and Bischoff, 1973], this basin is more active than the NUDB. As the middle segment of the SUDB is approached from the south (Figure 1.11), deformation lessens and the basin becomes shallower. This asymmetry in active faulting is, however, not evident in the fault density map (Figure 1.5), where both basins appear equally active.

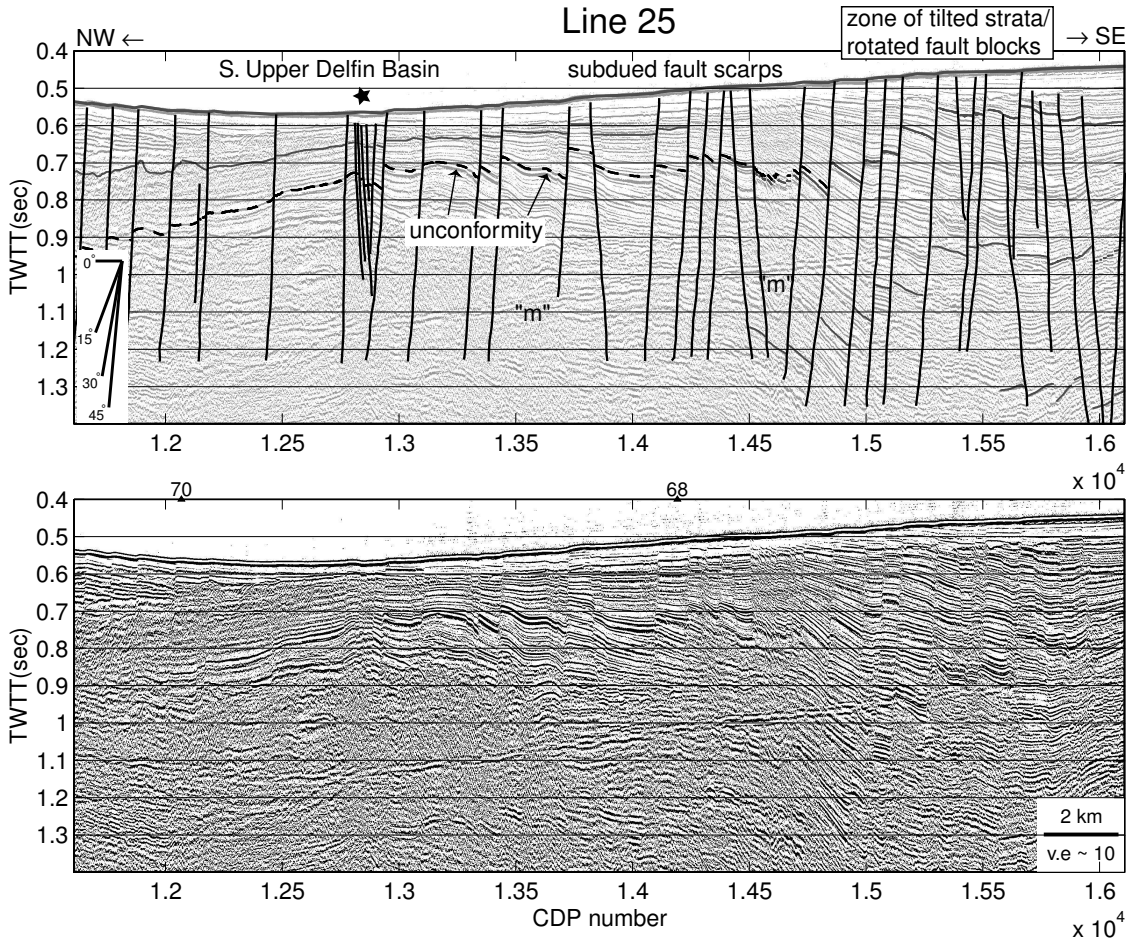

Figure 1.9: Seismic profile across the axis of the SUDB. The SUDB is subdued in this region, but is more active in its northeast and southwest segments. Strike-slip or oblique offset is suggested in the center of the image around CDP 13000 (marked by the star). Layers thicken both to the NW and SE of this zone of oblique offset. Prominent reflectors are highlighted in the top panel. The dashed line marks an unconformity.

Compared to faults in the SUDB, those in the NUDB are steeper (Figure 1.5) and reversals in the dip direction of faults are more common. As in the LDB, the same overall pattern of east-dipping faults in the NW flank of the rift basin and west-dipping faults in the SE flank is observed in the NUDB and northeast and southwest segments of the SUDB; the middle segment of the SUDB, however, shows the opposite sense of dip with outward facing faults common.

Figure 1.10 Compilation of MCS profiles, (a) 56, (b) 25 and (c) 29, which cross the Upper Delfín basins. Locations of the seismic profiles are shown in the map and figure 1.1b. Arrowheads mark the right end of the images. Boxes mark the location of other illustrations. See the caption in figure 1.4 for further details.

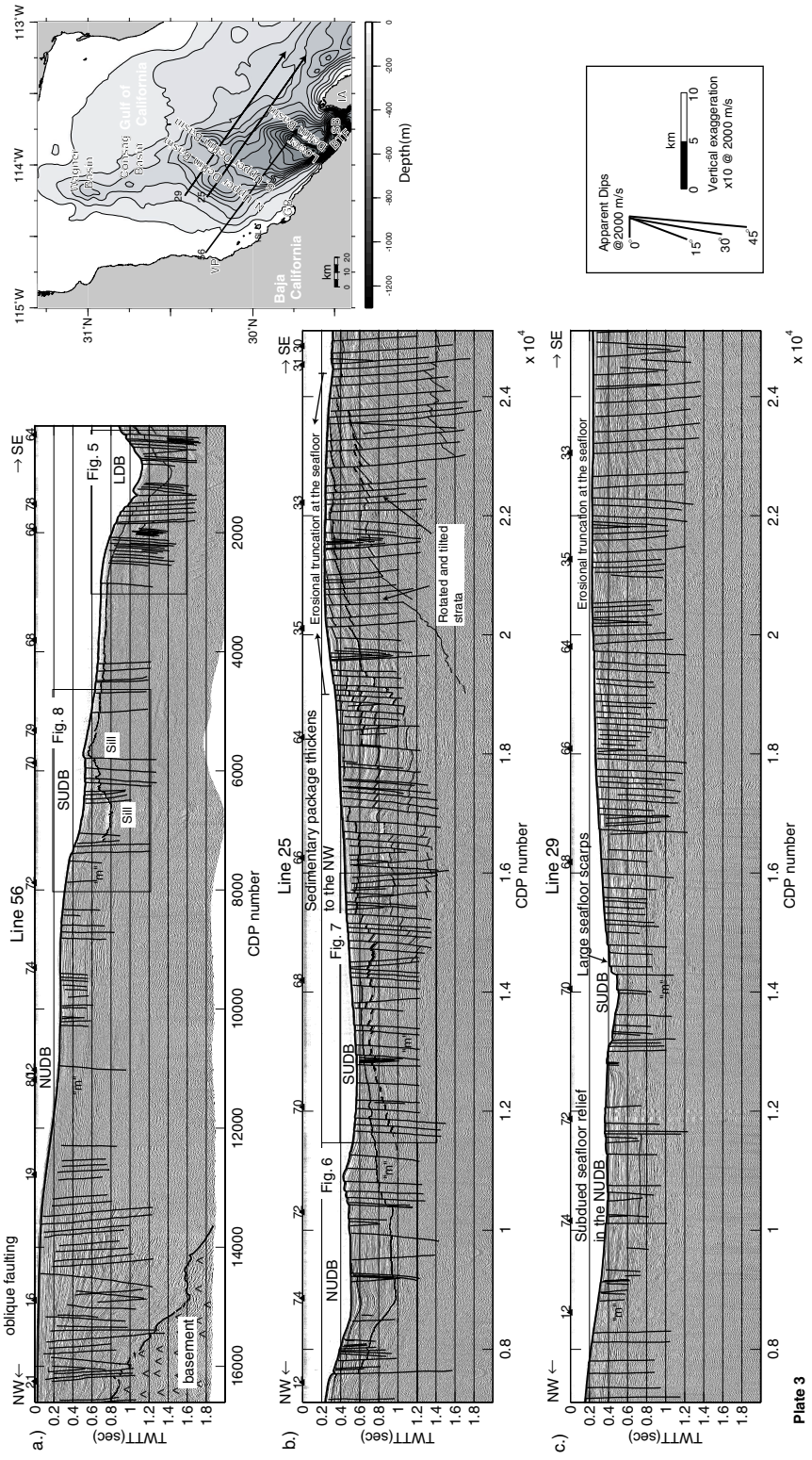

Figure 1.10: See previous page for caption.

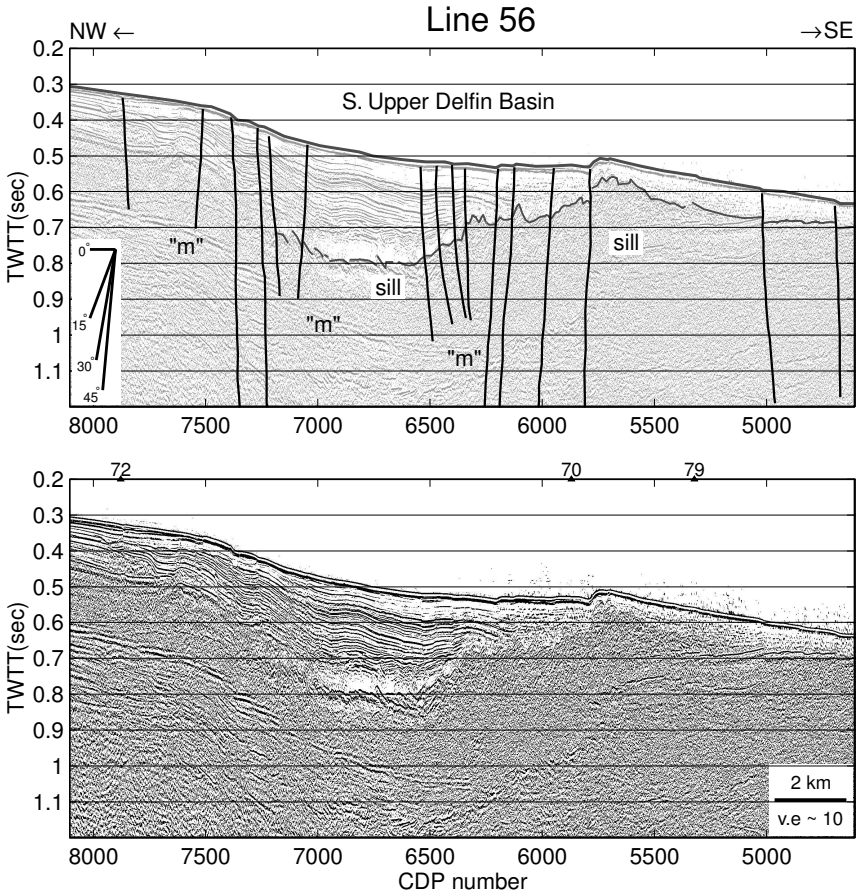

Figure 1.11: Seismic profile across the axis of the SUDB. Note that the seafloor relief of the SUDB is subdued and the fault scarps are not very large. This profile shows that extension is decreasing towards the middle of the basin. Chaotic reflectors are interpreted as sill intrusions. The thickness of the sill is difficult to determine as no coherent reflectors can be identified beneath the top contact. The sill underlies a more coherent package of reflectors, which is a few 100s m thick in deepest part of the basin.

In a region at 29.9°N, 113.3°W, centered in the middle of the Gulf (Figure 1.10b; CDP 22000, line 25), a zone of closely spaced faults (∼1 km apart) with opposing dips is associated with tilted strata. Evidence of erosional truncation in this area suggests that the strata were once domed up or tilted and exposed subaerially.

1.4.4 Wagner and Consag Basins

Fault scarps are smaller and less common than in the other major basins (Figure 1.12), but the density of faults is higher in the WB than in the Upper Delfín basins (Figure 1.5). Opposing fault dips are common in the axial region of the WB. There are

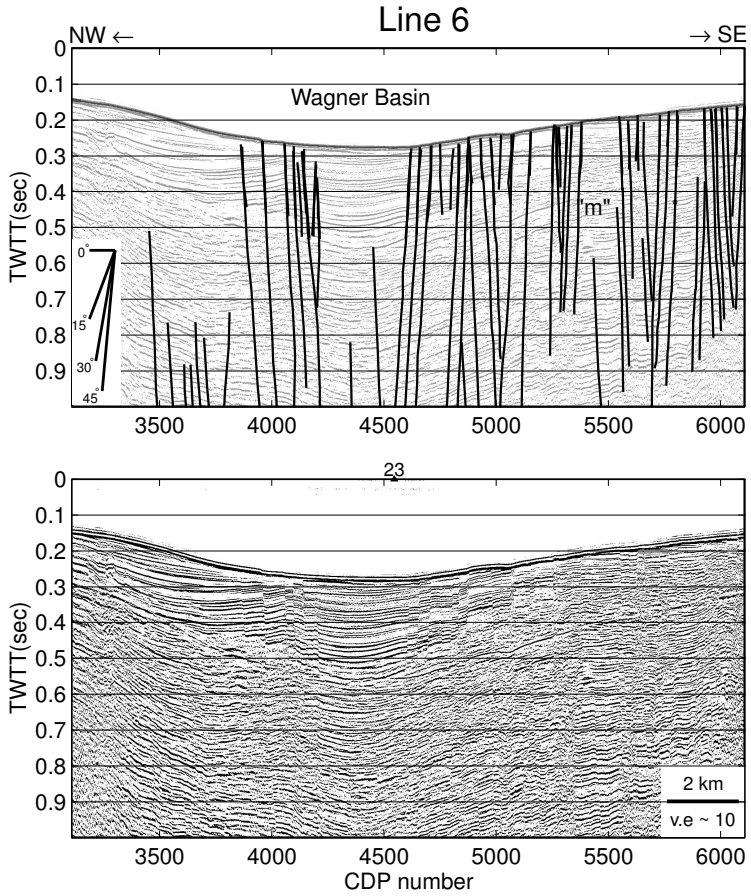

Figure 1.12: Seismic profile across the axis of the Wagner Basin. The sediment thickness is large here due to the high flux from the Colorado River located to the north. Note the high density of faults and their asymmetric distribution with respect to the center of the basin; more active faults are present on the SE side than on the NW side.

many steeply dipping faults and a wide range of fault dips (Figure 1.5). The structural pattern is asymmetric, with more active faults over a broader region in the SE flank of the basin and a narrower, less active fault zone in the NW side of the basin. The sedimentary package imaged in the area of the WB is at least 2 km thick; PEMEX wells W1 and W3 (Figure 1.1b) penetrated 3 km or more of Pleistocene sediments, below which the ages were either undetermined (W3) or still Pleistocene (W1). The thick Pleistocene sediments are faulted downward into the WB along normal faults with seafloor offsets averaging just a few meters. The Consag basin (Figure 1.13) to the south is generally shallower than the WB and may be a pull-apart in the left-stepping system of transform faults in the N. Gulf.

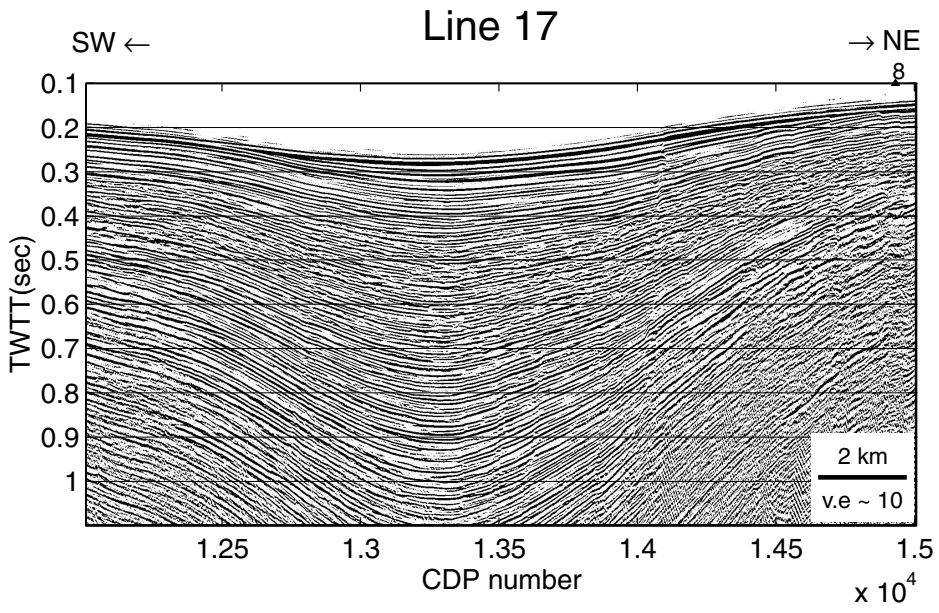

Figure 1.13: Uninterpreted seismic profile across the Consag Basin. It shows a large sediment-filled sag with very little faulting. This structure may be an accommodation zone.

1.5 Delineation of the Major Rift Basins

Isopach maps were used to identify the major active rift basins or depocenters in the N. Gulf (Figure 1.14). Due to the high density of faulting and disruption by igneous material, regional unconformities were not traceable throughout the major basins. We therefore chose a prominent reflector with good lateral continuity as the base of the youngest sediments. The thickness of the youngest sedimentary layer was then calculated by subtracting the thickness of the water column in two-way travel time. A velocity of 2000 m/s was used for the sediments to convert to thickness. The 150 m isopach was used to map the active basins (red lines in figure 1.14).

The trough of the LDB is outlined by the 800 m bathymetric contour. Based on the bathymetry, the basin trends N25°E. The 150 m isopach gives a length of 30 km and trend of N10°E. The LDB abuts the Ballenas transform to the SW, where it merges with the Salsipuedes basin (Figure 1.1b), the deepest of all of the N. Gulf basins. Due to the partial coverage, reliable isopach maps could not be produced for the Salsipuedes basin. The sedimentary package in the LDB is disrupted in many places by intrusions. The isopach map, however, clearly shows the segmentation of

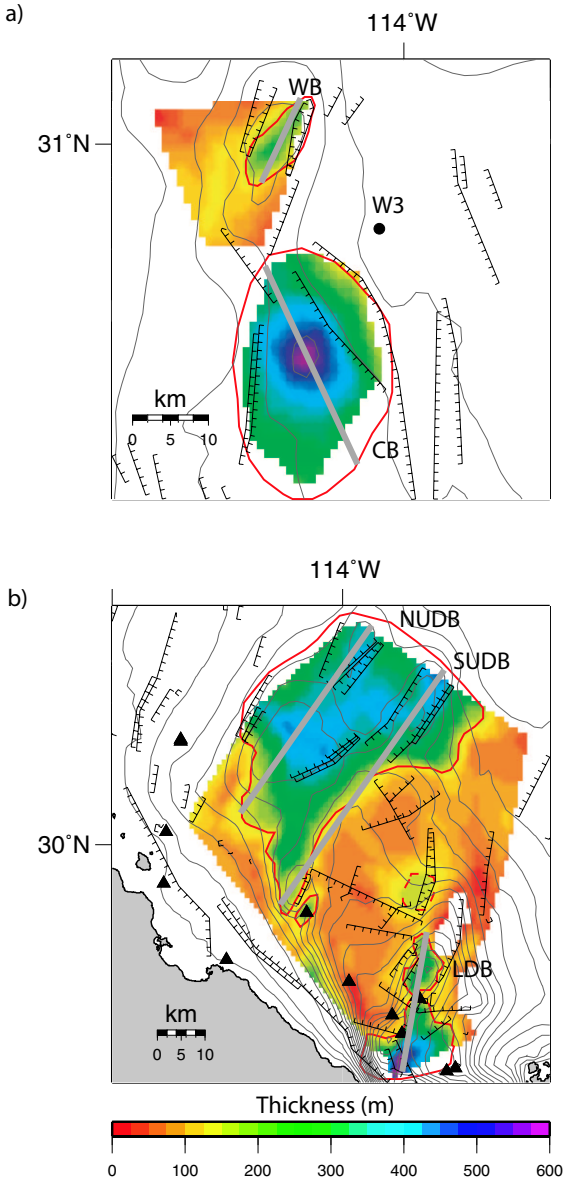

Figure 1.14: Isopach maps of the youngest sediments in a) the Wagner and Consag basins and b) the Upper Delfín and Lower Delfín basins. Thickness is given in meters below the seafloor. A velocity of 2000 m/s was used to convert TWTT to thickness. Solid red lines outline the major basins/depocenters. Thick gray lines represent the axes of the basins. These are based on the 150 m isopach. An additional small depocenter with no bathymetric expression is also shown (dashed red line). CB=Consag Basin; LDB=Lower Delfín Basin; NUDB=Northern Upper Delfín Basin; SUDB=Southern Upper Delfín Basin; W3=PEMEX well.

the LDB into two depressions (Figure 1.14) as is also observed in a seismic profile along the axis of the basin (Figure 1.4a). An additional small depocenter, just north of the two depressions, is interpreted as a structural continuation of the LDB or

another possibly younger segment of the basin (Figure 1.14).

The southern boundary of the Upper Delfín basins is located $\sim$ 30 km northwest of the LDB. Based on the bathymetric data, the NUDB and SUDB are two subparallel basins of similar size. Seafloor relief in these basins is not as pronounced as in the LDB. A low of 400-450 m depth marks the SUDB, while the NUDB has maximum water depths of 300-350 m. Both basins are segmented and trend N35°E based on bathymetry and the 150 m isopach (Figure 1.1b and 1.14). The isopach maps give lengths of 50 km and 60 km for NUDB and SUDB, respectively, and show the NUDB and SUDB as an irregularly shaped but mostly continuous basin, with a thicker sedimentary package in the center of the NUDB and the ends of the SUDB. This reflects the same structural connections suggested by active faulting.

Interestingly, the youngest layer is thickest in the Consag Basin (CB) (Figure 1.14). Similarly, from the 150 m isopach, this basin appears to be broader than the WB to the north. The axes of these basins are $\sim$ 15 km apart and the CB lies $\sim$ 30 km northwest of the northern boundary of the NUDB. Water depths in the CB and WB are less than 250 m (Figure 1.1b). The WB trends N15°E - N20°E (Figure 1.1b) based on bathymetry and N12°E based on the 150 m isopach (Figure 1.14). It has a length of 13 km. Based on seismic profiles and heat flow data, the WB has been interpreted either as a bend along a transform fault, or a transform fault with another spreading center located to the north [Henyey and Bischoff, 1973]. This contrasts with a geologic-tectonic interpretation of this basin as an active spreading center [Fenby and Gastil, 1991].

1.6 Relationship between Magmatism and Deformation

The Lower Delfín basin is magmatically the most active basin of those we surveyed. Along strike, the deepest part of the LDB is sandwiched between extrusive volcanic rocks to the northeast and the Baja California continental block to the southwest (Figure 1.4a; line 64). The axis of the LDB is intruded by volcanic rocks, which form small knolls on the seafloor (Figure 1.2 and 1.3). Intrusive bodies and volcanic knolls are elongate along the axis of the LDB, but are narrow across axis (see *

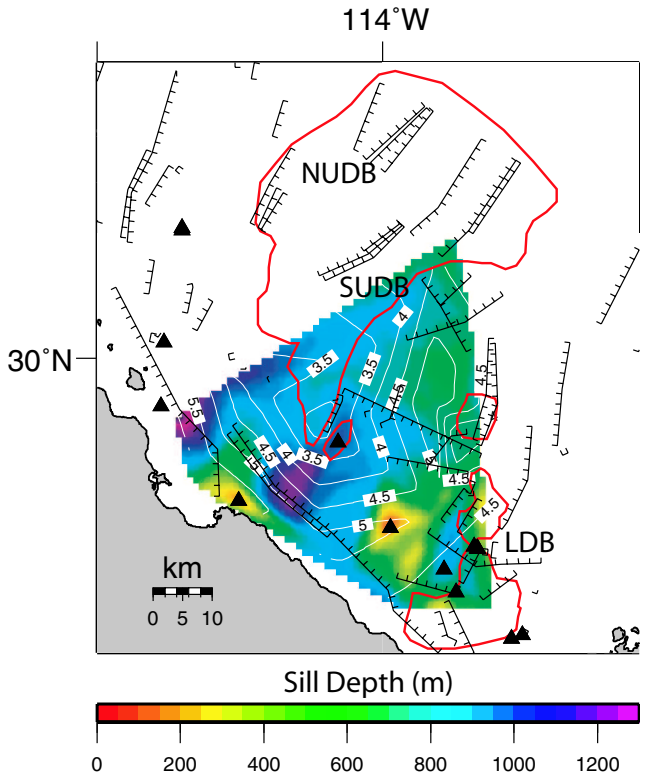

Figure 1.15: Map showing sill depth in meters below the seafloor overlain by contours (white lines) of P-wave velocities at 2.8 km depth below the sea surface. Contours are shown at 0.5 km/s intervals. The sill depths shown are for multiple sills and represent an interpolation between different bodies. The major basins are outlined in red, based on the 150m isopachs shown in figure 1.14. Triangles are volcanic knolls.

in Figure 1.4). Compared to the LDB, the NUDB and SUDB have fewer volcanic knolls. One of these is the large knoll located in the southwest segment of the SUDB (Figure 1.2 and 1.4c), which produced dredge samples of rhyolite pumice [Henyey and Bischoff, 1973]. Sills are, however, not uncommon, particularly in the deeper parts of these basins, where chaotic reflectors underlie a coherent package of sediments (e.g., Figure 1.11 and 1.10; line 56). The tops of sill bodies were interpreted and the depths are shown in figure 1.15. There seems to be some correlation between shallow sills, recent extrusive volcanism, high P-wave velocities and faulting (Figure 1.15). The one notable exception is the relatively large volcanic knoll in the southwest segment of the SUDB (Figure 1.4c, CDP 10000), which is associated with a velocity low.

Although no volcanic knolls were identified in the area of the WB, Consag Rock (Figure 1.1b), a small volcanic island west of the WB, may provide evidence for continued magmatic activity northward. Alternatively, it may be a remnant of older

volcanic rock, such as the pre-rift andesite from the early to middle Miocene volcanic arc found in the adjacent area of Baja California [Gastil et al., 1979]. The lack of identified extrusive and intrusive magmatism in the northern part of our survey may have resulted from the reduced ratio of igneous to sedimentary rock as the Colorado River delta is approached and the sedimentary column thickens, making this identification more difficult.

1.6.1 Basement

If the N. Gulf crust is new igneous material, one would expect any extended continental basement to be restricted to the margins of the Gulf and not underlie the entire survey area. Indeed, the acoustic basement in the top 2 km of the crust can only be mapped at certain locations to within a few kilometers of the Baja California coastline. The basement is imaged in a seismic profile directly offshore of Volcán Prieto, approximately 10 km from the Baja Peninsula coastline (Figure 1.1b and 1.4c; line 62) and has an apparent dip of $4 - 5^{\circ}$ southeastward into the Gulf. Just north of this profile, the basement depth increases from $\sim$0.63 s TWTT (630 m at a seismic velocity of 2000 m/s) close to the Baja Peninsula to >1500 m at $\sim$10 km away from the coastline, which may indicate an apparent northeastward dip also (Figure 1.10a; line 56). Further evidence for a northeastward dip is the depth of 2800 m to the altered andesite in the W2 well located to the north (Figure 1.1b). We correlate the acoustic basement with the altered andesite rather than with the quartz-rich diorite at 2950 m in the W2 well. This correlation suggests that the dip of the basement from the profile shown in figure 1.4a (line 56) to W2 is $\sim 5^{\circ}$. Fitting a plane to all of the basement depths interpreted in the reflection data gives a N-S strike and true dip of 5.2°E. This estimate supports the idea of a basement with relatively uniform dip and some local structure. The basement surface appears to be somewhat irregular and may indeed be affected by faulting; however, no large offset (>0.1 s TWTT) normal faults were interpreted in this area. Deciphering any lateral offsets of the basement is not presently possible.

Limited constraints on the composition of the deeper basement in the N. Gulf come from the sonobuoy data. From the analysis of refraction data, Phillips [1964] identified

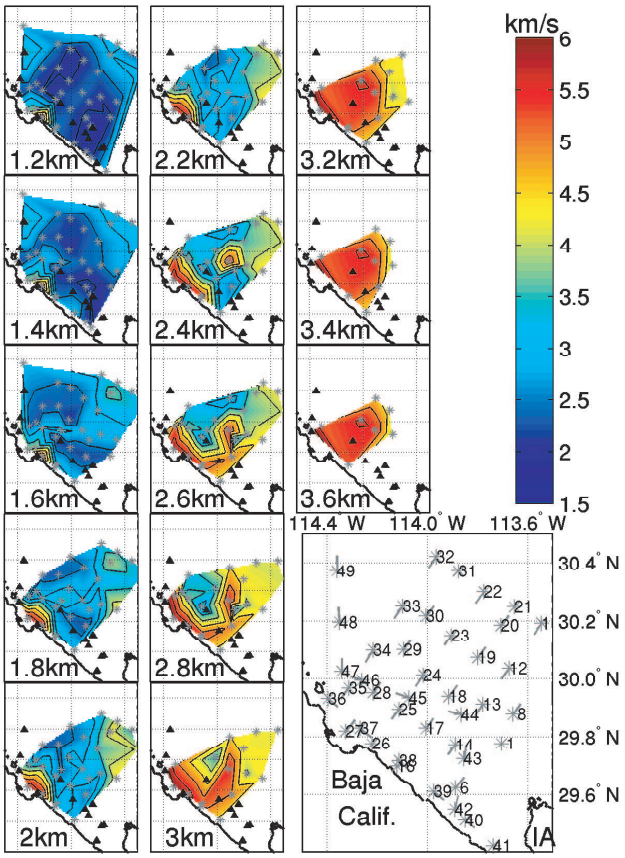

Figure 1.16: Depth slices showing interval velocities in the N. Gulf of California. Black triangles are volcanic knolls and gray stars mark the sonobuoy locations with tails pointing in the direction in which the ship was travelling. In each depth slice, the gray stars show the sonobuoys with data at that depth. IA=Isla Angel de la Guarda.

igneous and metamorphic basement with a seismic velocity of 5.53 km/s at a depth of ∼4 km in the N. Gulf. In addition, shallow magnetic horizons have been estimated at depths of 2.3-4.1 km below sea level [Sánchez-Zamora et al., 1991]. Our refraction data show a large jump (1 km/s or more) associated with every velocity change to ∼5.0 km/s. We interpret velocities >5.0 km/s as basement, possibly containing some amount of sedimentary material similar to that found in the Guaymas basin [Einsele et al., 1980].

Velocity highs seen at shallow depths (1.2 km) close to Gonzaga Bay and 30.2°N, -113.8°W are correlated with volcanic protrusions on the seafloor (Figure 1.16). The shooting tracks of the sonobuoys did not traverse every volcanic knoll in the area (e.g., those close to Isla Angel de la Guarda in the LDB do not all have sonobuoy coverage),

and we therefore cannot determine whether or not they all are associated with high velocities (Figure 1.16). Above 2 km, with the exception of the higher velocities in San Luis Gonzaga Bay, the velocities are $\leq$ 3.5 km/s (Figure 1.16). The fairly smooth increase in velocities with depth suggests a thick sequence of unconsolidated to consolidated sediments (Figure 1.16). At depths larger than 2 km, sonobuoys 14, 18, 24, 27, 35, 36 and 38 show basement velocities greater than $\sim$5 km/s. At the location of sonobuoy 36, basement velocity is 6.4 km/s. This is close to the Baja California coast and is probably volcanic basement similar to the basaltic andesites to rhyolites found in the nearby Holocene volcanic center of Isla San Luis [Paz Moreno and Demant, 1999]. The higher velocities between the middle segment of the SUDB and the LDB may indicate less extended igneous/metamorphic crust and a thinner sedimentary package between these basins.

1.7 Discussion

The N. Gulf of California displays a complex structural pattern which will be discussed in the context of onshore vs. offshore faulting, rift obliquity and the transition to seafloor spreading.

1.7.1 Onshore Versus Offshore Faulting

Here, we compare the offshore faults to the onshore structure of northeastern Baja California east of the Sierra San Pedro Mártir, between San Felipe (31° N) and Gonzaga Bay (29.8° N), where the spatial and temporal development of faulting is well established.

1.7.1.1 Synthesis of Offshore Structure

Based on our interpretation of the seismic data, faulting in the N. Gulf of California occurs over a broad depressed region, approximately 70 x 200 km encompassing multiple rift basins. Our map shows a broad zone of deformation, comprised of many oblique-slip faults with true dips of $\sim$60-80° and varying azimuths (Figure 1.5). No primary or throughgoing structures such as transform faults were identified in the N.

Gulf. In the axial regions of the Upper Delfín basins, most faults are NE-striking normal faults with some lateral offset. The Lower Delfín Basin has two mutually crosscutting sets of active faults (NE-striking normal and NW-striking oblique-normal faults) (Figure 1.17a). NW-striking, oblique-normal faults parallel the Baja California coastline. The uplifted zone north of Isla Angel de la Guarda may have accommodated extension created by listric ramp-flat faulting at depth. In the area of the Wagner and Consag basins, faults generally strike northerly. We expect the Wagner basin originated as part of an older extensional domain bounded by a major strike-slip fault located NE of Isla Angel de la Guarda, perhaps even outside of our survey area. We hypothesize that the orientation of the extensional component of this system was not significantly different than it is at present, since the Wagner basin is still a major part of the plate boundary.

The overall shallow structure in the N. Gulf is that of a pull-apart basin containing at least three major extensional domains or duplexes, the LDB, SUDB and NUDB. Extensional duplexes are known to form at releasing bends or offsets along strike-slip faults and on straight strike-slip faults [Woodcock and Fischer, 1986]. These duplexes appear to merge with transtensional branches from the BTF, forming a horsetail structure (Figure 1.17b). This indicates a transtensional fault zone NW of Isla Angel de la Guarda, where the small volcanic knolls are concentrated. This broad pull-apart basin is floored by basement of mixed igneous-sedimentary material, within which some blocks of older continental crust may exist. Structurally, the N. Gulf does not look like a typical mid-ocean ridge environment. There are no "ridges" and seafloor spreading is still not occurring.

1.7.1.2 Synthesis of Onshore Structure

We found no evidence for a continuation of the present onshore structures into the offshore in the N. Gulf. In contrast to the style of faulting in the offshore, onshore deformation consists of two structural regimes separated by the Puertecitos Volcanic Province (PVP) (Domains II and III in figure 1.17) and bounded to the west by the Main Gulf Escarpment (Domain I) [Dokka and Merriam, 1982]. A well-developed basin and range topography with E-dipping listric normal faults developed between

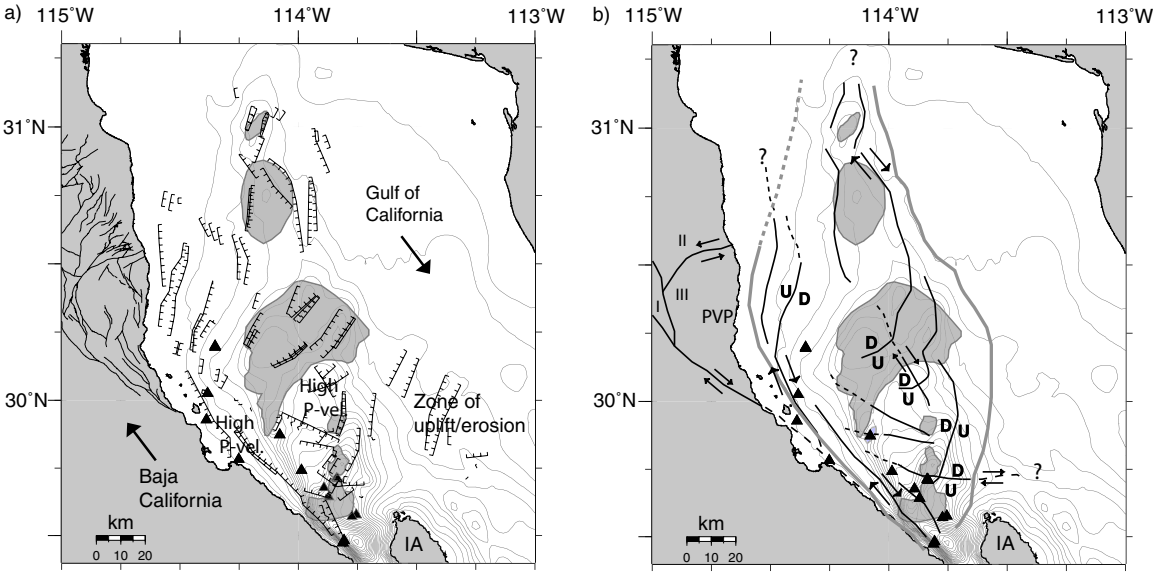

Figure 1.17: a) Summary map showing the faults interpreted in our reflection data (black lines with hachures on the downthrown side), bathymetric contours every 50 m (thin gray lines), the major basins determined from the 150 m isopach (gray fill) and areas of high P-velocities from our refraction data. Heavy black arrows indicate the current Pacific-North America relative plate motion direction, N37°W [Atwater and Stock, 1998]. Onshore faults are from Oskin et al. [2001]. b) Schematic drawing summarizing the major tectonic elements identified in the N. Gulf. The onshore structural domains (I, II and III) are after Dokka and Merriam [1982]. Black lines offshore represent the extensional strands of a broad shallow basin (outlined by thick gray lines) and faults that cut across the axis of the LDB. Arrows represent the sense of lateral slip. "U" and "D" refer to the sense of vertical slip. Black triangles are volcanic knolls. See text for discussion. PVP=Puertecitos Volcanic Province; IA=Isla Angel de la Guarda.

12 and 6 Ma north of the PVP in Domain II [Dokka and Merriam, 1982; Stock and Hodges, 1990], suggesting a period of E-W extension. Interpretation of kinematic data inversions along with published paleomagnetic data provide evidence for a W-E and SW-NE orientation of the axis of least principal stress in late Miocene time [Lewis and Stock, 1998b]. Sometime after 6 Ma the style of faulting in NE Baja California east of the rift margin, east of the San Pedro Mártir border fault, changed to E-W extension [Dokka and Merriam, 1982]. Pliocene to Recent extension along the western rift margin of the GEP remained E-NE directed [Nagy and Stock, 2000]. At about 3 Ma, extension within the Gulf Extensional Province was approximately oriented WSW-ENE [Lewis and Stock, 1998b] and NE-striking faults were rotated and reactivated with sinistral slip [Lewis and Stock, 1998a]. These faults have accommodated an

average of 30° of clockwise rotation of late Miocene tuffs around vertical axes [Lewis and Stock, 1998a]. In Domain III, south of Puertecitos there are no major NE-striking sinistral faults. A series of mostly <6.3 Ma old, NW-NNW striking, down-to-the-east, high-angle, normal faults exists between the PVP and Gonzaga Bay [Chapter 6 in Oskin, 2002; Stock and Hodges, 1990; Stock, 2000].

In Domain I, the active (Holocene) San Pedro Mártir fault, at the western margin of the Gulf Extensional Province north of the PVP records 5 km of vertical separation [Brown, 1978]. No evidence has been found for such large offsets on a single fault in the offshore. In order to image such offsets, deeper seismic data are required.

1.7.1.3 Comparison of Onshore and Offshore structure

Limited by the fact that our data do not penetrate the middle and lower crust, the present NE-striking onshore faults largely appear to terminate near the shoreline and are apparently not continuous out into the N. Gulf. Deformation in the shallow crust in the N. Gulf appears to be occurring in a different manner to that observed onshore within the continental extensional province. We speculate that the offshore structures may reflect a different and more recent stress regime than the onshore faults.

1.7.2 Influence of Rift Obliquity on Deformation

The angle, α, between the plate motion direction, N37°W [Atwater and Stock, 1998], and the rift trend or plate margin in the Gulf of California is approximately 20° or 30° [Withjack and Jamison, 1986]. Although obliquity can be locally related to different mechanisms such as excess magma injection compared to far field forces as in the case of Reykjanes Ridge [Abelson and Agnon, 1997], in this discussion we assume that obliquity is only a result of plate motion and hence, does not vary along the axis of the Gulf. Theory [Fossen and Tikoff, 1993] and kinematic modeling [Teyssier et al., 1995] have shown that strike-slip partitioning in continental crust is higher for higher rift obliquities (i.e., smaller α's) and wrench-dominated transtension occurs for $\alpha \leq 20°$. The fault pattern in the N. Gulf, however, suggests a limited degree of strike-slip partitioning, where faults with a larger/obvious strike-slip component

are concentrated close to the Baja California coast and faults with a dominantly extensional component are concentrated in the middle of the rift. Most of the faults are, however, interpreted as having oblique-slip rather than purely strike- or dip-slip indicating incomplete strain-partitioning.

Scaled analog experiments on displacement partitioning in basins and the lithosphere have shown that a viscous ductile layer at depth is needed to produce strike-slip partitioning during transpression [Richard and Cobbold, 1990]. This viscous ductile layer decouples the upper crust from the zone of shear at depth. In the absence of this layer, oblique slip faults will form instead of either purely strike-slip or purely dip-slip faults [Richard and Cobbold, 1990] because the transmission of basal shear forces to the upper and middle crust is more efficient. Strike-slip partitioning in the N. Gulf is incomplete. We suggest, therefore, that the lower crust in the N. Gulf of California is relatively thin or strong, the latter implying it is mantle-derived.

From analog experiments it is also known that the range of azimuths in a fault population should increase as rift obliquity increases (i.e., α decreases), with two orientations first becoming predominant at $\alpha \leq 30°$: one approximately rift-parallel and the other displacement-normal [Clifton et al., 2000]. For these obliquities, faults that develop within the rift have dip-slip, oblique-slip and strike-slip motion [Clifton et al., 2000]. Our observations in the N. Gulf of a predominantly rift-parallel fault population and overall large variations in fault orientations and dips partly confirm the results of analog models (Figure 1.5).

In addition, the rift basins are oriented approximately perpendicular to N37°W, the plate motion direction [Atwater and Stock, 1998], in the deepest parts of the N. Gulf, but oblique to the plate motion direction in the shallower areas. There are no large basin-bounding faults or well-defined zones of strike-slip or normal faulting. These structural styles are typical of mechanical models of oblique rifts. Mart and Dauteil [2000] showed that during analog experiments with rift obliquities of 15°, undulating rifts formed with central diapirs separated by threshold zones of diffuse extension.

Numerical results of purely strike-slip deformation in a pull-apart basin driven from below show that a wider basal shear zone produces a broader, longer and shal-

lower zone of surface deformation [Katzman et al., 1995]. By adding a small component of extension, a large component of regional subsidence is produced [ten Brink et al., 1996]. Based on the fact that brittle deformation in the N. Gulf is occurring by multiple small-offset faults in a broad zone of deformation, we also expect the basal shear zone beneath the crust to be wide. The fact that no local heat flow highs were identified in the N. Gulf [Henyey and Bischoff, 1973; Sánchez-Zamora et al., 1991] also supports a broad shear zone at depth.

1.7.3 Transition to Seafloor Spreading

If both the southern and northern parts of the Gulf have experienced the same amount of opening, why is there still no seafloor spreading in the northern part? Is it because of heterogeneities in thinning of the crust along the axis of the Gulf, or differences in initial crustal composition or physical properties such as crustal thickness and strength? Although a comparison with the southern Gulf is beyond the scope of this work, our results illuminate two points in which the northern and southern parts of the Gulf differ: i) strain-partitioning and ii) sediment thickness.

It has been suggested that the temporal overlap of 3-4 m.y. between continental rifting and seafloor spreading in the Gulf resulted from its obliquity [Fletcher and Munguía, 2000]. The overall structure of the Gulf of California is a series of long transform faults and short spreading centers. This geometry keeps the continental crust weak by dragging it past the spreading centers while suppressing active asthenospheric upwelling by cooling of the spreading center through lateral heat transfer to the continental crust; this prolongs the period of normal faulting in continental crust and increases interplate coupling [Fletcher and Munguía, 2000].

Although these arguments may apply to the southern and central parts of the Gulf, the absence of long transform faults in the N. Gulf requires a different mechanism for the long-lived continental rifting and the delay in the transition to seafloor spreading in this region. The N. Gulf has a complex fault system consisting of multiple oblique-slip faults over a broad area versus the transform fault-spreading center geometry of the S. Gulf. The former is likely to transfer less heat to the continental crust than the latter; therefore any mechanism that distributes deformation in the N. Gulf and

consequently slows the transition to seafloor spreading must also allow for an extended period of rifting in the continental crust unrelated to the structural geometry of the adjacent plate boundary. We suggest a broad zone of basal shear in the N. Gulf coupled with its inherent obliquity causes strain to be spatially distributed and the degree of strike-slip partitioning to be small. Deformation on the margins of the N. Gulf is thus maintained on two widely separated fault systems, the transpeninsular faults which merge into the Gulf Extensional Province and the Cerro Prieto transform fault. We further speculate that the westward jumps in extension in the N. Gulf over the last several million years may be related to the interaction of these two fault systems.

The delay in the transition to seafloor spreading in the N. Gulf may also be controlled by the higher sediment flux from the Colorado River [e.g., Einsele, 1986]. Deposition of cold sediments has an initial cooling effect. In the long term, however, a thick blanket of low thermal conductivity sediments acts as an insulator and inhibits the localization of deformation by keeping the crust equally weak everywhere. Thick porous sediments also facilitate the intrusion of sills [Einsele et al., 1980; McBirney, 1963; Saunders et al., 1982] rather than dikes, which would be needed for the development of a typical mid-ocean ridge.

1.8 Conclusions

The plate boundary in the N. Gulf of California is a wide zone of oblique faulting. Our results show a broad shallow basin, approximately 70 $\times$ 200 km with six 10-km scale subbasins spaced 15 or 30 km apart: an L-shaped depression (LDB and Salsipuedes basin), two subparallel rift basins (NUDB and SUDB) and a possible accommodation zone comprised of the WB and CB. All basins are segmented along axis. With the exception of the Salsipuedes basin, they all trend oblique to the plate motion direction. There are no clear structural connections such as transform faults between these three groups of basins; however, each group is morphologically distinct and the basins in each group show similarities in fault systematics and magmatism. Based on magmatic and fault activity, the LDB is the most active of the basins

surveyed. Most of the faults in the survey have apparent dips of ∼50-60° suggesting that the plate boundary is made up of mainly oblique-normal faults. Major faults have true dips of ∼70°. In general seafloor scarps are smaller in the northern part of the survey area (e.g., WB) than in the southern part (e.g., LDB), reflecting the influence of a higher sediment flux closer to the Colorado River delta. Fault density in the WB is, however, as high as in the LDB. From this we conclude that although it is likely that true seafloor will first be produced in the LDB based on the near-surface manifestations of active magmatism and faulting, the WB plays a significant and perhaps major role in active deformation in the N. Gulf.

Our reflection equipment imaged the top 2 km of the sedimentary package, which may be no older than Pleistocene in age, perhaps with some Pliocene in the lowest part we image. Throughout the area surveyed, our data show many faults spaced a few kilometers apart, with small offsets. There are no major faults that take up most of the extension. The N. Gulf consists of a complex network of predominantly NE-striking normal faults dissected in part by NW-striking oblique-normal faults. Some of the faults observed in the shallow crust may merge at depth into single fault planes with larger cumulative offset. Based on sonobuoy data, PEMEX well data and reflection profiles, the basement dips 5° E-SE adjacent to NE Baja California. A zone of predominantly strike-slip deformation lies along the peninsular coast (Figure 1.17), where some faults penetrate basement. This zone marks the northern extent of the Ballenas Transform Fault zone, but does not contain a simple transform fault. Volcanic knolls are located either along the transform fault zones or within the rifts close to these zones. This suggests that the transform fault is transtensional. The NW end of the Ballenas transform fault branches off into multiple rift basins forming a horse-tail structure (Figure 1.17). The rift basins of the N. Gulf represent many strands of the transform fault zone, which clearly possesses a tensional component north of Isla Angel de la Guarda. This is first expressed in the deep Salsipuedes basin. Moving from the LDB to the Upper Delfín basins, the transform fault loses offset with each additional rift. It becomes increasingly difficult to identify discrete zones of strike-slip offset.

We found no evidence for a continuation of the onshore structures into the off-

shore and fewer throughgoing structures than previous workers. Based on the fact that mainly oblique slip faults are present and active, we conclude that strike-slip partitioning is incomplete. The style of deformation we image may have resulted from shear at depth beneath a strong lower crust that effectively transmits the oblique stresses to the weaker upper crust.

It is likely that the early stages of rifting elsewhere closely resemble the current deformation in the N. Gulf, where wide zones of lower lithospheric shear, rift obliquity, sediment flux, crustal thickness and rheology influence the focusing of deformation within the rift. We have shown that deformation is distributed in the N. Gulf and suggest that this is typical of young oblique rifts. We further suggest that sediment supply plays a significant role in keeping deformation distributed.

References

Meir Abelson and Amotz Agnon. Mechanics of oblique spreading and ridge segmentation. *Earth and Planetary Science Letters*, 148:405–421, 1997.

Manuel Aragón-Arreola, Arturo Martín-Barajas, and Joann M. Stock. Estructura y evolución de las cuencas fósiles en el norte del Golfo de California a partir de sísmica de reflexión multicanal. *GEOS*, 22(2):181, 2002.

Tanya Atwater and Joann Stock. Pacific-North America Plate Tectonics of the Neogene Southwestern United States: An Update. *International Geology Review*, 40: 375–402, 1998.

Michael E. Badley. *Practical Seismic Interpretation*. IHRDC Boston, 1985.

Daniel H. Barker. Rift propagation, detachment faulting, and associated magmatism in Bransfield Strait, Antartica Peninsula. *Journal of Geophysical Research*, 103 (B10):24,017–24,043, 1998.

Richard A. Bennett, William Rodi, and Robert E. Reilinger. Global Positioning System constraints on fault slip rates in southern California and northern Baja, Mexico. *Journal of Geophysical Research*, 101(B10):21,943–21,960, 1996.

J. L. Bischoff and T. L. Henyey. Tectonic elements of the central part of the Gulf of California. *Geological Society of America Bulletin*, 85:1893–1904, 1974.

G. Boillot, D. Mougenot, J. Girardeau, and E. L. Winterer. Rifting Processes on the West Galicia Margin, Spain. In A. J. Tankard and H. R. Balkwill, editors, *American Association of Petroleum Geologists Memoir 46*, Extensional tectonics and stratigraphy of the North Atlantic margins, pages 363–377. 1989.

L. G. Brown. *Recent fault scarps along the eastern escarpments of the Sierra San Pedro Mártir, Baja California*. Masters Thesis, San Diego State University, San Diego, California, 1978.

Amy E. Clifton, Roy W. Schlische, Martha O. Withjack, and Rolf V. Ackermann. Influence of rift obliquity on fault-population systematics: results of experimental clay models. *Journal of Structural Geology*, 22:1491–1509, 2000.

James R. Cochran and Fernando Martinez. Evidence from the northern Red Sea on the transition from continental to oceanic rifting. *Tectonophysics*, 153:25–53, 1988.

Richard W. Couch, Gordon E. Ness, Osvaldo Sanchez-Zamora, Gustavo Calderón-Riveroll, Pierre Doguin, Thomas Plawman, Shane Coperude, Bruce Huehn, and William Gumma. Gravity Anomalies and Crustal Structure of the Gulf and Peninsular Province of the Californias. In J. P. Dauphin and B. R. T. Simoneit, editors, *American Association of Petroleum Geologists Memoir 47*, The Gulf and Peninsular Provinces of the Californias, pages 25–45. 1991.

J. R. Curray, D. G. Moore, L. A. Lawver, F. J. Emmel, R. W. Raitt, M. Henry, and R. Kieckhefer. Tectonics of the Andaman Sea and Burma. In J. S. Watkins, L. Montadert, and P. W. Dickerson, editors, *American Association of Petroleum Geologists Memoir 29*, Geological and Geophysical Investigations of Continental Margins, pages 189–198. 1979.

C. DeMets. A reappraisal of seafloor spreading lineations in the Gulf of California: Implications for the transfer of Baja California to the Pacific plate and estimates of Pacific-North America plate motion. *Geophysical Research Letters*, 22:3545–3548, 1995.

Roy K. Dokka and Richard H. Merriam. Late Cenozoic extension of northeastern Baja California, Mexico. *Geological Society of America Bulletin*, 93:371–378, 1982.

Neal W. Driscoll and Garry D. Karner. Lower crustal extension across the Northern Carnarvon basin, Australia: Evidence for an eastward dipping detachment. *Journal of Geophysical Research*, 103(B3):4975–4991, 1998.

Gerhard Einsele. Interaction between sediments and basalt injections in young Gulf of California-type spreading centers. *Geologische Rundschau*, 75(1):197–208, 1986.

Gerhardt Einsele, Joris M. Gieskes, Joseph Curray, David M. Moore, Eduardo Aguayo, Marie-Pierre Aubry, Daniel Fornari, Jose Guerrero, Miriam Kastner, Kerry Kelts, Mitchell Lyle, Yasumochi Matoba, Adolfo Molina-Cruz, Jeffrey Niemitz, Jaime Rueda, Andrew Saunders, Hans Schrader, Bernd Simoneit, and Victor Vacquier. Intrusion of basaltic sills into highly porous sediments and resulting hydrothermal activity. *Nature*, 283:441–445, 1980.

Scott S. Fenby and R. Gordon Gastil. Geologic-Tectonic Map of the Gulf of California and Surrounding Areas. In J. P. Dauphin and B. R. T. Simoneit, editors, *The Gulf and Peninsular Provinces of the Californias*, American Association of Petroleum Geologists Memoir 47, pages 79–83. 1991.

John M. Fletcher and Luis Munguía. Active continental rifting in southern Baja California, Mexico: Implications for plate motion partitioning and the transition to seafloor spreading in the Gulf of California. *Tectonics*, 19(6):1107–1123, 2000.

Haakon Fossen and Basil Tikoff. The deformation matrix for simultaneous simple shearing, pure shearing and volume change, and its application to transpression-transtension tectonics. *Journal of Structural Geology*, 15(3-5):413–422, 1993.

J. Frez and J. J. González. Crustal Structure and Seismotectonics of Northern Baja California. In J. P. Dauphin and B. R. T. Simoneit, editors, *American Association of Petroleum Geologists Memoir 47*, The Gulf and Peninsular Provinces of the Californias, pages 261–283. 1991.

G. S. Fuis and W. M. Kohler. Crustal structure and tectonics of the Imperial Valley Region, California. In A. C. Rigsby, editor, *The Imperial Basin-tectonics, sedcimentation and thermal aspects: Los Angeles, CA, Pacific Section*, S.E.P.M., pages 1–13. 1984.

R. G. Gastil, D. Krummenacher, and J. Minch. The record of Cenozoic volcanism around the Gulf of California. *Geological Society of America Bulletin*, 90:839–857, 1979.

John A. Goff, Eric A Bergman, and Sean C. Solomon. Earthquake Source Mechanisms and Transform Tectonics in the Gulf of California. *Journal of Geophysical Research*, 92(B10):10,485–10,510, 1987.

A. González-Fernández, J. J. Danobeitia, D. Córdoba, L. A. Delgado-Argote, R. Carbonell, and R. Bartolomo. Estructura de la litósfera en el alto Golfo de California a partir de datos de sísmica de reflexion multicanal, sísmica de gran ángulo y gravimetría. *GEOS*, 19(4):219, 1999.

T. P. Harding. Identification of Wrench Faults Using Subsurface Structural Data: Criteria and Pitfalls. *American Association of Petroleum Geologists Bulletin*, 74 (10):1590–1609, 1990.

J. Helenes and A. L. Carreño. Neogene sedimentary evolution of Baja California in relation to regional tectonics. *Journal of South American Earth Sciences*, 12: 589–605, 1999.

Christopher D. Henry and J. Jorge Aranda-Gómez. Plate interactions control middle-late Miocene, proto-Gulf and Basin and Range extension in the southern Basin and Range. *Tectonophysics*, 318:1–26, 2000.

T. L. Henyey and J. L. Bischoff. Tectonic elements of the northern part of the Gulf of California. *Geological Society of America Bulletin*, 84:315–330, 1973.

Bruce M. Herman, Roger N. Anderson, and Marek Truchan. Extensional Tectonics in the Okinawa Trough. In J. S. Watkins, L. Montadert, and P. W. Dickerson, editors, *American Association of Petroleum Geologists Memoir 29*, Geological and Geophysical Investigations of Continental Margins, pages 199–208. 1979.

Eugene D. Humphreys and Ray J. Weldon II. Kinematic Constraints on the Rifting of Baja California. In J. P. Dauphin and B. R. T. Simoneit, editors, *American Association of Petroleum Geologists Memoir 47*, The Gulf and Peninsular Provinces of the Californias, pages 217–228. 1991.

Daniel E. Karig and Wallace Jensky. The Proto-Gulf of California. *Earth and Planetary Science Letters*, 17:169–174, 1972.

Rafael Katzman, Uri S. ten Brink, and Jian Lin. Three-dimensional modeling of pull-apart basins: Implications for the tectonics of the Dead Sea Basin. *Journal of Geophysical Research*, 100(B4):6295–6312, 1995.

Kim D. Klitgord, John D. Mudie, James L. Bischoff, and Tom L. Henyey. Magnetic anomalies in the Northern and Central Gulf of California. *Geological Society of America Bulletin*, 85:815–820, 1974.

Roger L. Larson. Bathymetry, magnetic anomalies, and plate tectonic history of the mouth of the Gulf of California. *Geological Society of America Bulletin*, 83: 3345–3360, 1972.

Luc L. Lavier, W. Roger Buck, and Alexei N. B. Poliakov. Factors controlling normal fault offset in an ideal brittle layer. *Journal of Geophysical Research*, 105(B10): 23431–23442, 2000.

Lawrence A. Lawver, John G. Sclater, Thomas L. Henyey, and J. Rogers. Heat flow measurements in the southern portion of the Gulf of California. *Earth and Planetary Science Letters*, 12:198–208, 1973.

Claudia J. Lewis and Joann M. Stock. Paleomagnetic evidence of localized rotations during Neogene extension in the Sierra San Fermin, northeastern Baja California, Mexico. *Journal of Geophysical Research*, 103(B2):2455–2470, 1998a.

Claudia J. Lewis and Joann M. Stock. Late Miocene to Recent transtensional tectonics in the Sierra San Fermín. *Journal of Structural Geology*, 20(8):1043–1063, 1998b.

Jennifer L. Lewis, Steven M. Day, Harold Magistrale, Raul R. Castro, Luciana Astiz, Cecilio Rebollar, Jennifer Eakins, Frank L. Vernon, and James N. Brune. Crustal thickness of the Peninsular Ranges and Gulf Extensional Province in the Californias. *Journal of Geophysical Research*, 106(B7):13,599–13,611, 2001.

Peter Lonsdale. Geology and tectonic history of the Gulf of California. In D. Hussong, E. L. Winterer, and R. W. Decker, editors, *The Eastern Pacific Ocean and Hawaii*, volume N of *The Geology of North America*, pages 499–522. Geological Society of America Boulder, Colo., 1989.

Gianreto Manatschal and Daniel Bernoulli. Architecture and tectonic evolution of nonvolcanic margins; Present-day Galicia and ancient Adria. *Tectonics*, 18(6): 1099–1119, 1999.

I. Manighetti, P. Tapponnier, P. Y. Gillot, E. Jacques, V. Courtillot, R. Armijo, J. C. Ruegg, and G. King. Propagation of rifting along the Arabia-Somalia plate boundary: Into Afar. *Journal of Geophysical Research*, 103(B3):4947–4974, 1998.

Yossi Mart and Olivier Dauteil. Analogue experiments of propagation of oblique rifts. *Tectonophysics*, 316:121–132, 2000.

Alexander R. McBirney. Factors governing the nature of submarine volcanism. *Bull. Volcanol.*, 26:455–469, 1963.

Tim R. McHargue, Tom L. Heidrick, and Jack E. Livingston. Tectonostratigraphic development of the Interior Sudan rifts, Central Africa. *Tectonophysics*, 213:187–202, 1992.

Peter Molnar. Continental tectonics in the aftermath of plate tectonics. *Nature*, 335 (8):131–137, 1988.

Elizabeth A. Nagy and Joann M. Stock. Structural controls on the continent-ocean transition in the northern Gulf of California. *Journal of Geophysical Research*, 105 (B7):16,251–16,269, 2000.

Gordon E. Ness, Mitchell W. Lyle, and Richard W. Couch. Marine Magnetic Anomalies and Oceanic Crustal Isochrons of the Gulf and Peninsular Province of the Californias. American Association of Petroleum Geologists Memoir 47, pages 47–69. 1991.

A. Nicolas. Novel type of crust produced during continental rifting. *Nature*, 315(9??): 112–115, 1985.

M. Oskin. *Tectonic Evolution of the Northern Gulf of California, Mexico, Deduced from Conjugate Rifted Margins of the Upper Delfín Basin*. Ph.D. Thesis, California Institute of Technology, Pasadena, California, 2002.

M. Oskin, J. Stock, and A. Martin-Barajas. Rapid localization of Pacific-North America plate motion in the Gulf of California. *Geology*, 29(5):459–462, 2001.

Sergio Paz-López. *Procesamiento e Interpretación de Datos Sísmicos y Gravimétricos en el Norte del Golfo de California*. Masters Thesis, CICESE, Ensenada, Baja California, Mexico, 2000.

Francisco A. Paz Moreno and Alain Demant. The Recent Isla San Luis volcanic center: petrology of a rift-related volcanic suite in northern Gulf of California, Mexico. *Journal of Volcanology and Geothermal Research*, 93:31–52, 1999.

Guillermo A. Pérez-Cruz. Exploración Petrolera de la Porción Noroccidental del Golfo de California. *Boletin de la Asociación Mexicana de Geofísicos de Exploración*, 21 (3-4):81–128, 1980.

Richard P. Phillips. Seismic Refraction Studies in Gulf of California. In T. van Andel and G. G. Shor, editors, *Marine Geology of the Gulf of California*, American Association of Petroleum Geologists Memoir 3, pages 90–125. 1964.

P. Richard and P. Cobbold. Experimental insights into partitioning of fault motions in continental convergent wrench zones. *Annales Tectonicae*, IV(2):35–44, 1990.

O. Sánchez-Zamora, P. Doguin, R. W. Couch, and G. E. Ness. Magnetic anomalies of the northern Gulf of California: structural and thermal interpretations. In J. P. Dauphin and B. R. T. Simoneit, editors, *The Gulf and Peninsular Provinces of the Californias*, American Association of Petroleum Geologists Memoir 47, pages 377–401. 1991.

A. D. Saunders, D. J. Fornari, and M. Ann Morrison. The composition and emplacement of basaltic magmas produced during the development of continental-margin basins: the Gulf of California, Mexico. *Journal of the Geological Society of London*, pages 335–346, 1982.

Michael G. Sawlan. Magmatic Evolution of the Gulf of California Rift. In J. P. Dauphin and B. R. T. Simoneit, editors, *American Association of Petroleum Ge-*

ologists Memoir 47, The Gulf and Peninsular Provinces of the Californias, pages 301–369. 1991.

Michael S. Steckler, Francois Berthelot, Nicholas Lyberis, and Xavier Le Pichon. Subsidence in the Gulf of Suez; implications for rifting and plate kinematics. *Tectonophysics*, 153(1-4):249–270, 1988.

J. M. Stock and K. V. Hodges. Pre-Pliocene extension around the Gulf of California and the transfer of Baja California to the Pacific plate. *Tectonics*, 8:99–115, 1989.

J. M. Stock and K. V. Hodges. Miocene to Recent structural development of an extensional accommodation zone, northeastern Baja California, Mexico. *Journal of Structural Geology*, 12(3):315–328, 1990.

Joann M. Stock. Relation of the Puertecitos Volcanic Province, Baja California, Mexico, to development of the plate boundary in the Gulf of California. In H. Delgado-Granados, G. Aguirre-Díaz, and J. M. Stock, editors, *Cenozoic Tectonics and Volcanism of Mexico*, Geological Society of America Special Paper 334, pages 143–156. 2000.

Brian Taylor, Andrew Goodliffe, Fernando Martinez, and Richard Hey. Continental rifting and initial sea-floor spreading in the Woodlark basin. *Nature*, 374(6):534–537, 1995.

Brian Taylor, Andrew M. Goodliffe, and Fernando Martinez. How continents break up: Insights from Papua New Guinea. *Journal of Geophysical Research*, 104(B4): 7497–7512, 1999.

Uri S. ten Brink, Rafael Katzman, and Jian Lin. Three-dimensional models of deformation near strike-slip faults. *Journal of Geophysical Research*, 101(B7):16205–16220, 1996.

Christain Teyssier, Basil Tikoff, and Michelle Markley. Oblique plate motion and continental tectonics. *Geology*, 23(5):447–450, 1995.

Wayne Thatcher and James N. Brune. Seismic Study of an Oceanic Ridge Earthquake Swarm in the Gulf of California. *Geophys. J. R. Astr. Soc.*, 22:473–489, 1971.

Tjeerd H. Van Andel. Recent marine sediments of Gulf of California. In T. van Andel and G. G. Shor, editors, *Marine Geology of the Gulf of California*, American Association of Petroleum Geologists Memoir 3, pages 216–310. 1964.

Martha O. Withjack and William R. Jamison. Deformation produced by oblique rifting. *Tectonophysics*, 126:99–124, 1986.

Nigel H. Woodcock and Mike Fischer. Strike-slip duplexes. *Journal of Structural Geology*, 8(7):725–735, 1986.

Chapter 2 Deformation of the Brittle Crust in Wide and Soft Plate Boundary Zones

Abstract

Observations in some settings of oblique divergence such as the Sea of Marmara and the Dead Sea Transform show localized deformation. In contrast, faulting is distributed over a broad area in young oblique rifts such as the northern Gulf of California and some marginal seas such as the Okinawa Trough and Andaman Sea. Mechanisms such as thickening or strengthening of the crust, viscous flow and local or regional isostasy have been used to understand whether deformation stays localized in one area or is broadly distributed. However, other studies have shown that whether deformation is partitioned or distributed could depend on the applied bottom boundary conditions. We explore the effects of bottom-driven mechanisms on the style of brittle deformation using 2D+1D numerical models. Distributed deformation is produced in models with distributed basal shear, but not in purely edge-driven models or models with block-like basal shear. In the latter models deformation is always localized on one fault or a few faults. We further show that flow beneath the brittle crust can produce large enough shear stresses to cause faulting if the brittle crust is weak or thin and that this deformation is distributed over multiple faults. We also study how the style of deformation varies with obliquity and demonstrate that the style of delocalized faulting observed in the N. Gulf of California is reproduced in models with an obliquity of 0.7 and distributed basal boundary conditions. Our results are new in that several different styles of deformation are produced by varying only the basal boundary conditions and obliquity.

2.1 Introduction

Rifts come in a wide variety of styles. It is thought, that after a period of diffuse extension of the continental crust, the transition to seafloor spreading begins and deformation becomes focused in the weakest part of the rift. For example, the main phase of extension in the Red Sea began simultaneously along its length at $\sim$ 22 Ma [Omar and Steckler, 1995] and after a period of diffuse stretching and intrusion of about 250% extension [Joffe and Garfunkel, 1987] seafloor spreading initiated at discrete spreading centers starting at 5 Ma [Roeser, 1970] . Rift onset was synchronous along the full length of the Woodlark basin, Papua New Guinea at $\sim$6 Ma, which now has both active continental rifting and well-developed seafloor spreading [Taylor et al., 1999]. There are, however, also regions where this simple relationship does not seem to hold. For example, rifting in the Gulf of California also began at $\sim$6 Ma [Oskin et al., 2001] along the full length of the rift, but unlike the Woodlark basin, no seafloor magnetic reversals have been identified in the Gulf of California except in the southernmost rift segment (Alarcon Rise) [Klitgord et al., 1974; Larson et al., 1972; Lawver et al., 1973]. Also the style of deformation during early rifting is not always diffuse, akin to the nature of deformation in continental crust, nor is the later stage of deformation always focused. For example, the 60-100 km wide Gulf of Suez has been extended by 25–27 km [Steckler, 1985], suggesting that the active rift zone was never more than 100 km wide. In contrast, current deformation occurs over multiple faults in a 70 $\times$ 200 km wide zone in the northern Gulf of California [Persaud et al., 2003], which has experienced $\sim$255 km upper crustal separation [Oskin et al., 2001].

For a basic understanding of what causes deformation to be distributed over a broad region, we use numerical models to explore the effect of shear in the lithosphere on the deformation of the brittle part of the plate. We define delocalized deformation to be active deformation occurring over a region that is at least as wide as the thickness of the lithosphere. Delocalized deformation results from the broad distribution of the forces that drive plate tectonics in space and/or time over a wide area. This has been at the core of most models of deformation, but has often not been explicitly stated. Because it is difficult to produce multiple faults by simply

pulling on the sides of a homogenous elastic-plastic layer, many workers have combined edge-driven boundary conditions from plate tectonics with varying properties of the lithosphere (Figure 2.1a) to produce multiple faults in the brittle crust. In this approach, deformation becomes distributed over time, as a previously extending region is strengthened and the locus of extension is transferred to an adjacent region. Tradeoffs between strain rate and cooling [England, 1983; Bassi, 1993], strain rate, cooling and rheology [Bassi, 1995], initial crustal thickness and thermal state [Buck, 1991; Hopper and Buck, 1996] and the localizing effect of lithospheric necking and delocalizing effect of local crustal isostasy [Buck et al., 1999] have been modeled to demonstrate that the lithosphere may strengthen or weaken locally depending on its rheology and thermomechanical state. The underlying concepts in these models are as follows: weakening of the lithosphere leads to spatially localized deformation and strengthening of the lithosphere promotes deformation that occurs in different spots over a certain time period, but deformation is never spatially delocalized. The time-progressive nature of these models gives insight into the shifting of deformation in time from one place to another, but does not explain the existence of plate boundaries such as the Gulf of California where multiple faults are active all at once in a broad zone of deformation.

Models in which a broad zone of active deformation has been produced are less common. Lavier et al. [2000] have shown that multiple faults form in a thick elastic-plastic, brittle layer ($>$ 22 km), with an initial cohesion of 44 MPa, although these were not multiple faults forming all at once, but rather subsequent faulting due to strengthening of the rift zone by bending. These results were for side-driven models in which the brittle layer floated on an inviscid substrate. For a viscoelastic, two-layer crust, Roy and Royden [2000a] demonstrated analytically that the width of the deformation zone in the crust increased with time in cases with a low-viscosity lower crust. Deformation was driven in the mantle with a step-function of 3.5 cm/yr relative strike-slip. These results were confirmed in more complex numerical models with more realistic crustal rheology and failure criteria and velocities applied to both the sides and bottom of the crust [Roy and Royden, 2000b]. The first faults form in the center of the model, above the velocity discontinuity. Subsequent faulting

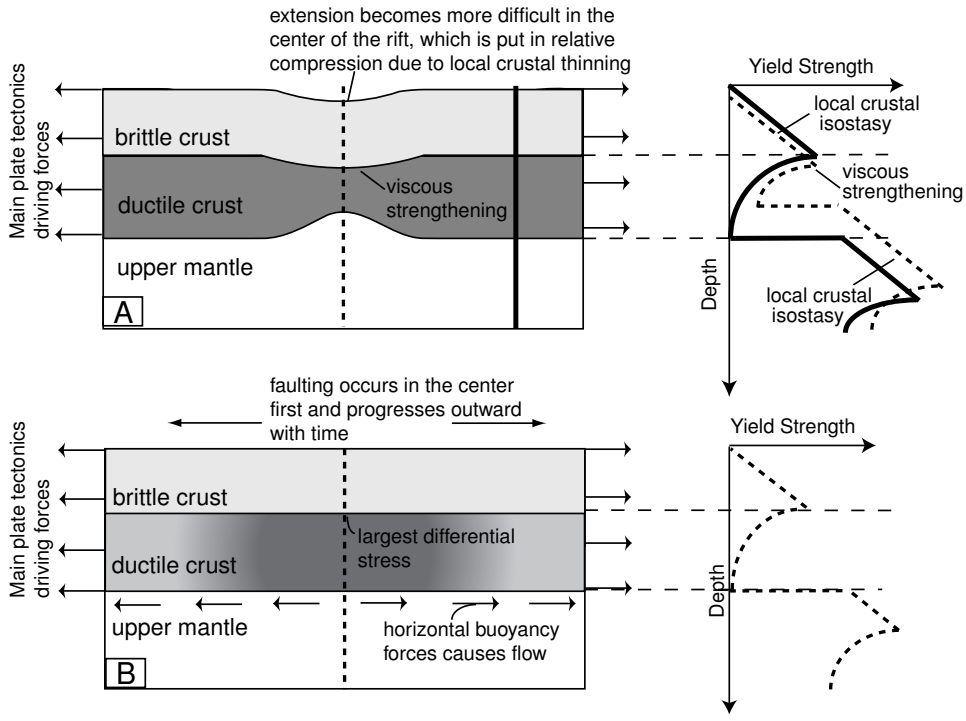

Figure 2.1: a) Edge-driven models of deformation [e.g., Buck et al., 1999] assume that mainly normal stresses at the edge of plates are important for driving deformation. Deformation is distributed into other areas as the deforming part of the rift (dashed line) is strengthened or put into relative compression. The corresponding strength profile is shown in the right panel by a dashed line. The relative decrease in strength outside the active rift zone (thick black line) is represented by the area under the thick black curve in the strength profile. b) Bottom-driven models of deformation [e.g., Roy and Royden, 2000a] assume that in addition to the edge forces, flow in the lower crust and mantle is significant for determining the style of deformation. Strengthening of the lithosphere and the redistribution of deformation to other areas as in model A is accompanied by flow beneath the brittle crust as a means of transmitting stresses to other areas. The multilayered structure of the lithosphere allows for attached or detached zones.

moves outward from the center as shear is maintained at the base of the crust. These models rely on the ductile properties of the lithosphere to distribute deformation. They thus emphasize the evolution of deformation in the soft part of the crust, which is manifested as faults in the brittle layer.

In a simple formulation of distributed deformation, Lamb [1994], building on the floating block model of McKenzie and Jackson [1986], demonstrated that ductile flow in the deep lithosphere could control the style of crustal deformation in wide and active continental plate boundary zones, if the average resistive shear stress on faults

in the brittle crust is much less than 100 MPa, and the underlying bulk effective viscosity is much greater than 10^{21} Pa s. Deformation in the crust in this model is thus dominated by the distributed stresses at the base of the brittle crust when the crust is weak. Although Lamb [1994] assumed that the faults already existed and therefore did not investigate the initiation of faults, his basic ideas set the stage for the work presented in this paper.

Recognizing that the distribution of shear stresses at the base of the brittle layer is a critical condition for distributed deformation, we first show that lower crustal flow can produce large enough, distributed shear stresses at the base of the crust to cause distributed faulting. In order to understand the effect of basal shear boundary conditions on the style of deformation in oblique extensional settings, we ran numerical experiments in which we varied only the obliquity and style of the basal boundary conditions. We show that faulting in an elastic-plastic layer is always distributed, if the basal velocities are distributed. The style of faulting produced in the models varies with the ratio of obliquity and realistically reproduces common geological structures. Finally we compare our model results to the style of active deformation in the northern Gulf of California.

2.2 Northern Gulf of California

The Gulf of California is a prime example of an obliquely-divergent plate boundary where the deformation may be basally driven. The fact that recognizable seafloor magnetic lineations are only present at the mouth of the Gulf, close to the East Pacific Rise [Lonsdale, 1989] supports an extended period lacking focused deformation typical of midocean-ridges. Additionally, no evidence for the formation of oceanic crust has been found in the northernmost one third of the Gulf, where the San Andreas transtensional fault system merges with the transpeninsular faults and the Gulf Extensional Province. Instead, the current plate boundary zone here is marked by a broad shallow pull-apart structure (Figure 2.2), ∼70 x 200 km, comprised of numerous oblique-normal faults and six ∼10-km wide segmented basins lacking well-defined transform faults [Persaud et al., 2003]. Active deformation is distributed

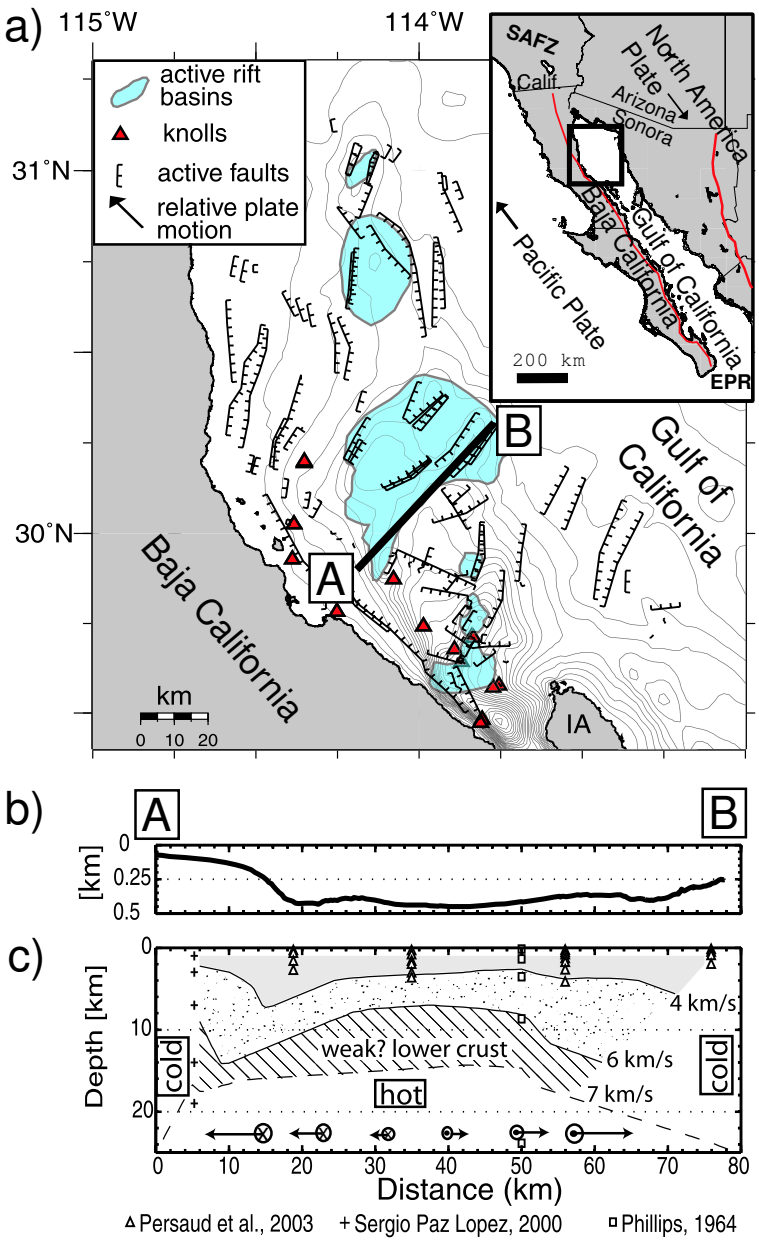

Figure 2.2: a) Map showing distributed faulting and multiple rift basins (light blue areas) in the N. Gulf of California after Persaud et al. [2003]. Black arrows show the Pacific-N. America relative plate motion [Atwater and Stock, 1998]. Red lines in the inset map show the eastern and western boundaries of the Gulf Extensional Province after Stock and Hodges [1989]. Solid black line marks the A-B cross-section represented below and in figure 2.7. b) Profile of shallow bathymetry along A-B. c) Cross section of crustal seismic velocities, showing the major crustal layers, with a possibly weak lower crust and deep strain gradient (black arrows).

across more than half of the northern Gulf's width, over many panels of small faults (up to 18 faults in 5 km) with average offsets of just a few meters [Persaud et al., 2003]. The broad *en echelon* extensional zones that form the rift basins and a recent plate boundary jump at 2 Ma [Stock, 2000; Lonsdale, 1989] indicate that diffuse rift zones, rather than narrow ridge segments, characterize extension in the northern Gulf [Persaud et al., 2003].

There is only indirect evidence that basal shear may be significant in the Gulf of California and on its margins. Evidence of the differential movement between crustal blocks has been used to infer that the Baja California peninsula is a microplate [DeMets, 1995], and hence that its coupling at the sides to either the North America or Pacific plates is incomplete. Differential motion between southern and northern Baja California has also been suggested based on the more westerly motion of the tip of the peninsula relative to locations in the northern Baja California [Dunn et al., 1996]. The spatial partitioning of deformation into three distinct fault systems across the southern Gulf and southwestern tip of the peninsula has been documented by Fletcher and Munguía [2000]. Additionally, distributed deformation in northeastern Baja California since 6 Ma has been documented by many workers [e.g., Dokka and Merriam, 1982; Stock and Hodges, 1990]. The role of basal shear can become significant in influencing the style of deformation, particularly in lithosphere that has been decoupled at the sides and transferred hundreds of kilometers. Two models for post 6 Ma block rotations in this region have been proposed: subhorizontal basal shear, and shear from bounding transform faults [Lewis and Stock, 1998a]. Some feel that the transform shear model is inconsistent with fault kinematics in this region and prefer ductile flow in the lower crust or basal shear [Dokka and Merriam, 1982]. We test this model here.

2.3 Models of Channel Drag

The following steps were taken to investigate whether flow in a lower crustal channel could produce large enough shear stresses at the base of the brittle crust to cause faulting:

1. We first perform a simple analysis of the drag generated by the flow in a crustal channel to investigate the magnitude of the resulting shear stresses at the base of the crust given that the viscosity of the channel should remain realistic.

2. We analytically determine the maximum frictional strength of the brittle crust in which faulting would occur if the shear stresses were as high as in 1.

3. To test whether faulting would occur in our models, we simulate in-and-out-of-the-plane flow over geologic time (Appendix A.2) by using velocity boundary conditions at the base of the lower crust to drive the flow.

To simplify the analysis of lower crustal flow, we use complete flow conditions that correspond to the steady-state one-dimensional channel flow of a Newtonian fluid with constant viscosity [Turcotte and Schubert, 1982; Kruse et al., 1991]. For a given channel thickness D, flow length, L, channel basal velocity v_0, crustal density ρ, crustal thinning Δh and time interval Δt, we first determine the channel viscosity, η for complete flow in a manner similar to Kruse et al. [1991]. We initially assume that the flow is a planar 1D Couette-Poiseuille flow, and can be driven by both the pressure gradient and the movement of the channel walls to demonstrate the effect of both. Kruse et al. [1991] limited themselves to just the effect of the average pressure gradient and approximated this as

$$\frac{dp}{dx} \approx \frac{-\rho g \Delta h}{L}, \tag{2.1}$$

with the flow rate needed in the lower crust in order for the flow to keep up with extension given by $\frac{\Delta h L}{4\Delta t}$. Note, $\frac{dp}{dx}$ is negative for flow in the positive x-direction. The flow rate has units of velocity $\times$ height, i.e., m^2/s.The viscosity is then given by

$$\eta \approx \frac{D^3(-\frac{dp}{dx})}{12(flowrate - \frac{v_0 D}{2})} \approx \frac{\rho g D^3 \Delta h \Delta t}{6L(\frac{\Delta h L}{2} - v_0 D \Delta t)}, \tag{2.2}$$

where g is the acceleration due to gravity. To use realistic conditions we choose the values shown in Table 2.1, and plot the resulting viscosity, η, as a function of channel thickness, D (dashed line Figure 2.4a). Note, we assume that the velocity of the channel wall is negligible; therefore $v_0 D \Delta t << \Delta h L$ and can be neglected when

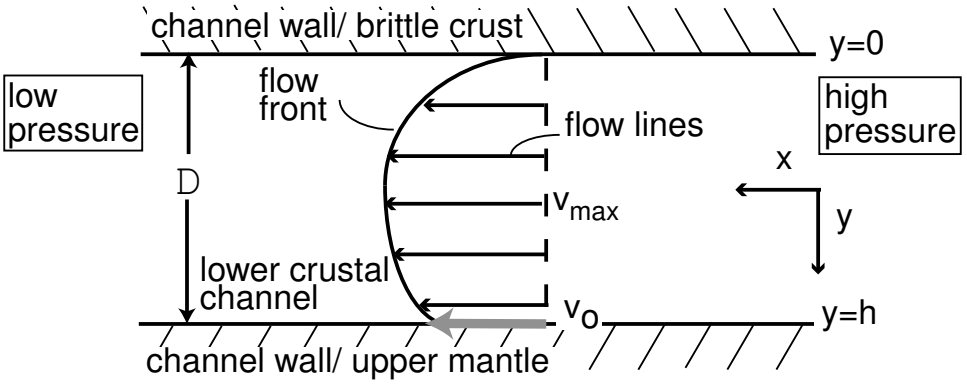

Figure 2.3: Schematic drawing of planar one-dimensional Couette-Poiseuille channel flow. The maximum velocity in the channel, v_{max}, is in the center of the channel when v_0 equals 0.

Table 2.1: Parameters for Channel Flow Approximation

Symbol	**Name**	**Value**
D	channel thickness	–
L	flow length	60 km
v_0	channel wall velocity	$\sim$0
ρ	crustal density	2600 $kg.m^{-3}$
Δh	crustal thinning	15 km
Δt	time for thinning	$2 \times 10^6 yr$
η	channel viscosity	–

determining the viscosity. However, if v_0 is on the order of mm/yr or larger, this term cannot be neglected, and Eq. 2.2 needs to be used in its full form.

In a 1D approximation, the shear stress, τ is given by

$$\tau = \frac{1}{2}\frac{dp}{dx}(2y - D) + \frac{\eta v_0}{D}. \tag{2.3}$$

The shear stress corresponding to complete flow is determined by substituting Eq. 2.1 into 2.3 and ignoring the last term in 2.3, since we assume that the flow is primarily driven by the pressure gradient and not by v_0. This gives

$$\tau \approx \frac{\rho g \Delta h D}{2L}. \tag{2.4}$$

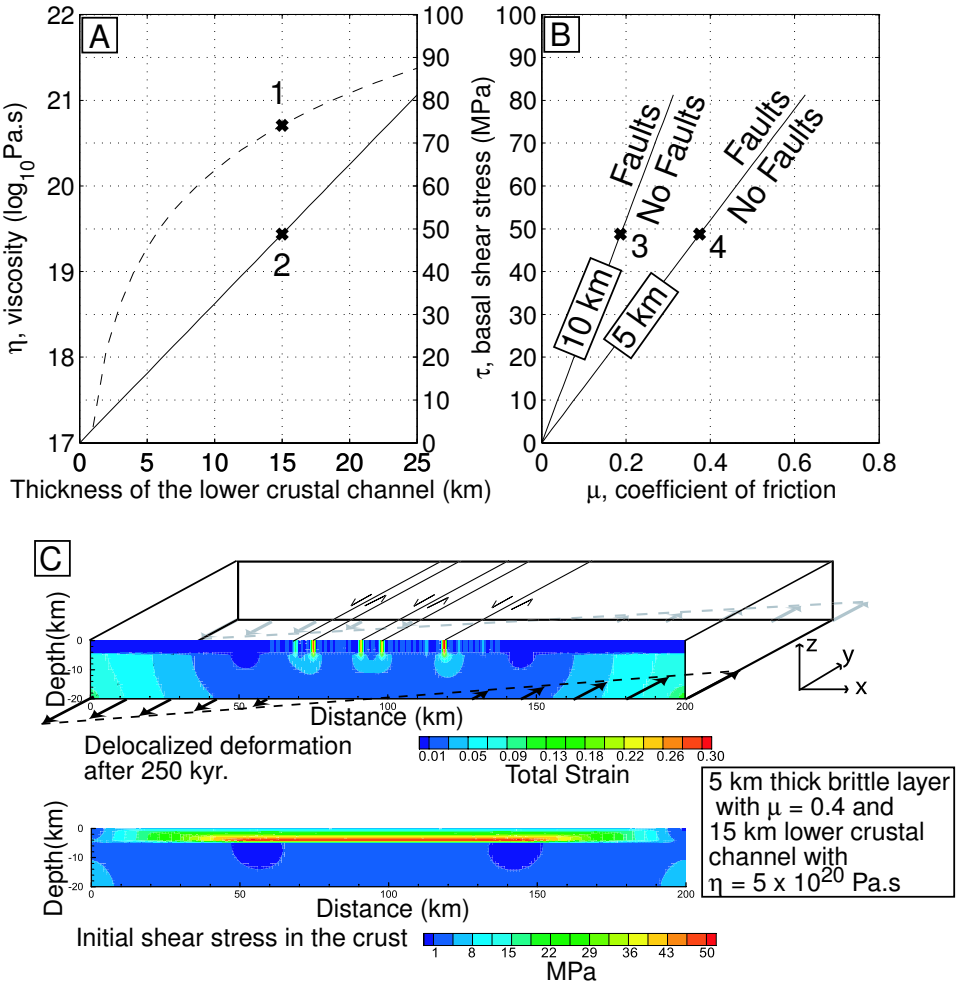

Figure 2.4: a) Viscosity (dashed line) and average shear stress (solid line) as a function of lower channel thickness using a simple channel flow approximation. 1 marks the value of viscosity determined for 15 km thick channel with a corresponding average shear stress marked by 2. b) Domains of fault formation. Faults will form if the basal shear stress is equal to or greater than the yield strength of the brittle layer, i.e., the coefficient of friction is smaller than the values on the line. Domains for a 10 and 5 km thick brittle layer are shown, with 3 and 4 marking the respective maximum coefficient of friction at which faults would form if the basal shear stress equals 50 MPa. c) Numerical models for a 5 km brittle layer.

at y=0, the base of the brittle layer. The corresponding values are reported in the same plot as the viscosity (solid line Figure 2.4a). The yield stress, σ_y at the base of the brittle layer can be estimated using

$$\sigma_y = \mu \rho g H, \tag{2.5}$$

where μ is the effective coefficient of friction and H the thickness of the brittle layer. To form a fault the shear stress, τ, must exceed the yield stress, σ_y. Setting (2.4) equal to (2.5), the maximum value of μ at which faults will form at a certain level of shear stress can be calculated. We plot μ as a function of τ for a 5 km thick and 10 km thick brittle layer and define the domain in which τ should be large enough to form faults in a brittle layer of a given frictional strength defined by μ (Figure 2.4b).

To determine whether such conditions would lead to distributed deformation in the case of distributed flow at the base of the brittle crust, we perform additional numerical experiments of the flow of an infinite viscous channel below an elastic-plastic layer in a plane perpendicular to the flow. We use a 2D+1D model formulation (Appendices A- C) to reproduce 'complete' flow in a channel driven at the base by linearly distributed velocity boundary conditions (Figure 2.4b). In the example shown in Figure 2.4, the deformation leads to the spontaneous formation of multiple localized strike-slip faults since the flow occurs in and out of the x-z plane. The conditions ($H = 5\ km$, $\mu = 0.4$, $\eta = 5 \times 10^{20} Pa.s$) are such that the average shear stress, τ, of 50 MPa (Figure 2.4b, initial shear stress) is larger than the yield stress at the base of the brittle crust. The resulting deformation leads to the formation of multiple faults distributed across the center of the box.

In summary, from Figure 2.4, one can see that for a reasonable range of geological parameters (5-10 km thick brittle layer, 15-20 km thick viscous channel and a channel viscosity of $0.5 - 5 \times 10^{20}$ Pa.s), the crust needs to be thin and fairly weak to very weak ($0 < \mu < 0.4$) to allow distributed faulting. Besides the magnitude and the distribution of the forces, other extrinsic factors can influence both the strength of the brittle layer and the style of deformation. For example, estimates of crustal and sedimentary rock frictional strength are on the order of $\mu = 0.6$ to 0.85 for dry rock [Byerlee, 1978], but fluid pore pressure and dike injection are known to decrease rock strength significantly [e.g., Brace and Kohlstedt, 1980]. Magmatism and the high sedimentation rate in the N. Gulf of California, ~3 m/1000yrs. [Van Andel, 1964] along with ~250 km of opening across the Gulf since ~6 Ma [Oskin et al., 2001] should lead to the formation of thick, fluid-rich igneous-sedimentary crust. In addition, the heat flow is high, $> 100\ mW/m^2$ [Lachenbruch et al., 1985]. Thinner than normal

continental crust and the likely high pore pressure conditions certainly gives support to the idea that the integrated strength of the crust is low. These observations are all consistent with a basally-driven mechanism for the distributed deformation in the N. Gulf.

2.4 Models of Oblique Extension

Deformation in transtensional settings is commonly partitioned into strike-slip and tensional components [e.g., Umhoefer and Dorsey, 1997]. Teyssier et al. [1995] suggested that the angle between the rift margin and the direction of relative plate motion, θ, controls the efficiency of partitioning, with the transition between partitioned and non-partitioned deformation occurring at $\theta = 20°$. These results were from strain models of transpression, which in terms of strain, is the numerical inverse of transtension; therefore, these models and also apply here. A slightly smaller angle for strain partitioning was determined by Burbidge and Braun [1998]. Considering strain partitioning as the kinematic response of a deformation system to the applied boundary conditions [Tikoff and Teyssier, 1994], we test these predictions by examining how the style of deformation varies with obliquity.

The brittle crust is modeled as a single 10 km thick, 100 km wide, frictional and cohesional elastic-plastic material (Appendix A) with quartz rheology. We use two types of basal boundary conditions as end members, step or linear functions of velocity (Figure 2.5). A step function of velocity represents one extreme form of basal shear, where shear is focused on a narrow fault zone and blocklike behavior is expected. A linear function of velocity is one representation of distributed shear, chosen for its simplicity. The basic model setup and weakening on the fault follows Lavier et al. [2000]. Appendix B outlines the manner in which velocities, forces and stresses are handled. Obliquity, r, is given as

$$r = \frac{v_y}{v_x + v_y}, \tag{2.6}$$

where $v_x = v_0 sin\theta$ is the extensional component of velocity and $v_y = v_0 cos\theta$ is the strike-slip component. r is 0 for purely extensional and 1 for purely strike-slip bound-

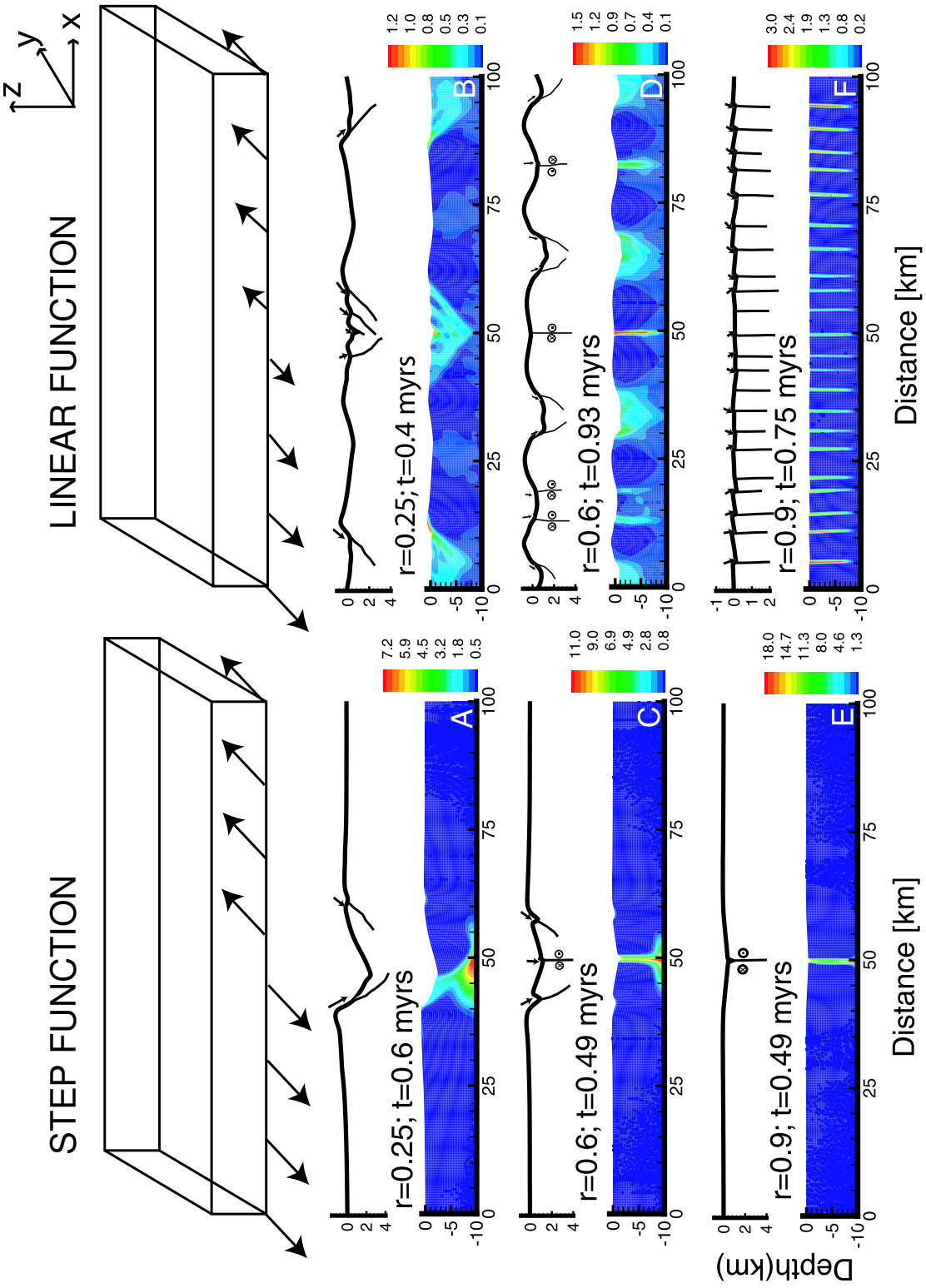

Figure 2.5: Models with step basal-boundary conditions (left panel) and linear basal-boundary conditions (right panel), with varying obliquity, r = 0.25, 0.6 and 0.9. The time for each model run, t, is indicated next to the obliquity. The total plastic strain ($\times$ 100%) is shown in all cases with hot colors representing zones of high strain. Velocity boundary conditions are schematically shown in the top panel.

ary conditions (see Figure 2.4c for axes). In all cases, a constant total plate velocity, $v_0 = 5\ cmyr^{-1}$, was applied to the sides of the models, which moved apart at different obliquities. The relationship between r and θ is

$$\frac{1-r}{r} = tan\ \theta. \tag{2.7}$$

The models in Figure 2.5 show a very wide range of structural styles, similar to that observed in rifts. In the case of a step-function like drag, by varying only the obliquity, we obtain localized rift structures ranging from half-graben (Figure 2.5a) to flower structures, (Figure 2.5c) to a single sag above a highly-oblique fault (Figure 2.5e). These environments are similar to areas such as the Dead Sea Rift [Rümpker et al., 2003] or the East African Rifts [Birt et al., 1997]. In all models with step functions of basal velocity, deformation is localized on a single or few faults in the middle of the layer above the velocity discontinuity at 50 km (Figure 2.5, left panel). Low-angle ($\sim 45°$ dip) oblique-normal faults form at low values of obliquity, r < 0.35 (Figure 2.5a), similar to the purely extensional cases of Lavier et al. [2000]. At higher obliquities, a single near-vertical fault forms in the center of the layer. This is accompanied by a set of conjugate normal faults if r < 0.9. Slight normal offset on the near-vertical faults is evident in the topographic profiles (Figure 2.5c and e) even when normal faults co-exist, indicating incomplete strain partitioning.

For the cases with linear basal velocity boundary conditions, the deformation comprises a series of widely spaced half-graben with multiple oblique faults for a low obliquity (Figure 2.5b), and a series of sag basins separated by strike-slip faults accumulating normal offset for an intermediate obliquity (Figure 2.5d). Finally, for high obliquity, deformation is distributed over many strike-slip faults, each accumulating a small amount of normal offset (Figure 2.5f). When, at high obliquity, deformation becomes partitioned between normal faults and strike-slip faults, the blocks stuck between strike-slip and normal faults show differential rotation, forming structures typical in transtensional settings (Figures 2.5 and 2.7). A fully 3-D model would be necessary to assess the validity of such model features. Any of these styles of deformation can be encountered in settings of oblique divergence, or even in a single

transtensional environment, e.g., the Gulf of California [Persaud et al., 2003].

In all experiments with linear basal velocity boundary conditions, deformation is distributed across the entire width of the model (Figure 2.5, right panel). In these cases, multiple basins and oblique-normal faults form at low obliquities, r = 0.25 (Figure 2.5b). Starting at r = 0.6 ($\theta = 34°$), intrabasinal zones of steeply-dipping faults develop, and strain is incompletely partitioned. We expect this from theory [Tikoff and Teyssier, 1994], but what we also see is a transition from shallower to steeper dips, with increasing obliquity and a closer spacing between faults as the strike-slip component increases. This was also noted in analog experiments on oblique convergence with solely basal boundary conditions [Burbidge and Braun, 1998].

To understand what determines the style of faulting in our models, we first analyze the stress system under which incipient faulting occurs, then the spatial and temporal evolution of that stress system (extension is treated as negative). For oblique-slip faulting to occur in intact rock, at most one of the three principal stress axes can lie in the xz reference coordinate frame (model plane) [Williams, 1958]. The relationship between the angle, α between the x-axis and the largest horizontal principal stress and r is given by [Burbidge and Braun, 1998].

$$\frac{1-r}{r} = \frac{\partial w_x}{\partial w_y} = \frac{1}{tan\ 2\alpha}, \tag{2.8}$$

where w_x and w_y are the displacements in the x and y directions respectively (Figure 2.6). Substituting (2.7) into (2.8) gives $tan\ \theta = (tan\ 2\alpha)^{-1}$. This is only true for the initial faults formed and assumes that one principal stress axis is vertical and the other two are horizontal. One principal stress, σ_2, thus makes an angle α with the x-axis and the other σ_3 trends at α to the y-axis. As the obliquity, r increases, θ decreases and α increases. The horizontal principal stress axes thus become less aligned with the xz plane with increasing obliquity. If faults form, the plunge of the slip vectors which are defined with respect to the principal stress axes, are steeper in the xz reference frame. The faults have a constant strike in and out of the model plane and the true dips are defined in the xz plane. As faulting progresses, Eq. **??** and the derived relationship between α and θ are no longer valid, since the state

of stress in the models is modified by 1) the spacing between the faults and the number of faults formed, 2) the amount and sense of offset on neighboring faults, 3) the thickness of the blocks, and 4) the reduction of cohesion with strain (A.2). This causes α to progressively change, whereas θ remains constant. Fault block rotations depend on all of the above and this in turn affects the geometry of faults over time (B.3), particularly in models with multiple faults and large dip variations (Figure 2.5d).

In these models, the number of faults formed during the initial and long-term evolution of the model is highly dependent on how much normal offset a given fault can accumulate before the state of stress along that fault becomes unfavorable for continued slip and a new fault forms. This depends on the dip of the fault [Forsyth, 1992] and the amount and rate of strength loss on the fault [e.g., Lavier et al., 2000]. In the models presented here, the amount and rate of weakening on the faults increase as the offset on the fault increases (A.2). The relationship is such that, the larger the offset a fault accumulates, the weaker it becomes, and the likelihood of forming another fault decreases. Forsyth [1992] showed that a fault with a low dip has a more favorable stress state for continued slip than a fault with high dip.

As shown before, the fault dip in our model is controlled by the obliquity. At high obliquity, we obtain steep dips, whereas at low obliquity, faults form with low dips. Therefore a simple way of explaining the fact that many more faults form in the highly oblique distributed case is that a given fault cannot accumulate much slip before another fault forms (Figure 2.5f). On the other hand, at low obliquity, faults with shallower dips form and they can accumulate larger offsets before other faults form (Figure 2.5b). In the long-term evolution of the models, this results in a lower fault density across the box.

2.5 Why Are Transform Faults Missing in the N. Gulf?

Using the obliquity of the Gulf of California, with a 10 km thick crust and linear basal-boundary conditions, we were able to match the style of faulting observed. Because of the smooth transition in fault dips towards the center of the rift basins (Figure 2.7),

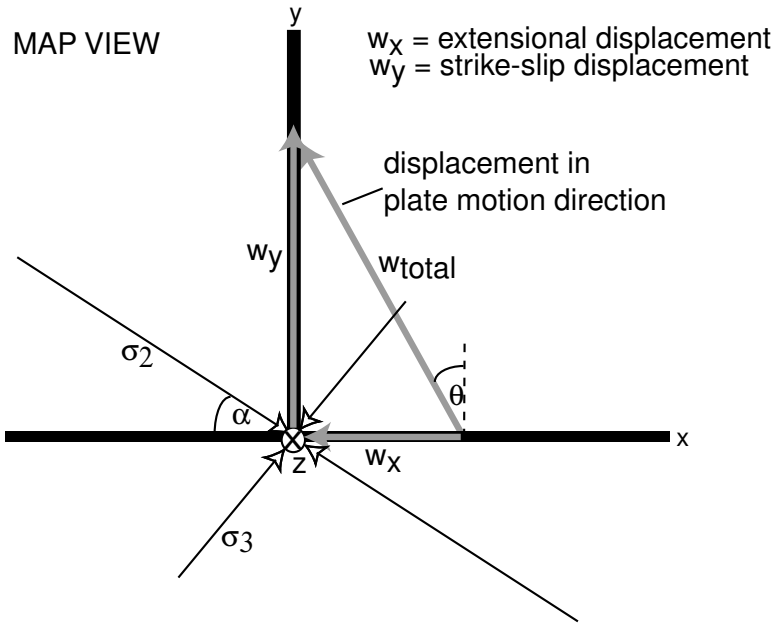

Figure 2.6: Map view schematic diagram showing the orientation of the principal stresses, $\sigma_{2,3}$ with respect to the model space (xz plane, in-and-out of the paper) during oblique-slip faulting. θ = angle between the the rift margin and the plate motion vector; α = angle between the largest horizontal principal stress and the x-axis.

single through-going transform faults are not needed to connect the major rift basins; rather, a zone of oblique-slip faults accommodates both the lateral and vertical offset. Hence, the rift basins are shallow and diffuse structures. The rift basins may indeed be partial flower structures, which commonly have concave upward fault planes in cross-section. These structures are not reproducible in our models based on the use of the Mohr-Coulomb failure criterion. With the failure criterion we used, the orientation of the Riedel shears (conjugate faults) does not depend on the overburden pressure; there is, therefore, no rotation of the fault plane with increasing depth [Braun, 1994].

The dips of faults in the N. Gulf lie between 60 and 75°, similar to the model. The rift basins in the model are variable in size, have multiple bounding faults and are unevenly spaced, similar to structures across the pull-apart structure in the N. Gulf [Persaud et al., 2003]. The fault offsets, however, do not match (model max. = 1 km; data max. = a few 100 m) due to the high sedimentation rate in the Gulf of California, which is not included in the model. Along the strike of the pull-apart structure, multiple basins can be explained by using the model with r=0.25 and

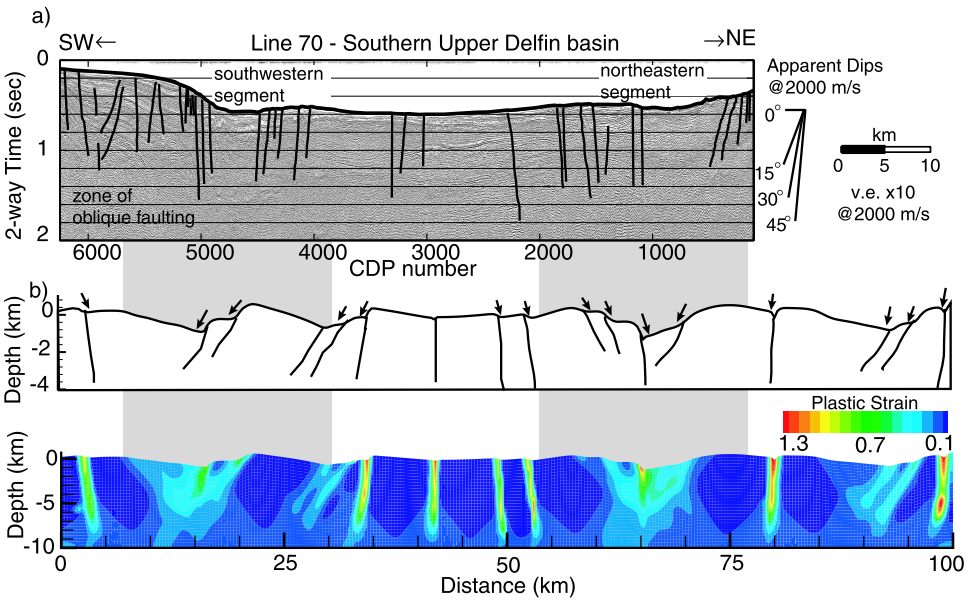

Figure 2.7: Comparison between a) a representative seismic profile across the N. Gulf and b) model with linear basal-boundary conditions. This model was run 800,000 yrs. with r = 0.7 ($\theta = 23°$), the obliquity determined for the Gulf [Umhoefer and Stone, 1996]. Note the tilted fault blocks and multiple rift basins (gray zones) with varying fault dips present in both model and data.

linear-basal boundary conditions (Figure 2.5b). In this model, multiple ∼10 km wide basins separated by ∼25 km are produced. This is similar to the observations shown in Figure 2.2.

2.6 Discussion and Conclusions

Our numerical models show that for a fixed crustal composition and thickness, the style of brittle deformation in a soft plate boundary zone depends on the driving mechanism. In this study, we make no assumptions about the lower crustal strength or tradeoffs between crustal buoyancy and lithospheric necking effects, since no clear pattern based on these properties has been established for obliquely-extending regions. We instead use distributed velocity boundary conditions as an analog for flow in a lower crustal channel. We first estimate bounds on the viscosity of the material in the channel based on complete flow conditions [Kruse et al., 1991], then show that the resulting basal shear is enough to break weak or thin crust. In this case, deformation occurs over multiple faults and the flow essentially drives the deformation. Lower

crustal flow is only likely to occur where the crustal thickness exceeds 20 or 25 km [McKenzie et al., 2000]. Estimates of the present crustal thickness in the N. Gulf range from 13 km [Couch et al., 1991] to 20-25 km [Phillips, 1964] (Figure 2.2). It is therefore unlikely that lower crustal flow is currently driving the distributed deformation observed in the N. Gulf although it may have done so in the past.

Here, we discuss alternative mechanisms for driving basal drag. Although mantle drag is presumably small and hence thought to be insignificant for driving the plates and furthermore for breaking the plates, there is no doubt that some drag must exist [Forsyth and Uyeda, 1975; Bokelmann and Silver, 2002; Teyssier et al., 2002]. Estimates of sublithospheric drag are limited by the thermal stability of the mantle and are strongly dependent on estimates of viscosity and the thickness of the subcrustal layer within which flow occurs. These stresses may range from almost null to on average a few MPa in magnitude [Melosh, 1977; Bokelmann and Silver, 2002] and do not definitively resolve the question of whether or not continental splitting is controlled by drag on the base of lithospheric plates. The first alternative for producing larger than normal shear stresses at the base of the crust is based on a hypothesis by Hey [1998] for the opening the Gulf by basally driven shear. This involves the transfer of lithosphere from the Farallon plate to the Pacific plate and subsequent subduction of that lithosphere. Hey [1998] proposed that the resulting shear stresses produced by drag of the subducted lithosphere beneath the North America plate are enough to break the plate if i) the mantle is relatively strong, ii) a few thousand km^2 of the lithosphere is subducted and iii) the thickness of the mantle shear zone is on the order of a few hundred meters [Hey, 1998]. We disagree with the details of these estimates since they involve enormous shear stresses, but adopt the idea of deep shear resulting from the differential movement between partly attached or transferred layers.

A second and simpler mechanism may explain the current style of deformation in the N. Gulf. Presently, the edges of the Gulf of California are cold and the center is hot. With a weak center and strong edges, there could easily be a deep strain gradient between the axis and the western and eastern edges, which follow the Pacific and N. America plates respectively (Figure 2.2). The weak underlying sediments might easily detach and exhibit deformation patterns that reflect that deep strain.

The deep strain pattern may or may not be ductile, since the lower crust is likely new basalt, diabase or gabbro, which, when dry, could have above average strength even at high temperatures. A strong contrast in ductility from axis to edge is however, certain.

Additional mechanisms that rely more heavily on rift architecture are edge-driven convection in the mantle beneath rifts, which could result in sublithospheric mantle flow velocities of up to 3 cm/yr [King and Anderson, 1998], and along-strike flow, e.g., that occurring from the Red Sea to the Gulf of Suez [Steckler et al., 1998]. There is no doubt that basal shear stress can be large and in some cases it is large enough to facilitate the subduction of chunks of continent; e.g., basal shear from the Pacific plate in a 300 km wide zone under the Bird's Head region of eastern Indonesia is driving it under the Australian Plate [Stevens et al., 2002]. Efforts to quantify the influence of basal forces on deformation using geodetic measurements have thus far proved inconclusive [Jackson and Molnar, 1990; Bourne et al., 1998b,a] and have been complicated by arguments on the strength of the mantle versus the strength of the lower crust [Lamb, 2002] and which one drives versus which one follows [Tikoff et al., 2002]. We believe the deformation record gives insight into the regional distribution of the forces rather than their magnitudes, which assumes some global average. The edge-driven model approach popular in studies of plate driving mechanisms only works for deforming strictly rigid plates along single large offset faults. Oceanization of soft and broad plate boundaries such as the Gulf of California, or opening of marginal seas such as the Okinawa Trough, requires the modeling of non-zero bottom boundary conditions and geophysical investigations of the deep crust and upper mantle for a better understanding.

Appendix A Rheology

A.1 Brittle Rheology

Our model uses an approach similar to *FLAC*, an explicit finite difference program that performs a Lagrangian analysis of continua [Lavier et al., 2000]. We assume that the yield stress of a brittle material is given by a linear Mohr envelope or Coulomb failure criterion. When that criterion is met, flow follows a rule for non-associated plasticity [e.g., Poliakov and Buck, 1998]. This formulation allows localization of plastic deformation in shear zones or faults. The shear stress at yield, τ, is given by Coulomb theory:

$$\tau = \mu\sigma_n + C(\varepsilon_{ps}), \tag{A.1}$$

where μ is the coefficient of friction, σ_n is the normal stress, and C is the cohesion, which depends on the total plastic strain, ε_{ps} . The plastic strain is the non-recoverable strain accumulated when the stress in the layer is locally greater than the yield stress. The cohesion is reduced with increasing strain after yielding. Up to the point where the material loses all cohesion, the reduction of cohesion with strain is linear,

$$C(\varepsilon_{ps}) = C(0)(1 - \frac{\varepsilon_{ps}}{\varepsilon_c}), \tag{A.2}$$

where $C(0)$ is the initial cohesion of the layer, corresponding to $C(0)$=44 MPa in these models, after Lavier et al. [2000]. We define ε_c as a characteristic value of the plastic strain. When the plastic strain reaches ε_c the fault is cohesionless. However, as seen in all models allowing for the localization of deformation [e.g., Cundall, 1989], the width of the fault, Δw, is consistently about three times the grid size. Thus, for a given fault displacement the strain is dependent on the grid size. In order to scale the characteristic strain and the rate of cohesion weakening between two models with different grid sizes, we use characteristic offset, $\Delta x_c = \varepsilon_c \Delta w$ rather than ε_c as a measure of the amount of deformation needed to form a cohesionless fault [Lavier

et al., 2000].

A.2 Visco-elasticity

To model the viscous part of the lithosphere, we used the Maxwell viscoelastic constitutive equations relating the deviatoric stresses, σ_{ii} to the deviatoric strains, ε_{ii}:

$$\frac{\partial \sigma_{ii}}{\partial t} = E\frac{\partial \varepsilon_{ii}}{\partial t} - \frac{\sigma_{ii}}{\tau_M}, \tag{A.3}$$

where E is the Young's modulus and τ_M is the Maxwell time defined as $\tau_M = 2\eta/E$ with η being the effective viscosity. The subscript i corresponds to the component on x, y or z of the stress and strain tensors. In our lithospheric model in which deformation is driven from the bottom, the viscosity is kept constant to satisfy the full channel flow conditions defined analytically by Kruse et al. [1991].

Appendix B Mechanical Equilibrium

For each numerical time step, the modeling involves direct solution of the equation of motion for every grid point including the effects of inertia [Cundall, 1989](Figure B.1):

$$\rho \frac{\partial v_i}{\partial t} - \frac{\partial \sigma_{ij}}{\partial x_j} - \rho g_i = 0, \tag{B.1}$$

where v_i is the velocity at each grid point, g_i is the acceleration due to gravity, ρ is the mass density and σ_{ij} is the stress in each grid element. We model strike-slip deformation in and out of the plane f_y by calculating the strain resulting from the shear stresses applied in and out of the plane as [Roy and Royden, 2000a]:

$$f_y = \frac{\partial \sigma_{yz}}{\partial z} + \frac{\partial \sigma_{yx}}{\partial x}. \tag{B.2}$$

In order to approximate quasi-static processes, the effects of inertia must be damped in a way akin to oscillations in a damped oscillator. Starting from a non-equilibrium state, the forces present at each grid point are summed ($f_i = \rho \delta v_i / \delta t$). The corresponding out-of-balance forces and the mass at the grid point give rise to

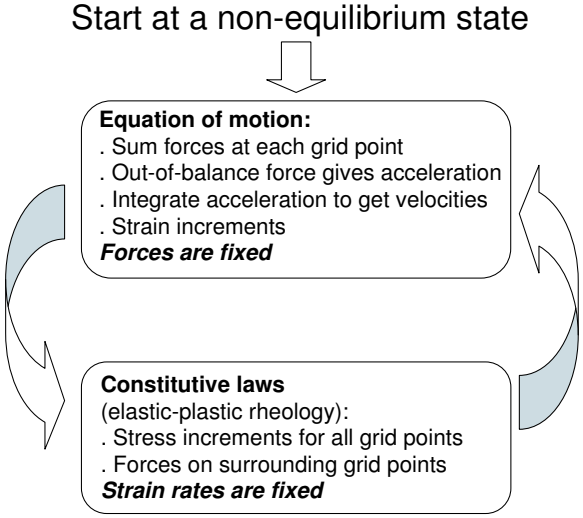

Figure B.1: Flow diagram outlining the major steps in the numerical model approach. Modified from Cundall.

acceleration. The accelerations are integrated to calculate the new velocities which are used to determine the incremental strain, ε_{ij} at each grid point. During a single time step, finite rotations also change the stress tensor, which is defined with respect to a fixed frame of reference. Before the incremental strains are determined, the stress tensor is updated to take these rotations into consideration as follows.

$$\sigma_{ij(new)} = \sigma_{ij(old)} + (\omega_{ik}\sigma_{kj} - \sigma_{ik}\omega_{kj})\Delta t, \tag{B.3}$$

where Δt is the time step and ω_{ij}, the rotation per unit time, is given in terms of the velocity derivatives by

$$\omega_{ij} = \frac{1}{2}\left(\frac{\partial v_i}{\partial x_j} - \frac{\partial v_j}{\partial x_i}.\right) \tag{B.4}$$

By using the constitutive law for elastic, viscous and plastic rheologies described in **A1**, the corresponding stress increments are determined from the strain increments, and the forces that they produce on the surrounding grid points are summed to determine the new out-of-balance forces and velocities. This dynamic response is then damped to approach a quasi-static equilibrium.

FLAC is a very powerful technique for simulating non-linear rheological behavior at very high resolution because the explicit time-marching scheme does not require the storage of the large matrices that are needed for implicit methods. The time step of the calculation scales with the elastic-plastic property of our model. If the problem is purely elastic, the time step of the dynamic response scales with the velocity of the elastic wave propagating through the elements. This time step is of the order of a few hundredths of a second. Therefore, the resolution of the domains studied and the timescale needed for our numerical experiments would yield very long run times. In order to decrease the CPU time needed to perform the numerical experiments, we increase the speed of calculation by setting the boundary displacement per time step to a fraction of the grid spacing. To set the boundary displacement, we choose a ratio of boundary velocity to sound velocity of $10^{-6} - 10^{-5}$. We find that this ratio allows for fast enough runs and at the same time minimizes the error in the strain calculation.

Appendix C Re-meshing

The initial mesh of the model is made of quadrilaterals subdivided into two pairs of superimposed constant-strain triangular zones. The use of triangular zones eliminates the problem of "hourglassing" deformation sometimes experienced in finite differences [Cundall, 1989]. Since this method is Lagrangian (i.e., the numerical grid follows the deformations), the simulation of large deformations (locally more than 50%) involves re-meshing to overcome the problem of degradation of numerical precision when elements are distorted. We trigger re-meshing when one of the triangles in the grid elements is distorted enough that one of its angles becomes smaller than a given value. Every time re-meshing occurs, strains at each grid point are interpolated between the old deformed mesh and the new undeformed mesh using the barycentric coordinates of the nodes and Gauss points of the new elements in the old deformed mesh. The new state of strain is then used with the rheological laws to calculate the stress and resulting out-of-balance forces to start the time step cycle again. Also every time we re-mesh, errors in the interpolation of the state variables result in an increase in the out-of-balance force, and artificial accelerations and oscillations may occur. For this reason the solution may not be in equilibrium immediately after re-meshing. We have tested different criteria to trigger re-meshing in order to reduce the oscillations and chose to use a minimum angle before re-meshing of 15°.

References

Tanya Atwater and Joann Stock. Pacific-North America Plate Tectonics of the Neogene Southwestern United States: An Update. *International Geology Review*, 40: 375–402, 1998.

G. Bassi. Contrasting styles of rifting: models and examples from the eastern Canadian margins. *Tectonics*, 12(3):639–655, 1993.

G. Bassi. Relative importance of strain-rate and rheology for the mode of continental extension. *Geophysical Journal International*, 122:195–210, 1995.

C. S. Birt, P. K. H. Maguire, M. A. Khan, H. Thybo, G. R. Keller, and J. Patel. The influence of pre-existing structures on the evolution of the southern Kenya Rift Valley - evidence from seismic and gravity studeies. *Tectonophysics*, 278:211–242, 1997.

Götz Bokelmann and Paul G. Silver. Shear stress at the base of the shield lithosphere. *Geophysical Research Letters*, 29(23):2091, doi:10.1029/2002GL015925, 2002.

S. J. Bourne, T. Arnadottir, J. Beavan, D. J. Darby, P. C. England, B. Parsons, R. I. Walcott, and P. R. Wood. Crustal deformation of the Marlborough fault zone in the South Island of New Zealand: Geodetic constraints over the interval 1982-1994. *Journal of Geophysical Research*, 103(B12):30147–30165, 1998a.

S. J. Bourne, P. C. England, and B. Parsons. The motion of crustal blocks driven by flow of the lower lithosphere and implications for slip rates of continental strike-slip faults. *Nature*, 391(12):655–659, 1998b.

W. F. Brace and D. L. Kohlstedt. Limits on Lithospheric Stress Imposed by Laboratory Experiments. *Journal of Geophysical Research*, 85(B11):6248–6252, 1980.

Jean Braun. Three-dimensional numerical simulations of crustal-scale wrenching using a non-linear failure criterion. *Journal of Structural Geology*, 16(8):1173–1186, 1994.

W. R. Buck. Modes of continental lithospheric extension. *Journal of Geophysical Research*, 96:20,161–20,178, 1991.

W. R. Buck, Luc L. Lavier, and Alexei N. B. Poliakov. How to make a rift wide. *Philosophical Transactions of the Royal Society of London A*, 357:671–693, 1999.

David R. Burbidge and Jean Braun. Analogue models of obliquely convergent continental plate boundaries. *Journal of Geophysical Research*, 103(B7):15221–15237, 1998.

J. Byerlee. Friction of Rocks. *Pure and Applied Geophysics*, 116:615–626, 1978.

Richard W. Couch, Gordon E. Ness, Osvaldo Sanchez-Zamora, Gustavo Calderón-Riveroll, Pierre Doguin, Thomas Plawman, Shane Coperude, Bruce Huehn, and William Gumma. Gravity Anomalies and Crustal Structure of the Gulf and Peninsular Province of the Californias. In J. P. Dauphin and B. R. T. Simoneit, editors, *American Association of Petroleum Geologists Memoir 47*, The Gulf and Peninsular Provinces of the Californias, pages 25–45. 1991.

P. A. Cundall. Numerical experiments on localization in frictional materials. *Ing. Arch.*, 58:148–159, 1989.

C. DeMets. A reappraisal of seafloor spreading lineations in the Gulf of California: Implications for the transfer of Baja California to the Pacific plate and estimates of Pacific-North America plate motion. *Geophysical Research Letters*, 22:3545–3548, 1995.

Roy K. Dokka and Richard H. Merriam. Late Cenozoic extension of northeastern Baja California, Mexico. *Geological Society of America Bulletin*, 93:371–378, 1982.

P. J. Dunn, J. W. Robbins, J. M. Bosworth, and R. Kolenkiewicz. Crustal deformation around the Gulf of California. *Geophysical Research Letters*, 23(2):193–196, 1996.

Philip England. Constraints on Extension of Continental Lithosphere. *Journal of Geophysical Research*, 88(B2):1145–1152, 1983.

John M. Fletcher and Luis Munguía. Active continental rifting in southern Baja California, Mexico: Implications for plate motion partitioning and the transition to seafloor spreading in the Gulf of California. *Tectonics*, 19(6):1107–1123, 2000.

Donald Forsyth and Seiya Uyeda. On the Relative Importance of the Driving Forces of Plate Motion. *Geophysical Journal of the Royal Astronomical Society*, 43:163–200, 1975.

Donald W. Forsyth. Finite extension and low–angle normal faulting. *Geology*, 20: 27–30, 1992.

Richard N. Hey. Speculative propagating rift-subduction zone interactions with possible consequences for continental margin evolution. *Geology*, 26(3):247–250, 1998.

John R. Hopper and W. Roger Buck. The effects of lower crustal flow on continental extension and passive margin formation. *Journal of Geophysical Research*, 101(B9): 20175–20194, 1996.

James Jackson and Peter Molnar. Active Faulting and Block Rotations in the Western Transverse Ranges, California. *Journal of Geophysical Research*, 95(B13):22,073–22,087, 1990.

Sam Joffe and Zvi Garfunkel. Plate kinematics of the circum Red Sea - a re-evaluation. *Tectonophysics*, 141:5–22, 1987.

Scott D. King and Don L. Anderson. Edge-driven convection. *Earth and Planetary Science Letters*, 160:289–296, 1998.

Kim D. Klitgord, John D. Mudie, James L. Bischoff, and Tom L. Henyey. Magnetic anomalies in the Northern and Central Gulf of California. *Geological Society of America Bulletin*, 85:815–820, 1974.

Sarah Kruse, Marcia McNutt, Jason Phipps-Morgan, and Leigh Royden. Lithospheric Extension Near Lake Mead, Nevada: A Model for Ductile Flow in the Lower Crust. *Journal of Geophysical Research*, 96(B3):4435–4456, 1991.

Arthur H. Lachenbruch, J. H. Sass, and Jr. S. P. Galanis. Heat Flow in Southernmost California and the Origin of the Salton Trough. *Journal of Geophysical Research*, 90(B8):6709–6736, 1985.

Simon Lamb. Is it all in the crust? *Nature*, 420:130–131, 2002.

Simon H. Lamb. Behavior of the brittle crust in wide plate boundary zones. *Journal of Geophysical Research*, 99(B3):4457–4483, 1994.

Peggy A. Larson, John D. Mudie, and Roger L. Larson. Magnetic Anomalies and Fracture-Zone Trends in the Gulf of California. *Geological Society of America Bulletin*, 83:3361–3368, 1972.

Luc L. Lavier, W. Roger Buck, and Alexei N. B. Poliakov. Factors controlling normal fault offset in an ideal brittle layer. *Journal of Geophysical Research*, 105(B10): 23431–23442, 2000.

Lawrence A. Lawver, John G. Sclater, Thomas L. Henyey, and J. Rogers. Heat flow measurements in the southern portion of the Gulf of California. *Earth and Planetary Science Letters*, 12:198–208, 1973.

Claudia J. Lewis and Joann M. Stock. Paleomagnetic evidence of localized rotations during Neogene extension in the Sierra San Fermin, northeastern Baja California, Mexico. *Journal of Geophysical Research*, 103(B2):2455–2470, 1998a.

Peter Lonsdale. Geology and tectonic history of the Gulf of California. In D. Hussong, E. L. Winterer, and R. W. Decker, editors, *The Eastern Pacific Ocean and Hawaii*, volume N of *The Geology of North America*, pages 499–522. Geological Society of America Boulder, Colo., 1989.

D. McKenzie and J. Jackson. A block model of distributed deformation by faulting. *Journal of the Geological Society of London*, 143:349–353, 1986.

Dan McKenzie, Francis Nimmo, James A. Jackson, P. B. Gans, and E. L. Miller. Characteristics and consequences of flow in the lower crust. *Journal of Geophysical Research*, 105(B5):11029–11046, 2000.

Jay Melosh. Shear Stress on the Base of the Lithospheric Plate. *Pure and Applied Geophysics*, 115(1-2):429–439, 1977.

Gomaa I. Omar and Michael S. Steckler. Fission Track Evidence on the Initial Rifting of the Red Sea: Two Pulses, No Propagation. *Science*, 270(24):1341–1344, 1995.

M. Oskin, J. Stock, and A. Martin-Barajas. Rapid localization of Pacific-North America plate motion in the Gulf of California. *Geology*, 29(5):459–462, 2001.

P. Persaud, J. M. Stock, M. S. Steckler, A. Martin-Barajas, J. B. Diebold, A. Gonzalez-Fernandez, and G. S. Mountain. Active deformation and shallow structure of the Wagner, Consag and Delfín Basins, Northern Gulf of California, Mexico. *Journal of Geophysical Research*, 108(B7):2355, doi:10.1029/2002JB001937, 2003.

Richard P. Phillips. Seismic Refraction Studies in Gulf of California. In T. van Andel and G. G. Shor, editors, *Marine Geology of the Gulf of California*, American Association of Petroleum Geologists Memoir 3, pages 90–125. 1964.

A. N. B. Poliakov and W. Roger Buck. Faulting in mid-ocean ridges; formation of abyssal hills. *Annales Geophysicae*, 16(1):33pp, 1998.

Roeser. A Detailed Magnetic Survey of the Southern Red Sea. *Geologisches Jahrbuch*, D13:131–153, 1970.

Mousumi Roy and Leigh H. Royden. Crustal rheology and faulting at strike-slip plate boundaries 1. An analytic model. *Journal of Geophysical Research*, 105(B3): 5583–5597, 2000a.

Mousumi Roy and Leigh H. Royden. Crustal rheology and faulting at strike-slip plate boundaries 2. Effects of lower crustal flow. *Journal of Geophysical Research*, 105 (B3):5599–5613, 2000b.

Georg Rümpker, Trond Ryberg, Günter Bock, and Desert Seismology Group. Boundary–layer mantle flow under the Dead Sea transform fault inferred from seismic anisotropy. *Nature*, 425:497–501, 2003.

Michael S. Steckler. Uplift and extension at the Gulf if Suez: indications of induced mantle convection. *Nature*, 317:135–139, 1985.

Michael S. Steckler, Shimon Feinstein, Barry P. Kohn, and Luc L. Lavier. Pattern of mantle thinning from subsidence and heat flow measurements in the Gulf of Suez: Evidence for the rotation of Sinai and along-strike flow from the Red Sea. *Tectonics*, 17(6):903–920, 1998.

Colleen W. Stevens, Robert McCaffrey, Yehuda Bock, Joachim F. Genrich, Manuel Pubellier, and Cecep Subarya. Evidence for Block Rotations and Basal Shear in the World's Fastest Slipping Continental Shear Zone in NW New Guinea. In Seth Stein and Jeffrey T. Freymueller, editors, *Plate Boundary Zones*, volume 30 of *Geodynamic Series*, pages 87–99. 2002.

J. M. Stock and K. V. Hodges. Pre-Pliocene extension around the Gulf of California and the transfer of Baja California to the Pacific plate. *Tectonics*, 8:99–115, 1989.

J. M. Stock and K. V. Hodges. Miocene to Recent structural development of an extensional accommodation zone, northeastern Baja California, Mexico. *Journal of Structural Geology*, 12(3):315–328, 1990.

Joann M. Stock. Relation of the Puertecitos Volcanic Province, Baja California, Mexico, to development of the plate boundary in the Gulf of California. In H. Delgado-Granados, G. Aguirre-Díaz, and J. M. Stock, editors, *Cenozoic Tectonics and Volcanism of Mexico*, Geological Society of America Special Paper 334, pages 143–156. 2000.

Brian Taylor, Andrew M. Goodliffe, and Fernando Martinez. How continents break up: Insights from Papua New Guinea. *Journal of Geophysical Research*, 104(B4): 7497–7512, 1999.

Ch. Teyssier, B. Tikoff, and J. Weber. Attachment between brittle and ductile crust at wrenching plate boundaries. *EGS Stephan Mueller Special Publication Series*, 1:119–144, 2002.

Christain Teyssier, Basil Tikoff, and Michelle Markley. Oblique plate motion and continental tectonics. *Geology*, 23(5):447–450, 1995.

B. Tikoff, Ch. Teyssier, and Ch. Waters. Clutch tectonics and the partial attachment of lithospheric layers. *EGS Stephan Mueller Special Publication Series*, 1:93–117, 2002.

Basil Tikoff and Christain Teyssier. Strain modeling of displacement-field partitioning in transpressional orogens. *Journal of Structural Geology*, 16(11):1575–1588, 1994.

Donald L. Turcotte and Gerald Schubert. *Geodynamics, Applications of Continuum Physics to Geological Problems*. John Wiley & Sons, 1982.

Paul J. Umhoefer and Rebecca J. Dorsey. Translation of terranes: Lessons from central Baja California, Mexico. *Geology*, 25(11):1007–1010, 1997.

Paul J. Umhoefer and K. A. Stone. Description and kinematics of the SE Loreto basin fault array, Baja California Sur, Mexico: a positive field test of oblique-rift models. *Journal of Structural Geology*, 18(5):595–614, 1996.

Tjeerd H. Van Andel. Recent marine sediments of Gulf of California. In T. van Andel and G. G. Shor, editors, *Marine Geology of the Gulf of California*, American Association of Petroleum Geologists Memoir 3, pages 216–310. 1964.

Alwyn Williams. Oblique-slip faults and rotated stress systems. *Geological Magazine*, 95(3):207–218, 1958.

Chapter 3 Crustal Thickness Variations in the Continental Margins of the Gulf of California from Receiver Functions

Abstract

Receiver functions (RFs) from teleseismic events recorded by the NARS-Baja array were used to map crustal thickness in the continental margins of the Gulf of California, a newly forming ocean basin. Although the upper crust is known to have split apart simultaneously along the entire length of the Gulf, little is known about the behavior of the lower crust in this region. The RFs show clear P-to-S wave conversions from the Moho beneath the stations. The delay times between the direct P and P-to-S waves indicate thinner crust closer to the Gulf along the entire Baja California peninsula. The thinner crust is associated with the eastern Peninsular Ranges batholith (PRB). Crustal thickness is uncorrelated with topography in the PRB and the Moho is not flat, suggesting mantle compensation by a weaker than normal mantle based on seismological evidence. The approximately W-E shallowing in Moho depths is significant with extremes in crustal thickness of ∼20 and 40 km. Similar results have been obtained at the northern end of the Gulf by Lewis et al. [2001], who proposed a mechanism of lower crustal flow associated with rifting in the Gulf Extensional Province for thinning of the crust. Based on the amount of pre-Pliocene extension possible in the continental margins, if the lower crust did thin in concert with the upper crust, it is possible that the crust was thinned during the early stages of rifting before the opening of the ocean basin. In this case, we suggest that when breakup occurred, the lower crust in the margins of the Gulf was still behaving ductilely. Alternatively, the lower crust may have thinned after the Gulf opened. The implications of these mechanisms are discussed.

3.1 Introduction

Oblique rifts are abundant in the geological record. Examples are the modern Dead Sea-Gulf of Aqaba system and late Mesozoic Ivory Coast-Ghana margin [Wilson, 1965]. The Gulf of California, at the southern end of the Pacific-North America plate boundary is a ∼1400 km long, highly-sedimented, oblique rift characterized by long transform faults and short spreading centers [Lonsdale, 1989]. It is one of the few places where the poorly understood process of continental breakup can be directly studied. Here, continental rifting began after a period of minor extension [Stock and Hodges, 1989] above a subduction-related volcanic arc [Gastil et al., 1979], which was supposedly oriented oblique to the extension direction. Current Pacific-North America plate motion is taken up primarily by distributed faulting. This has been documented in the southern Gulf and on its margins [Fletcher and Munguía, 2000], as well as in the northern one third of the Gulf, where multiple small-offset faults instead of throughgoing transform faults exist [Persaud et al., 2003]. The diffuse nature of deformation, despite ∼6 Ma of fast spreading (5 cm/yr full rate), is curious and is manifested in the lack of organized seafloor spreading throughout the Gulf [Lonsdale, 1989]. It is thought that wide rifts result from the extension of thick, hot crust when the mantle lithosphere is weak and the lower crust is weak, but not so weak that core complexes form [Buck, 1991]. If this is the case in the Gulf, then the lower crust there could conceivably contain some continental crust from the margins, thus making it weak.

To help us understand the evolution of deformation at this plate boundary and what processes delay the transition to seafloor spreading, we seek to constrain the nature of the crust beneath the Gulf. Recent cross-Gulf tiepoints in the form of ∼255 km dextral offset of 6.3 Ma pyroclastic flow deposits [Oskin et al., 2001] support the exact fit of the rifted conjugate margins in the Upper Delfín Basin, with only a few tens of kilometers of dextral displacement occurring between 12.6 and 6.3 Ma [Oskin et al., 2001]. On this basis, very little upper continental crust is expected beneath the Gulf at least not in this one basin segment. Basement rocks in the southern California and northern Baja California consist of the Jurassic-Cretaceous Peninsular Ranges

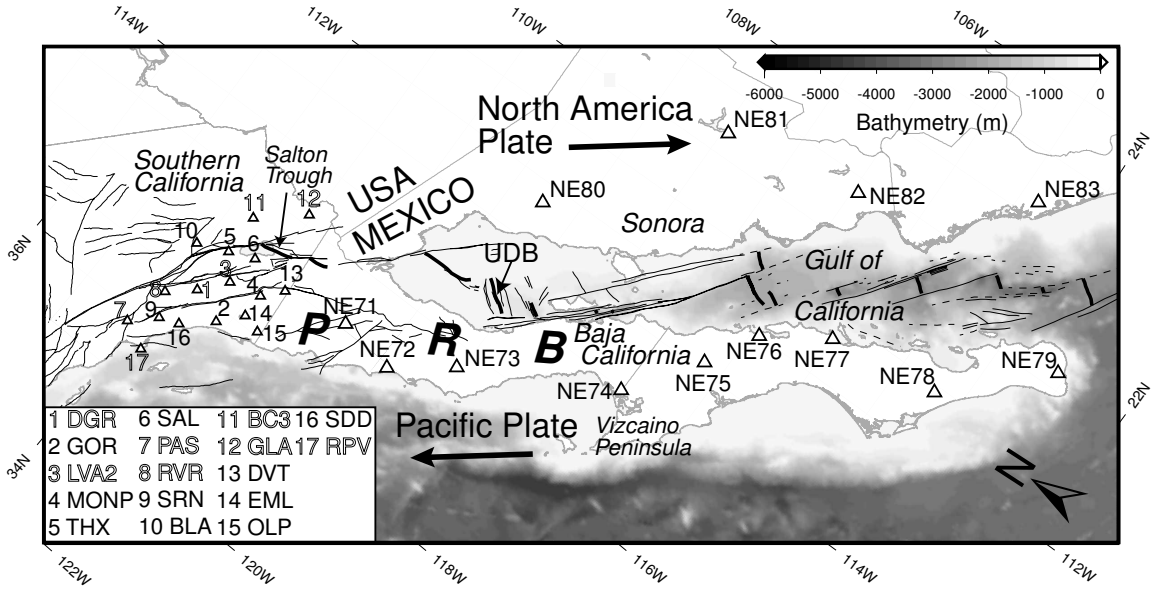

Figure 3.1: Map showing the major faults along the Pacific-North America plate boundary in southern California [Jennings, 1994] and the Gulf of California [Fenby and Gastil, 1991], and the station locations used in this study. Southern California stations are numbered according to the legend (bold text are stations that were also analyzed by Zhu and Kanamori [2000]. See also table 3.1). The 13 stations prefixed with NE are part of the NARS-Baja array. The bathymetry of the region is grayshaded and emphasizes the very shallow water depths in the northern Gulf. Thick black arrows indicate the current Pacific-North America relative plate motion direction N37°W [Atwater and Stock, 1998]. PRB = Peninsular Ranges Batholith; UDB=Upper Delfín basin.

batholith (PRB). The batholith is well exposed north of the Vizcaino peninsula in the Peninsular Ranges, which are part of a larger geologic province that extends to the tip of the Baja California peninsula [Oliver, 1980] (Figure 3.1). Although no direct constraints on the degree of extension of the lower crust in the continental margins exist, one study along a profile in northern Baja California found that the crust closer to the Gulf was thinner than the crust on the Pacific side of the peninsula [Lewis et al., 2001]. Lewis et al. [2001] explained this thinning as resulting from diffuse lower crustal extension in response to rifting in the Gulf Extensional Province, however, the timing of this extension remains unclear. Our purpose is, therefore, to examine the variation in crustal thickness in the continental margins around the entire Gulf of California and to use this information to suggest bounds on the amount of lower continental crust that could exist within the Gulf.

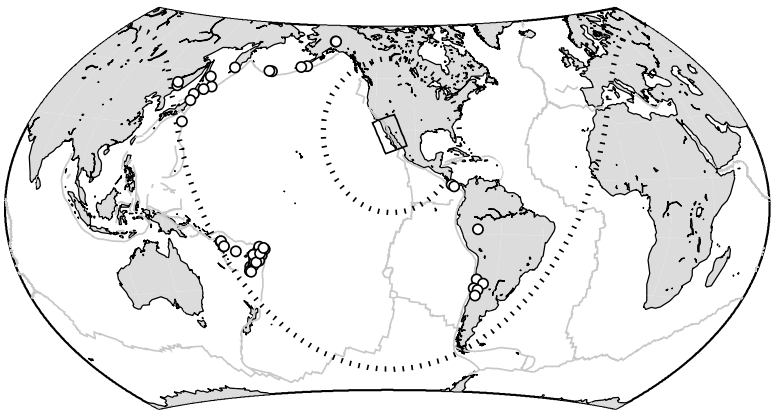

Figure 3.2: Map showing the distribution of the 64 events considered in this study. The black box marks the Gulf of California study area shown in figure 3.1. Dotted lines at distances of 30°and 90° away from the center of the study area enclose the selected events.

We estimate the variation of crustal thickness in Baja California and Sonora, Mexico, the continental margins of the Gulf of Calfornia using broadband seismic data from the NARS-Baja network (Figure 3.1) to calculate receiver functions (RFs). This technique has been widely used to map the depth to the Mohorovičić discontinuity (Moho) [e.g. Dahl-Jensen et al., 2003] and the results can be interpreted in a fairly straightforward manner in areas of extension where the lithospheric structures are mainly flat-lying. Along with the inferences on the lower crustal composition beneath the Gulf, this study provides Moho depth estimates and V_p/V_s values for parts of Baja California and Sonora, Mexico, where the regional crustal thickness is only grossly known [e.g., Urrutia-Fucugauchi, 1986]. This study is now possible with the new data collected by the NARS-Baja network.

3.2 Data

Starting in 2001, 18 broadband seismic stations were deployed, as part of the Network of Autonomously Recording Seismographs (NARS)-Baja network in Baja California and Sonora, Mexico. The recordings from these stations provide a new dataset and a unique opportunity to map the crustal thickness on a regional scale around the entire Gulf of California. We use data from 13 NARS-Baja stations, 9 in Baja California and 4 in Sonora, along with 17 southern California stations (Figure 3.1 and

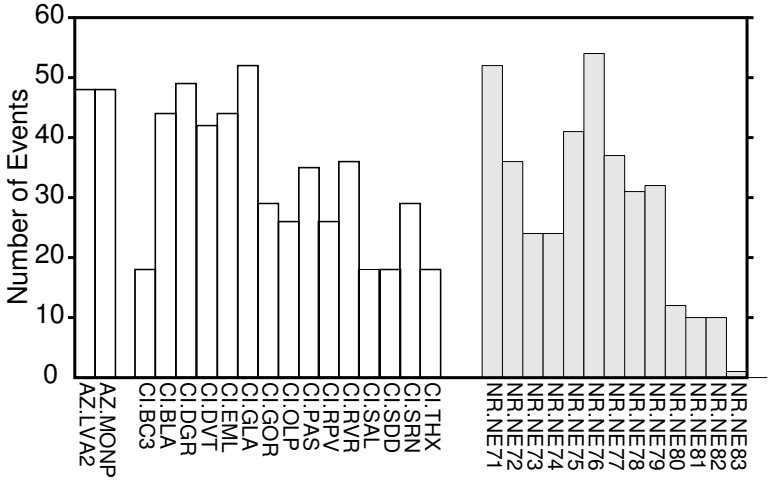

Figure 3.3: Histogram showing the number of good quality records per station considered. RFs were calculated for all of these events, but only approximately 50% of these events gave usable RFs. Note the number of good quality teleseismic records for the NARS-Baja stations is directly comparable to those for the stations in southern California, which were selected because they had high quality data.

Table 3.1). The southern California stations were selected for an evenly spaced distribution from latitude 34° southward, as well as good data availability and quality within our time period. In this study, the RFs from the southern California stations are essentially used as a quality check on the RFs from the NARS-Baja network. We note that the data quality of the coastal stations is considerably poorer than that of the inland stations. Since published Moho depth estimates for southern California based on receiver function studies are largely confirmed by our work (Table 3.1 and Appendix C), we do not analyze our results in southern California in detail. Instead, we focus on our results for the NARS-Baja stations. From an initial 133 teleseismic events with magnitudes above 5.9 M_w that occurred between April 2002 and March 2003, we selected a total of 64 events (Figure 3.2 and Table 3.2). From these events, data for individual stations were selected if they met the following conditions: the event was located within a $\sim 30 - 90°$ distance range and the P-wave was readily identifiable. The final distribution of events per station is shown in Figure 3.3.

Table 3.1: Stations Used in Teleseismic Receiver Function Analysis

Station	**Lat.** [°]	**Long.** [°]	**Altitude [m]**	**Events**	**Moho Depth [km]**	$\mathbf{V_p/V_s}$
AZ.LVA2[1]	33.35160	-116.56150	1435.00	17	29.463(28.859,30.241)	1.804(1.776,1.831)
AZ.MONP	32.89270	-116.42250	1920.00	19	30.135(29.515,31.061)	1.785(1.756,1.812)
CI.BC3[2]	33.65484	-115.45309	1080.00	7	25.389(24.553,26.381)	1.793(1.749,1.842)
CI.BLA	34.06970	-116.38890	1214.00	17	31.067(30.541,31.526)	1.845(1.823,1.868)
CI.DGR[3]	33.64996	-117.00948	609.00	11	32.963(31.77,34.014)	1.791(1.761,1.826)
CI.DVT	32.65910	-116.10059	870.00	15	30.706(29.3,31.464)	1.735(1.707,1.771)
CI.EML	32.89083	-116.84566	131.00	16	31.396(30.836,32.442)	1.897(1.875,1.899)
CI.GLA[4]	33.05107	-114.82779	514.00	23	27.544(26.747,28.113)	1.667(1.635,1.692)
CI.GOR	33.16000	-117.23000	46.00	12	30.575(29.49,31.607)	1.679(1.643,1.762)
CI.OLP	32.60783	-116.93036	130.00	10	28.907(28.143,29.85)	1.793(1.748,1.837)
CI.PAS[5]	34.14844	-118.17117	257.00	19	24.516(23.091,25.554)	1.834(1.78,1.89)
CI.RPV[6]	33.74329	-118.40426	64.00	7	23.462(22.563,24.451)	1.73(1.69,1.768)
CI.RVR[7]	33.99351	-117.37545	232.00	15	31.089(30.068,31.998)	1.813(1.779,1.845)
CI.SAL	33.27989	-115.98617	-22.00	6	18.01(17.264,18.943)	1.747(1.68,1.827)
CI.SDD	33.55259	-117.66171	85.00	3	38.059(36.349,39.645)	1.748(1.695,1.802)
CI.SRN	33.82843	-117.78938	181.00	12	29.403(28.234,30.27)	1.79(1.749,1.841)
CI.THX	33.63481	-116.16402	-44.00	3	22.905(21.924,24.042)	1.62(1.6,1.683)
NR.NE71	31.68973	-115.90526	1155.00	25	33.742(33.077,34.19)	1.798(1.784,1.818)
NR.NE72	30.84843	-116.05857	17.00	9	31.996(30.982,32.678)	1.834(1.795,1.889)
NR.NE73	30.06510	-115.34847	489.00	9	39.979(37.652,41.58)	1.779(1.707,1.837)
NR.NE74	28.00751	-114.01380	21.00	4	30.794(29.765,32.272)	1.885(1.8,1.899)
NR.NE75	27.29334	-112.85649	137.00	21	27.357(26.665,27.968)	1.802(1.77,1.834)
NR.NE76	26.88894	-111.99905	35.00	14	20.917(20.355,21.456)	1.827(1.798,1.861)
NR.NE77	26.01577	-111.36133	40.00	9	24.466(23.617,25.469)	1.75(1.705,1.805)
NR.NE78	24.39820	-111.10643	82.00	7	34.673(33.36,36.5)	1.628(1.602,1.66)
NR.NE79	23.11937	-109.75611	225.00	13	26.042(25.114,26.723)	1.682(1.641,1.746)
NR.NE80	30.50000	-112.31993	225.00	7	39.571(38.069,40.706)	1.859(1.812,1.893)
NR.NE81	28.91834	-109.63626	295.00	6	27.894(26.943,29.398)	1.735(1.693,1.782)
NR.NE82	26.91566	-109.23084	183.00	4	21.793(20.89,22.5)	1.87(1.828,1.898)
NR.NE83	24.73088	-107.73933	28.00	1	22.051(20.832,23.133)	1.688(1.634,1.747)

[1] 29.6±0.9 km, 1.80±0.05
[2] 25.1±1.6 km, 1.84±0.09
[3] 32.8±1.3 km, 1.80±0.06
[4] 27.0±0.6 km, 1.72±0.04
[5] 28.0±1.0 km, 1.73±0.07
[6] 21.5±0.7 km, 1.84±0.05
[7] 30.7±0.9 km, 1.83±0.04

Table 3.1 Events are the number of events used in the determination of the Moho depth and V_p/V_s. NR stations are part of the NARS-Baja network, AZ stations are part of the ANZA regional network and CI stations are part of the Caltech regional seismic network. AZ and CI stations are located in southern California. The 90% confidence intervals for Moho depths and V_p/V_s are given. Moho depths are not corrected for altitude. V_p/V_s values are for a fixed $V_p = 6.3$ km/s. Superscripted stations 1-7 were also analyzed by Zhu and Kanamori [2000] (bold text in figure 3.1).

3.3 Method

Receiver functions are time series that provide us with an image of the earth structure close to the receiver. The technique involves the isolation of the local response from

Table 3.2: Locations and Magnitudes of Events Used in Teleseismic Receiver Function Analysis

Event ID	**Lat. [°]**	**Long. [°]**	**Depth [km]**	**M_w**
9775029	-29.5	-71.1	69	6.4
9777469	-14.4	167.6	10	5.9
12880392	16.9	-100.8	33	6.1
12880404	-27.3	-70	61	6.6
12880408	-16.4	173.2	33	5.9
12887656	-56.2	-122.1	10	6.2
12881052	13.1	144.5	76	7.2
13115436	-17.9	-174.6	131	6.3
13359428	53.9	-161.3	33	6
13487432	-28.9	-66.6	21	6
13658260	8.7	-83.9	33	6.2
13658244	-17.8	-178.7	564	5.9
9792597	-12.6	166.3	33	6.7
9792721	-30.8	-70.9	52	6.5
9795541	-13.3	167	187	5.9
9795905	43.8	130.7	566	7.2
9800261	-12.4	166.5	33	6.2
9796365	-22.1	179.1	620	6.1
9799465	43.6	-127.2	10	5.9
9804941	8.1	-82.6	33	5.9
9805773	29.3	139	424	6.2
9815881	-16.2	-176.3	364	6.1
9815885	-19.5	169	114	6
9809281	14.2	146.1	62	6.5
9811425	-21.8	-179.5	579	7.4
9811437	-23.8	178.4	694	7.7
9811621	-23.8	178.3	682	6
9811933	31	141.9	10	6.2
13811732	-20	-176.2	211	5.9
13819524	-22.7	178.8	619	6
13813032	44.9	130.1	578	6.5
9827425	-31.4	-68.9	117	6.4
9827509	-10.5	161.1	33	6.2
9827697	-10.5	161	33	6.2
9827849	-10.6	161.2	33	6.3
9830809	23.4	-108.4	10	6.3
9850213	-8.3	-71.5	536	6.8
9850509	-14.7	-175.4	33	6
9852585	41.3	142.1	58	6.1
9851361	51.9	157.3	102	6.2
9851421	-15.7	-173	33	6.3
9851553	-19.7	-178.6	589	6.2
9852093	44.3	149.8	33	6.2
9855193	-20.5	-178.6	552	6.2
9852973	63.6	-148	10	6.7
9856397	38.9	141.9	49	6.1
9856489	63.7	-147.7	10	7.9
13911652	51.3	179.4	33	6.3
13911540	51.3	179.4	33	6.3

continued on next page.

Table 3.2 Event location and magnitudes are from the Southern California Earthquake Data Center (SCEDC). Waveform data were retrieved from SCEDC with STP (Seismogram Transfer Program).

Table 3.2 cont.

Event ID	Lat. [°]	Long. [°]	Depth [km]	M_w
13911544	13.8	-91.1	33	6
13911656	13.8	-91.1	33	6
13911524	48	146.3	507	7.5
13913348	-14.4	167.8	33	6.8
9871197	-50	-114	10	6
9871201	-24.1	179.1	531	6.1
9877157	-20.6	-177.7	377	6.5
9877713	-33.6	-69.8	111	6
9880477	44.3	-129.1	10	6
9881337	-10.4	160.7	33	7.5
9881501	13.7	-90.8	33	6.3
9881693	18.8	-103.9	33	7.3
9889609	53.5	-164.6	3	6.5
13947104	-17.3	-175.3	275	6.1
13948052	51.5	177.9	33	6.8
13948068	51.4	177.7	33	6.2
13950664	-15.3	-173.5	41	5.9

the source effects [Phinney, 1964; Vinnik, 1977]. Rays ending in a P-leg that arrive at the receiver have more energy on the vertical component seismograms and than those ending in S-legs (Figure A.1). The vertical component seismograms are therefore used to enhance or isolate the P-to-S conversions that occur close to the receiver by deconvolving the vertical from the horizontal components. This technique is well-suited for analyzing flat-lying structures, with little or no dip.

For each event-station pair, data were selected within the distance ranges of $30 - 90°$ and initially windowed 30 s before and 120 s after the P-wave pick. Only signals with a good signal-to-noise ratio and a clearly identifiable P-wave arrival were used. The records were rotated to the Z-vertical R-radial and T-transverse coordinate system, the trend and mean were removed, and a 5% cosine taper was applied. The taper helps to reduce the noise in the deconvolution.

An additional rotation into LQT (a ray-based coordinate system) was carried out by finding the eigenvectors of the covariance matrix and minimizing the rotation [Vinnik, 1977; Husebye et al., 1975; Kanasewich, 1973] (Appendix A). This is intended to focus the P-wave energy on the L-component, the SV-energy on the Q component and the SH-energy on the T component. Here it is important that gain is applied correctly to the signals and that the window over which the covariance is calculated contains the first few cycles of the P-wave and no anomalous spikes.

Receiver functions can be modelled in either the frequency domain [Phinney, 1964; Langston, 1979; Owens et al., 1984] or time domain [Vinnik, 1977]; both require the deconvolution of the vertical component seismogram from the horizontal components. We found the results of both approaches very similar and chose the less CPU intensive frequency domain deconvolution. The LQT signals were then transformed into the frequency domain for the deconvolution; here the Q and T signals are each divided by the L signal. A waterlevel is first applied to the L signal to avoid division by zero and enhancement of noise [Clayton and Wiggins, 1976]. The possible waterlevel parameters considered were: 0.0001, 0.001, 0.01 and 0.1. The waterlevel is determined by adding a fraction (determined by the waterlevel parameter) of the maximum of the L-signal to the sample if the sample is below this value. After deconvolution the receiver functions were first filtered with a Gaussian filter before transformation back into the time domain. The width of the Gaussian filter used is either 2.5 or 5. The narrower filter width is used when the level of high-frequency noise in the RFs is high.

To determine the Moho depth for each station, we calculate the weighted sum of the amplitudes of each receiver function at P-Pms, P-PmpPs and either P-PmpSs or P-PmsPs travel times for a range of depths, H and V_p/V_s or κ values [Zhu and Kanamori, 2000] (Figure 3.4). This approach uses the differential tau or difference in travel times between the P and Ps waves or reverberations as a "moveout" correction before stacking in a plane-wave approximation, assuming a locally flat crust-mantle boundary. Although the V_p value can be varied with each H-κ domain calculation, it is fixed at the start of each calculation and is generally 6.3 km/s. The V_s value varies over a certain range to give a corresponding range for κ. The maximum of the H-κ stack gives an estimate of the crustal thickness and κ value. The uncertainties are calculated from the distribution of the maxima of the stacks of 200 bootstrap samples of the receiver functions. Simulated annealing was used to search for the maxima. The receiver functions shown here have been filtered for display purposes only, using a singular value decomposition filter after Chevrot and Girardin [2000].

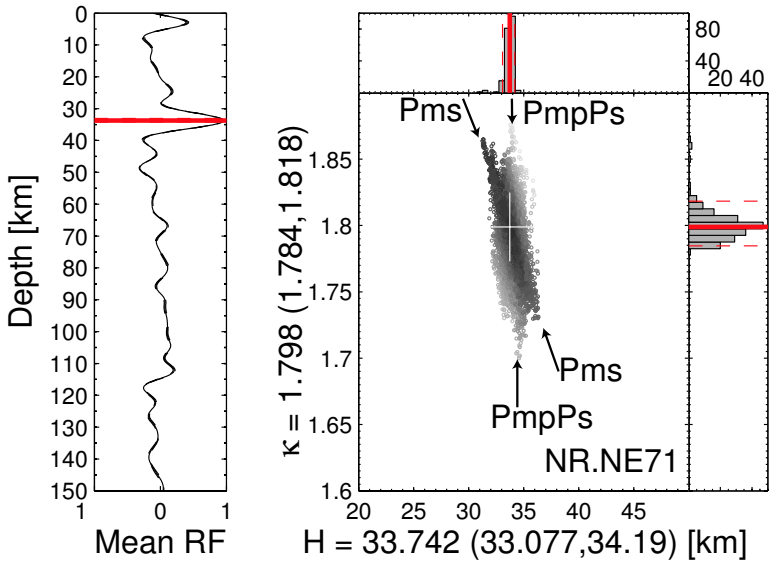

Figure 3.4: An example of the depth-V_p/V_s, H-κ stacking for station NR.NE71. The left panel shows the mean RF plotted in depth vs. normalized amplitude. The upper and lower limits of the 90% confidence interval almost exactly coincide with the RF and are therefore barely visible at this scale. The red line marks the maximum determined by 200 bootstrap resamplings of the RFs and stacking in the H-κ domain (see text for details). The Moho P-to-S conversion and a multiple are indicated. The right panel shows the results of the stacking with the 90% confidence interval marked in red.

3.4 Depth and Nature of the Moho in Baja California

In general, there is very little detectable azimuthal variation in Moho depth at individual stations. In the case of a 35 km thick crust and a near-vertical, 1 Hz incident S wave, the P-to-S conversions from the Moho sample a circle with a radius of ∼7 km around the station. Because of the natural bias in source regions, the events used in this study cluster both in back azimuth and epicentral distance. The NW and SE quadrants of back azimuth are well sampled, whereas the SW is only poorly sampled, and events from the NE are almost absent (Figure 3.5). Epicentral distance ranges of $\sim 70 - 90°$ are the most common (Appendix B). At these distances, the differential moveout of the Ps phase relative to the P is minimal. For these reasons, the expected changes in arrival time of the Ps on the radial RF due to a dipping Moho or the expected changes in the Ps amplitudes with changing back azimuth [Cassidy, 1992] might go undetected, especially for shallow dips. Keeping these limitations in mind,

we first examine the radial (Q) and transverse (T) receiver functions at and around the time of the P-to-S conversion from the Moho (Pms) and search for indications of anisotropic layers directly beneath the Moho.

Pms is easily identified in all of the RFs. In most cases, it appears as a single positive swing at around $\sim$ 2-5 s after the P arrival (e.g., Figure 3.6-3.7 and Appendix B). In some instances, it is a composite pulse, made up of two positive swings, which arises from the interference with a P-to-S conversion from a shallow crustal layer that has a smaller relative moveout. The sharp one-sided nature of Pms indicates that the Moho is a sharp transition [Levin et al., 2002]. However, in most cases, the presence of energy from Pms in the transverse RFs is an indication of anisotropy in the mantle beneath the Moho [Bostock, 1997]. This is particularly clear in the RFs in figures 3.6 and B.7, which leads to a possible interpretation of the Moho beneath these stations as the upper boundary of an anisotropic zone that is gradational beneath the Moho [Levin and Park, 2000]. Other evidence for anisotropy in the mantle is discussed below.

Using the H-κ stacking procedure, we stack all of the RFs for each station to determine the Moho depth. These values are shown with the corresponding error in Table 3.1. The poor quality of the RFs from station NE74 is likely due to its location near a semi-closed bay near the Vizcaino peninsula. The ringy nature of the data may thus be the result of seismic wave focusing related to the coastline geometry. Our Moho depth estimate of 31 km beneath this station is based on only four poor quality receiver functions but is similar to the value of 30 km reported in maps by Urrutia-Fucugauchi [1986]. In contrast to NE74, NE71 has exceptionally good data quality. This is reflected in the tightness of the H and κ 90% confidence interval (Figure 3.4). The Pms is the most prominent arrival at around 4.5 s (33.7 km). The multiples from conversions at the Moho with positive and negative polarity arrive close to 14 and 17.5 s respectively and are easily identifiable (Figure 3.7). Similarly, the RFs from NE75 show a clear Pms arrival at around 3.5 s (27.5 km) with corresponding multiples at 12 and 15 s (Figure 3.6). The polarity reversal of the multiple at 15 s may indicate a Moho with dip in the direction of incoming positively polarized multiples [Cassidy, 1992]. Based on this and the larger moveout with distance for the negative

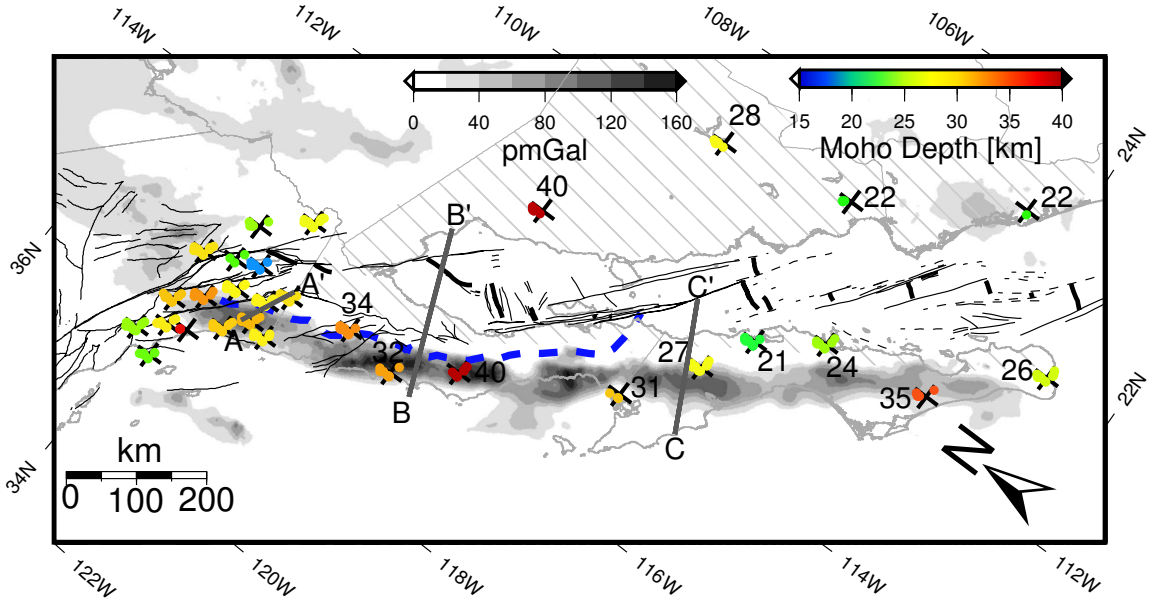

Figure 3.5: Map of crustal thickness. Moho depths have been corrected for altitude and are relative to sealevel. Crosses at the station locations indicate the four compass quadrants with the colored dots indicating the Moho pierce points, assuming a Moho depth of 30 km and an IASP91 velocity model. See Figure 3.1 for station names. Thick gray lines are the profiles shown in Figure 3.8. The grid of magnetic potential (pseudogravity) from Langenheim and Jachens [2003] is shown to illustrate the existence of the western Peninsular Ranges batholith along the full length of the peninsula. Dashed blue line is the magnetite/ilmenite boundary from Gastil et al. [1990]. Striped region marks the Gulf Extensional province as defined by Stock and Hodges [1989]. See text for a discussion.

polarities, we conclude that the Moho beneath this station may have a shallow dip to the S-SE. A dipping Moho is also suggested for NE79 (Figure B.7), which is located at the tip of the peninsula.

The overall trend in crustal thickness is the crust closer to the Gulf is consistently thinner than the crust on the western side of the Baja California peninsula (Figure 3.5). The thinner crust (21 - 26 km thick) is associated with stations NE76, NE77 and NE79, located in the southern half of the peninsula. Combining these results with those of Lewis et al. [2001] gives an $\sim$ 50 km wide zone of thin crust along the eastern peninsula. We map thicker crust (27-40 km) along the entire western side of the peninsula, based on our results from the other 6 peninsular stations.

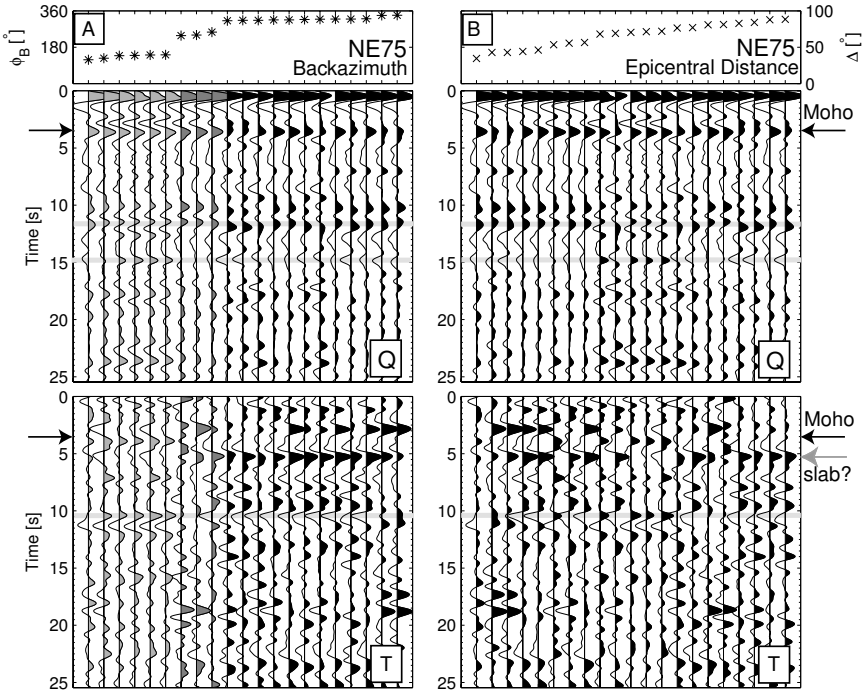

Figure 3.6: In the left panel, the Q (middle) and T (bottom) components of the receiver functions of NR.NE75 are shown. The RFs are sorted by back azimuth as indicated in the top plot, A. RFs in the same back azimuth quadrant are filled with the same color. The right panel shows the same RFs but sorted by epicentral distance as indicated in B. Gray horizontal lines on the Q-components at 12 and 15 s mark the multiples discussed in the text. On the T-components the gray line at 10 s marks the evidence for anisotropy. The gray arrow points to evidence for a slab beneath this station. Crustal thickness is 27.3 km and V_p/V_s is 1.8.

3.5 Moho Depths in Southern California

Our estimates of the Moho depths in southern California range from 18 km for CI.SAL located in the Salton Trough to 38 km for CI.SDD located at the coast (Figure 3.5). No systematic variation in Moho depths can be noted from these results, except that a fairly uniform crustal thickness appears to be associated with the Peninsular Ranges in southern California and thin crust exists beneath the Salton Trough. The average crustal thickness is ∼28 km, which is similar to the results of another teleseismic receiver function study in southern California [Zhu and Kanamori, 2000]. In detail, however, their estimate of 28 km for PAS is 3.5 km thicker than ours and does not lie within the error bounds of our estimate, even though our Moho depths for the other 6 stations analyzed in both studies match theirs very closely (Table 3.1). We

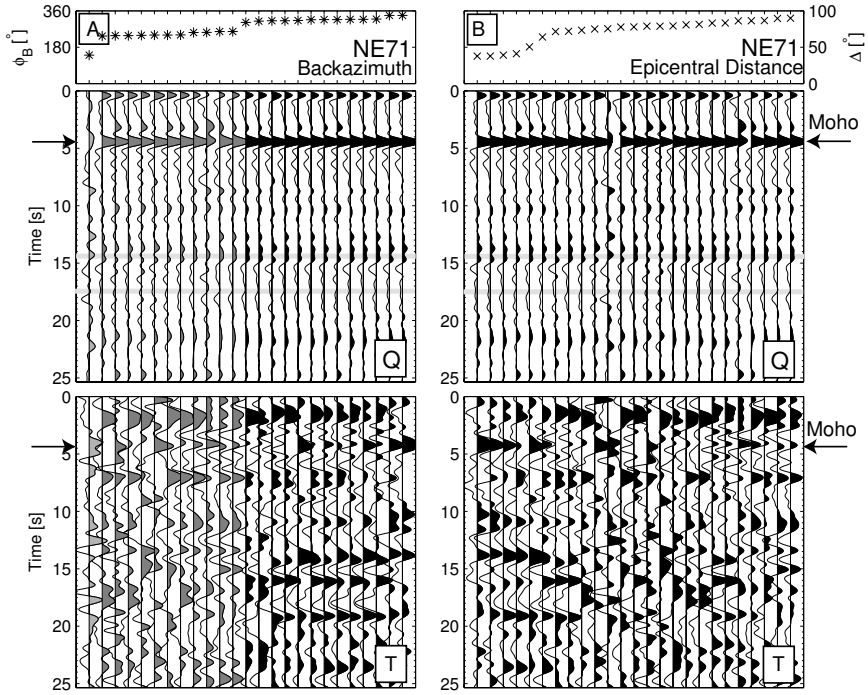

Figure 3.7: In the left panel, the Q (middle) and T (bottom) components of the receiver functions of NR.NE71 are shown. The RFs are sorted by back azimuth as indicated in the top plot, A. RFs in the same back azimuth quadrant are filled with the same color. The right panel shows the same RFs but sorted by epicentral distance as indicated in B. Gray horizontal lines on the Q-components at 14 and 17.5 s mark the multiples discussed in the text. Crustal thickness is 33.7 km and V_p/V_s is 1.8.

attribute the difference at Pasadena to the choice of maxima particularly at close distances. Our method resulted in the first pulse of the doublet being chosen as the Ps conversion, while the choice of the later pulse would give a thicker crust and smaller V_p/V_s ratio as in the case of Zhu and Kanamori [2000]. The doublet pulse for a shallow Ps conversion was previously interpreted as a shallow crustal discontinuity by Langston [1989] based on his effort to accept the deeper Moho depth estimate of 31 km by Hearn and Clayton [1986]. Langston [1989], however, did note that the Moho could be no deeper than 27 km if the observed Ps conversion was indeed from the Moho.

Lewis et al. [2000] and Ichinose et al. [1996] have shown that the crust thins from west to east across a compositional boundary in the Peninsular Ranges of southern California. This boundary was first identified by Gastil [1975], who separated the Peninsular Ranges batholith into eastern and western zones based on structural and

petrographic differences. We did not find a similar pattern of crustal thinning in the southern California region, but our results do not rule out the eastward thinning of the crust. We note that their station density was much higher than ours, but the delay times of Pms for AZ.MONP, CI.EML and CI.DVT, our stations close to Ichinose et al. [1996] (profile A-A', Figure 3.8), are close and based on our estimates of crustal thickness, the crust appears to be thinned by only 1 km in this region and not 10 km over a lateral distance of 30 km as estimated by Ichinose et al. [1996].

3.6 Other Results

Pre-Moho arrivals are likely due to layering in the crust or multiples from a crustal interface above the Moho. The first arrival on the Q-component is probably a shallow basin multiple, i.e., a P-SV conversion from the base of the sediments like that observed by Kind et al. [1995]. In almost all RFs, this arrival is the largest and has a delay time with respect to direct P of 0.5-1 s. This arrival is present in most radial RFs and also in some transverse RFs, which suggests polarization of P-to-S conversion that produces P-to-SH energy. A low-velocity surface layer tends to broaden the direct P-arrival. Due to the high-velocity contrast, a Ps conversion also results from this layers. The absolute amplitudes of the RFs are very sensitive to near-surface high-velocity contrasts [Ammon, 1991]. This Ps phase arrives directly after the P and may not be resolvable in the conventional ZRT coordinate system [Cassidy, 1992]; however, the LQT rotation separates the direct P-arrival from the horizontal components, so that the Ps conversion from the shallow layer is resolvable.

Due to the lack of complete azimuthal coverage in the data, a thorough analysis for anisotropy is not possible here. We, however, briefly discuss the indications of anisotropic layers evident in the RFs. Arrivals below the Moho may give an indication of anisotropy since they show a polarity reversal on the T-component and have larger amplitudes than would be expected from a dipping layer (e.g., at $\sim$10 s in Figures 3.6 and B.4). Based on the apparently 180° symmetry in transverse energy at 10 s, e.g., symmetry about the S and N back azimuths in the case of NE75, we assume that the anisotropic layer beneath this station has a horizontal symmetry axis polarized

in a N-S direction [Savage, 1998]. Station NE76 is more complex, showing a polarity reversal at 10 s around 360° back azimuth, but no polarity reversal at 180° (based only on a single RF), however, an anisotropic layer similar to that beneath NE75 may exist here. A delay time of 10 s with respect to the P-arrival translates to ∼100 km depth, therefore one explanation for these observations may be that the anisotropy is derived from shearing at the base of the lithosphere. Based on a similar reasoning, we suggest that an anisotropic layer exists directly beneath the Moho of NE79 (Figure B.7).

We have also found some evidence for a slab beneath NE75. The T-component RFs show a prominent arrival between 5–6 s that is either not clear in the Q-components or is polarity reversed (Figure 3.6). A polarity reversal in the Q-components could be an indication of anisotropy, with the negative polarity in the Q-component being indicative of the slab top.

3.7 Discussion and Conclusions

Our crustal thickness estimates along the Baja California peninsula are summarized in Figure 3.8. This is a projection of all of the RFs for stations NE71-NE79 (Figure 3.1) from their estimated P-to-S conversion points (30 km depth based on the IASP91 model) onto a N60°E profile that crosses the peninsula (profile C-C' in Figure 3.5) with some of the RFs unavoidably extending into the Gulf. This clearly demonstrates that the continental crust in the margins of the Gulf of California is thinnest closer to the Gulf. Similar results have been obtained in the Peninsular Ranges in southern California [Ichinose et al., 1996] (A-A' in Figure 3.5) and northern Baja California [Lewis et al., 2001] (B-B' in Figure 3.5). These authors propose a mechanism of diffuse lower crustal extension for thinning of the crust and suggest that the thinned crust is the eastern Peninsular Ranges batholith (PRB) and the thicker crust is the stronger, more mafic, western PRB. They propose that the change in crustal thickness is associated with a "compositional" boundary between the two batholiths [Ichinose et al., 1996; Lewis et al., 2001]. This "compositional" boundary has only been mapped in the northern half of the peninsula where the batholith is exposed [Gastil et al., 1990]. Recently, Langenheim and Jachens [2003] used magnetic data to show that

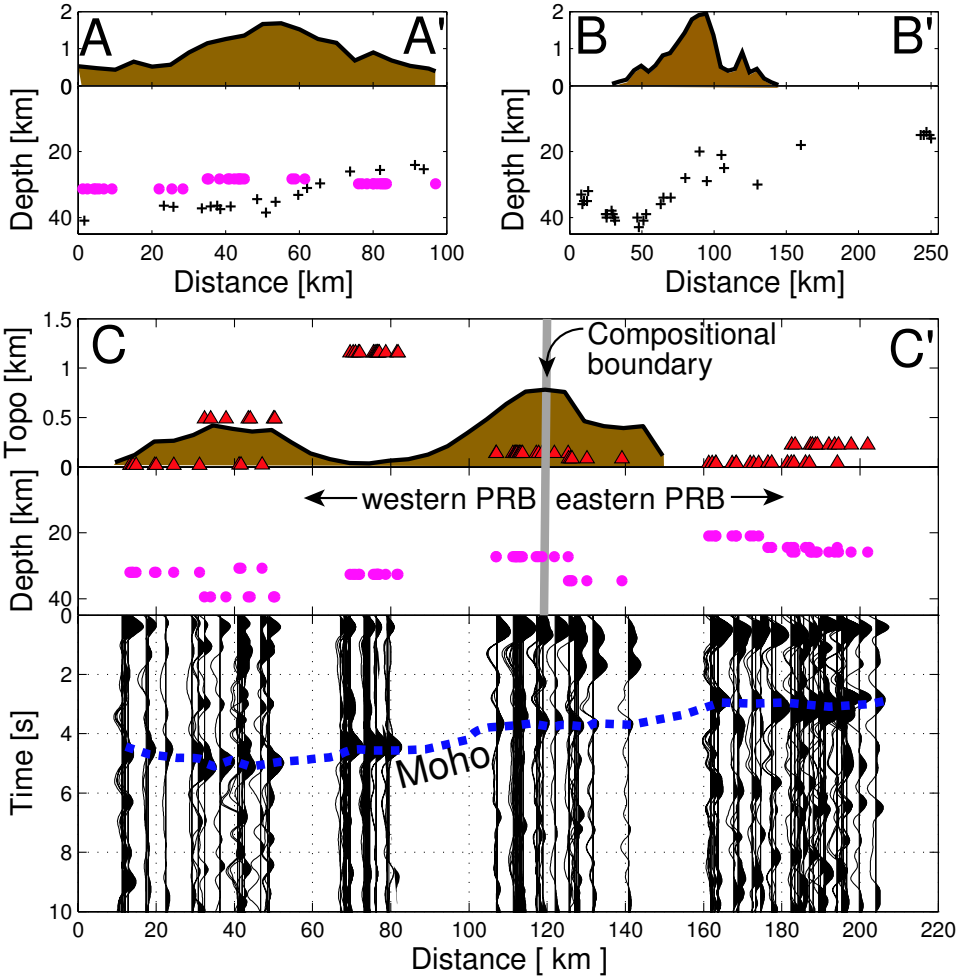

Figure 3.8: Profiles of Moho depth based on receiver function analysis: profile A-A' after Ichinose et al. [1996], profile B-B' after Lewis et al. [2001] and profile C-C' this study. Map view profile locations are shown in Figure 3.5. Topography is shown in the top panel of each profile. Dots in profile A-A' are the projection of Moho depths from stations AZ.MONP, CI.EML and CI.DVT (this study); crosses are the results of Ichinose et al. [1996]. Profile C-C' is a projection of the RFs from 9 NARS-Baja stations located in Baja California: the dashed blue line marks the Moho P-to-S conversion; red triangles are the station elevations; dots are the calculated Moho depths; the thick gray line indicates the compositional boundary approximated from magnetic potential Langenheim and Jachens [2003] (Figure 3.5). The RFs were projected from their individual Moho pierce points, assuming a Moho depth of 30 km and an IASP91 velocity model.

the western PRB extends along the full length of the peninsula, i.e., ∼1200 km northwest from the southern tip of the peninsula. Their results lend support to the hypothesis of Stock and Hodges [1989], that since the opening of the Gulf, the Baja California peninsula (south of the Agua Blanca fault) has behaved as a rigid block.

Langenheim and Jachens [2003] further proposed that the location of Gulf rifting was influenced by the mafic western PRB, which was stronger than the surrounding crust. They suggested that the pattern of crustal thinning observed to the north by Lewis et al. [2001] may also extend the full length of the peninsula. This suggestion is supported by our large-scale observations of thinner crust along the eastern peninsula, likely associated with the eastern PRB and thicker crust along the western peninsula associated with the western PRB. The implications of these results are discussed below.

From our results and assuming an original crustal thickness of ∼40 km (similar to the western PRB) the eastern PRB appears to have been stretched by a factor of 2 or extended by 100% if it was all thinned uniformly. Note that we define the eastern PRB to also include the Gulf Extensional Province defined by Stock and Hodges [1989], which extends in a thinner belt along the eastern Baja California peninsula (Figure 3.5). It is not unlikely, but cannot be proved here, that this pervasive thinning of the crust may have occurred in the Miocene, before the opening of the Gulf. In the margins of the Gulf, possible values of upper crustal extension in the late Miocene range from 20% to 200%, with varying amounts of total extension possible throughout the Gulf Extensional Province [Stock and Hodges, 1989]. This extension was ENE directed and similar in structural style to extension in the Basin and Range province [Stock and Hodges, 1989]. Although more detailed mapping is needed before an accurate estimate of the total post-mid Miocene upper crustal extension can be made, local values range from 5% to 50% [Stock and Hodges, 1989]. Thus, more extension may have occurred in the lower crust of the eastern PRB than the upper crust.

Two possible mechanisms exist for pervasive thinning of the lower crust with little extension of the upper crust: lower crustal flow and "oceanization" of continental crustal blocks. Lower or mid-crustal flow has been suggested as a mechanism for maintaining a smooth Moho topography in the Basin and Range where thickened crust is thinned usually as a result of surface topography-related pressure gradients to accommodate regional extension [Block and Royden, 1990; Kruse et al., 1991]. Lower crustal flow is, however, only likely when the crustal thickness exceeds 20 or 25 km and is accompanied by uplift and significant tilting without faulting [McKenzie

et al., 2000]. For the viscosity of the lower crust to be low enough for flow, the heat flow is expected to be higher than the continental average. Based on only sparse measurements, the heat flow values for the Baja California peninsula range from 42-84 mW/m^2 [Urrutia-Fucugauchi, 1986]. Alternatively, shear within the continental crust may decrease the viscosity of the lower crust and facilitate flow as has also been proposed for the Dead Sea basin, where the heat flow is 45-54 mW/m^2, close to the continental average [Al-Zoubi and ten Brink, 2002]. This mechanism for facilitating flow in the lower crust would only apply if the eastern PRB was thinned after the Gulf opened and major transform faults started to develop. Whether shear- or topography-related, lower crustal flow acts to smooth out variations in crustal thickness, which implies that if the lower crust of the eastern PRB did flow, the flow was eastward, and the western PRB was not involved.

Crustal thickness along the Baja California peninsula appears to be uncorrelated with topography (Figure 3.8). Non-Airy type compensation as in the case of the southern Sierra Nevada [Wernicke et al., 1996] is supported. The Moho beneath the Peninsular Ranges is, however, not flat nor is the crustal thickness anti-correlated with crustal density. Because the lower-density eastern PRB is thinner than the higher-density western PRB, a Pratt-type root as suggested for the southern Sierra Nevada can be ruled out. We suggest instead compensation by upper mantle density variation or the flexural rigidity of the lithosphere supports the load of the eastern PRB. Seismic observations show that P-waves traveling through the upper mantle beneath the Gulf are 5-10% slower than normal [Thatcher and Brune, 1971] and S-wave velocity in the uppermost 200 km of the upper mantle is 6-8% slower than in the PREM model [e.g. Ritsema and van Heijst, 2000]. Therefore, our preferred choice is compensation by density variations in the upper mantle. This does not require lower crustal flow, rather it allows for thinning of both the crust and mantle with no decoupling in the lower crust, e.g., in the Woodlark basin, Papua New Guinea, where the overall crust is thin beneath areas of the greatest surface extension [Abers et al., 2002]. The Moho is indeed not flat in this region, and compensation is accomplished through mantle buoyancy and not crustal thickening [Abers et al., 2002].

Another mechanism for thinning the crust is through the "oceanization" of crustal

blocks. This has been reported from the Gulf of Guinea, where the ghost of tilted fault blocks is still seen beneath the reflection Moho [Rosendahl et al., 1992]. The "oceanization" of continental fault blocks is a gradual process and involves the progressive lateral replacement of continental fault blocks with oceanic crust. The reflection Moho marks the transition to a more ductile regime at depth. The implications of lower crustal flow versus "oceanization" of continental fault blocks are significant, since the latter requires that thinning occurred after the Gulf opened and no continental crust would be expected within the Gulf. The view of lower crustal flow allows for the presence of continental crust within the Gulf and thus inherently weaker crust there. The question then is: was the middle or lower continental crust behaving ductilely as the Gulf opened?

Presumably, the eastern PRB had the current thickness of the western PRB, i.e., ∼40 km, before any Gulf-related extension began [Schmidt, 2000]. If the eastern PRB underwent 100% of pre-Gulf extension, then its thickness at the opening of the Gulf was 20 km and the lower limit of the strain rate is 10^{-15} s^{-1}, assuming a 12-6 Ma period of stretching. Since the Gulf opened above a volcanic arc, the geotherm was probably elevated in the eastern PRB at the time. A comparison with the "young lithosphere" stretching model of Pérez-Gussinyé et al. [2001] gives some insight into the conditions at final breakup. The young lithosphere model is based on the Woodlark basin, Papua New Guinea, where rifting of hot thick crust at high strain rates, 10^{-14} s^{-1} produced a narrow ocean-continent transition and lower crust that was still behaving ductilely at breakup [Pérez-Gussinyé et al., 2001, and references therein]. We note that this model is for uniform pure shear of the entire crust, which limits its direct application to the eastern PRB, where the amount of the surface extension occurring before 6 Ma was probably not 100% [e.g. Henry and Aranda-Gómez, 2000]. Based on this model, it is likely that at breakup, the lower crust in the continental margins of the Gulf, like that in the Woodlark basin, was still behaving ductilely, and as a result, some lower continental crust may exist within the current Gulf.

In summary, we have shown that overall the crust is thinnest (21-27 km) in a strip no wider than 50 km along the eastern Baja California peninsula and that this

coincides with the eastern PRB and includes the Gulf Extensional Province. The western PRB is thicker (31-40 km) and may indeed have behaved as a rigid block during the opening of the Gulf. It is possible that extension of the eastern PRB (including the Gulf Extensional Province) may have occurred during the Miocene before the Pacific-North America plate boundary was fully located in the Gulf of California. The timing of this extension is important for understanding the mechanism of thinning and its relationship to the current Gulf. If the eastern PRB was thinned after the Gulf opened by lower crustal flow then the amount of lower continental crust within the Gulf may be significant.

Appendix A Rotation from ZRT to LQT Coordinate System

The following steps were used to rotate the Z(Vertical), R(Radial), and T(Transverse) components of the seismograms to the corresponding L, Q and new T components. This method is based on that of Kanasewich [1973]. First the covariance, i.e., the products of the deviations from the means is calculated in 1 s windows centered at every time point, $t_j (j = 1, 2, ..., M)$ in a larger 30 s window around the P-wave arrival time. We therefore consider a time window of length $N\Delta t$, M times; where N the number of time points in the window, and Δt is the sampling interval. Here, $N\Delta t = 1$ and $M = 30$. The mean, μ_1 of N observations of $X_{1i} (i = 1, 2, ..., N)$ is given by

$$\mu_1 = \frac{1}{N} \sum_{i=1}^{N} X_{1i}. \tag{A.1}$$

The covariance between N observations of X_1 and X_2 is

$$Cov[X_1, X_2] = \frac{1}{N} \sum_{i=1}^{N} (X_{1i} - \mu_1)(X_{2i} - \mu_2). \tag{A.2}$$

Considering the Z, R and T components, the covariance matrix is given by

$$V = \begin{pmatrix} Var[R] & Cov[R,T] & Cov[R,Z] \\ Cov[R,T] & Var[T] & Cov[T,Z] \\ Cov[R,Z] & Cov[T,Z] & Var[Z] \end{pmatrix}, \tag{A.3}$$

where Var is the autocovariance or variance, e.g., $Cov[X_1, X_1]$, and Cov is the covariance as defined in Eq. A.2. Evaluating V, M times results in a matrix, Q with the dimensions $(3 \times 3 \times M)$ given by

$$Q = V(t_j), \tag{A.4}$$

where $V(t_j)$ is V evaluated as in Eq. A.4 at the points $t_j(j = 1, 2, ..., M)$. We take the average of Q along the third dimension to minimize the influence of anomalous spikes, thus reducing the Q matrix to a 3×3 matrix, W as follows

$$W = \frac{1}{M} \sum_{j=1}^{M} \begin{pmatrix} Q(1,1,j) & Q(1,2,j) & Q(1,3,j) \\ Q(2,1,j) & Q(2,2,j) & Q(2,3,j) \\ Q(3,1,j) & Q(3,2,j) & Q(3,3,j) \end{pmatrix}, \tag{A.5}$$

The eigenvalues of W are λ_1, λ_2 and λ_3, where λ_1 represents the largest eigenvalue and λ_2 represents the smallest eigenvalue. The corresponding eigenvectors are e_1, e_2 and e_3. In an ideal case, the transformation matrix for the rotation into the LQT coordinate system is $[e_1; e_2; e_3]$, and the transformation is carried out as follows

$$\begin{pmatrix} L \\ Q \\ newT \end{pmatrix} = \begin{pmatrix} e_1... \\ e_2... \\ e_3... \end{pmatrix} \begin{pmatrix} Z \\ R \\ T \end{pmatrix}. \tag{A.6}$$

This rotation can be problematic since the e_1, e_2 and e_3 eigenvectors do not necessarily always explain decreasing variance in the data. We have found that the variance often fails to provide a reasonable rotation of the data and have therefore used the maximum component of the eigenvector to determine which new axes that eigenvector best explains. We have also found that two instead of three eigenvectors will in a small number of cases sufficiently explain the data. This ambiguity is then resolved by using the eigenvalues. After the rotation the Q and T components are shifted 15 s forward in time with respect to the L component by clipping 15 s of pre P-wave noise from the beginning of the L component and 15 s from the end of the Q and T signals. The clipped ends of the signals are tapered. The Q and T components are conceptually the convolved signals, therefore applying this time shift before the deconvolution allows for 15 s of pre P-wave noise at the beginning of the deconvolved receiver function. The level of this pre-signal noise is low for stable deconvolutions.

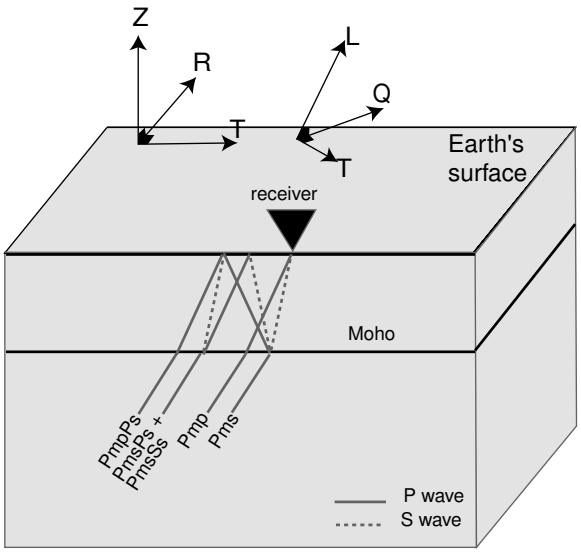

Figure A.1: Schematic drawing showing the ZRT and LQT coordinate systems. Ray conversions at the Moho and multiples are discussed in the text.

Appendix B Receiver Functions from NARS Baja Stations

In Figures B.1-B.7, we show the Q and T components of the receiver functions for the NARS-Baja stations, NE72, NE73, NE74, NE76, NE77, NE78 and NE79, located on the Baja California peninsula (Figure 3.1). These RFs are also compiled along with those from stations NE71 and NE75 in the map in Figure 3.5 and profile in Figure 3.8c. RFs in the same back azimuth quadrant are filled with the same color.

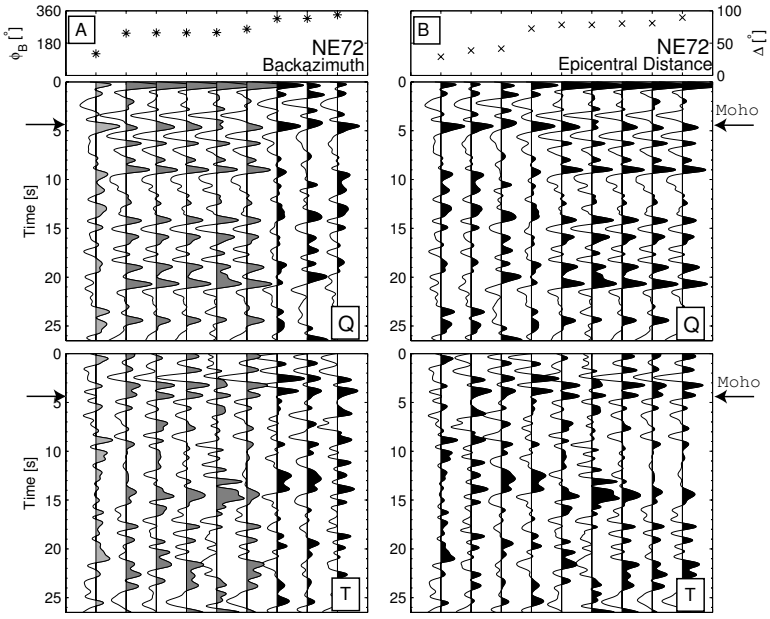

Figure B.1: In the left panel, the Q (middle) and T (bottom) components of the receiver functions of NR.NE72 are shown. The RFs are sorted by backazimuth as indicated in the top plot, A. The right panel shows the same RFs but sorted by epicentral distance as indicated in B. Crustal thickness is 32 km and V_p/V_s is 1.834.

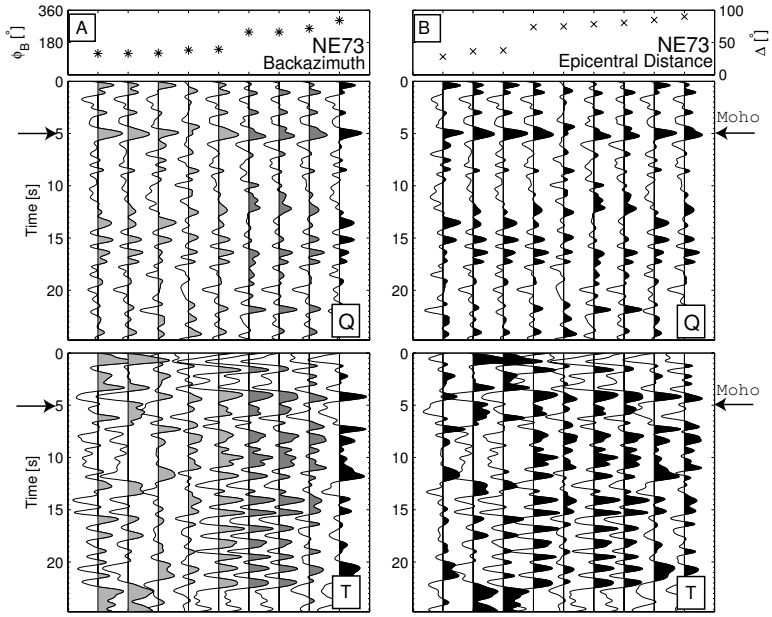

Figure B.2: In the left panel, the Q (middle) and T (bottom) components of the receiver functions of NR.NE73 are shown. The RFs are sorted by backazimuth as indicated in the top plot, A. The right panel shows the same RFs but sorted by epicentral distance as indicated in B. Crustal thickness is 40 km and V_p/V_s is 1.779.

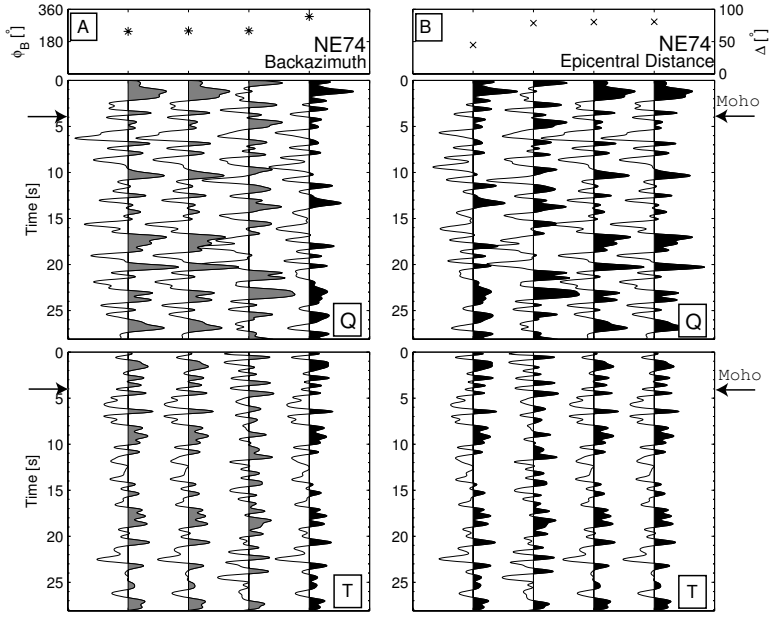

Figure B.3: In the left panel, the Q (middle) and T (bottom) components of the receiver functions of NR.NE74 are shown. The RFs are sorted by backazimuth as indicated in the top plot, A. The right panel shows the same RFs but sorted by epicentral distance as indicated in B. Crustal thickness is 31 km and V_p/V_s is 1.885.

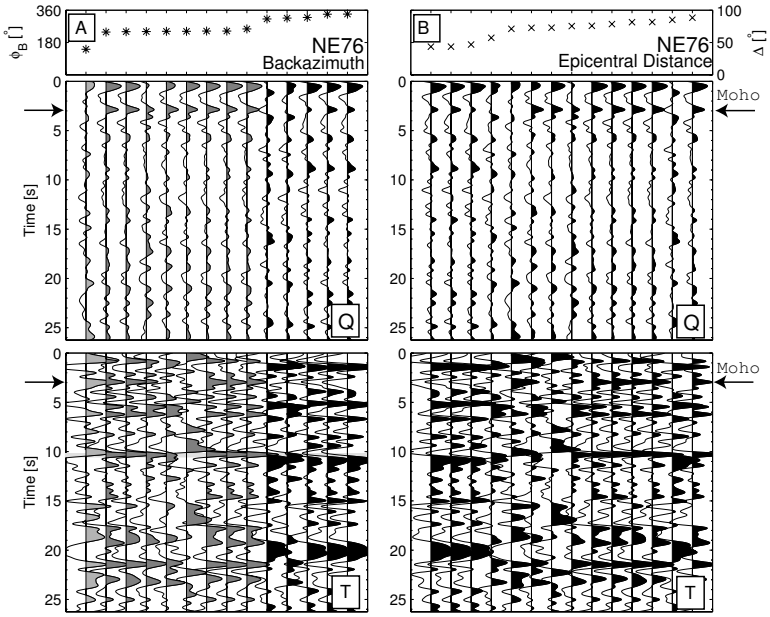

Figure B.4: In the left panel, the Q (middle) and T (bottom) components of the receiver functions of NR.NE76 are shown. The RFs are sorted by backazimuth as indicated in the top plot, A. The right panel shows the same RFs but sorted by epicentral distance as indicated in B. Crustal thickness is 21 km and V_p/V_s is 1.827.

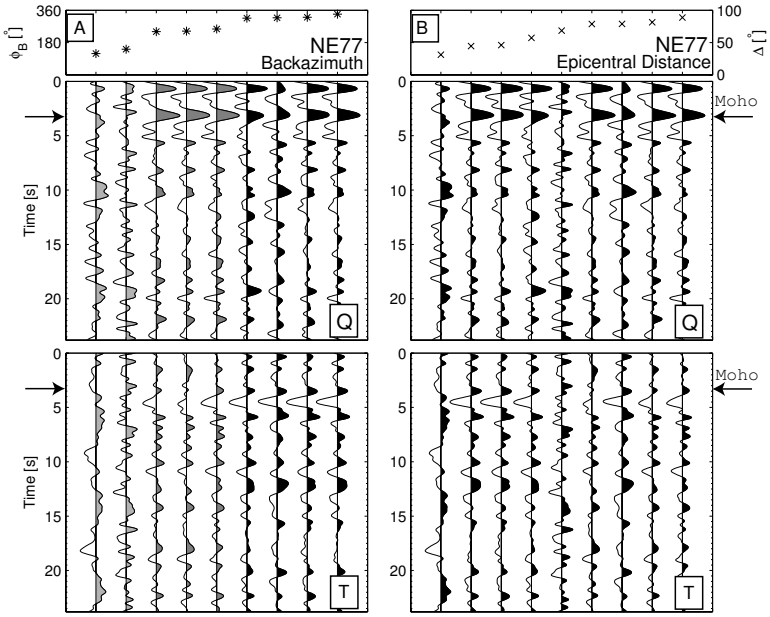

Figure B.5: In the left panel, the Q (middle) and T (bottom) components of the receiver functions of NR.NE77 are shown. The RFs are sorted by backazimuth as indicated in the top plot, A. The right panel shows the same RFs but sorted by epicentral distance as indicated in B. Crustal thickness is 24 km and V_p/V_s is 1.75.

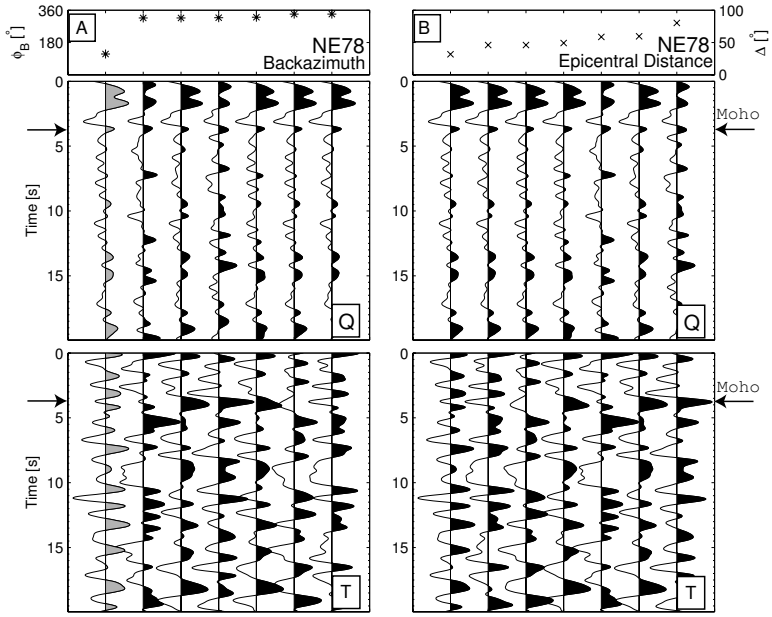

Figure B.6: In the left panel, the Q (middle) and T (bottom) components of the receiver functions of NR.NE78 are shown. The RFs are sorted by backazimuth as indicated in the top plot, A. The right panel shows the same RFs but sorted by epicentral distance as indicated in B. Crustal thickness is 35 km and V_p/V_s is 1.628.

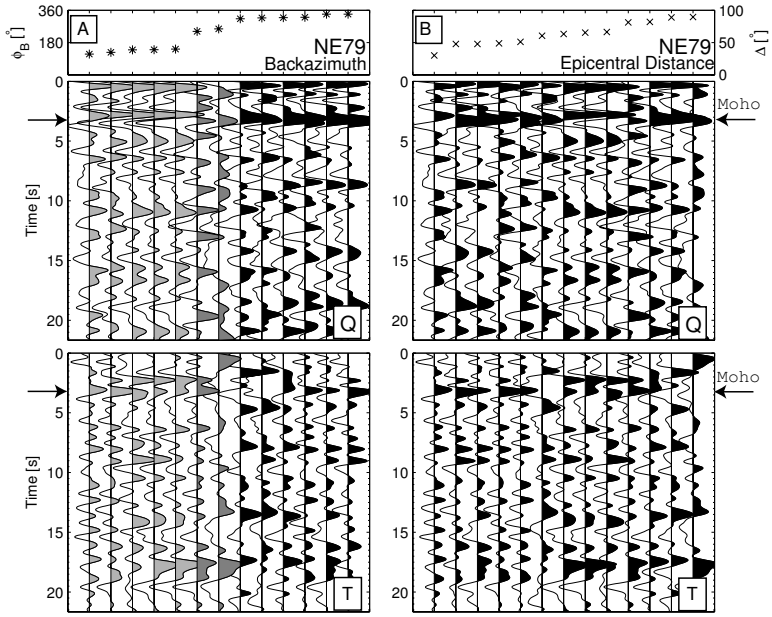

Figure B.7: In the left panel, the Q (middle) and T (bottom) components of the receiver functions of NR.NE79 are shown. The RFs are sorted by backazimuth as indicated in the top plot, A. The right panel shows the same RFs but sorted by epicentral distance as indicated in B. Crustal thickness is 26 km and V_p/V_s is 1.682.

Appendix C Receiver Functions from Southern California Stations

In Figures C.1-C.3, we show the moved out Q-component receiver functions for all of the southern California stations. The station locations are given in Figure 3.1. The receiver functions are SVD filtered, moved out and sorted by back azimuth. The moveout for the Moho P-s conversion was applied to align these arrivals. RFs in the same back azimuth quadrant are filled with the same color. See Table 3.1 for Moho depths, V_p/V_s values. Ray parameter, p ($\circ$) and back azimuth ϕ_B (*) are shown below each set of receiver functions.

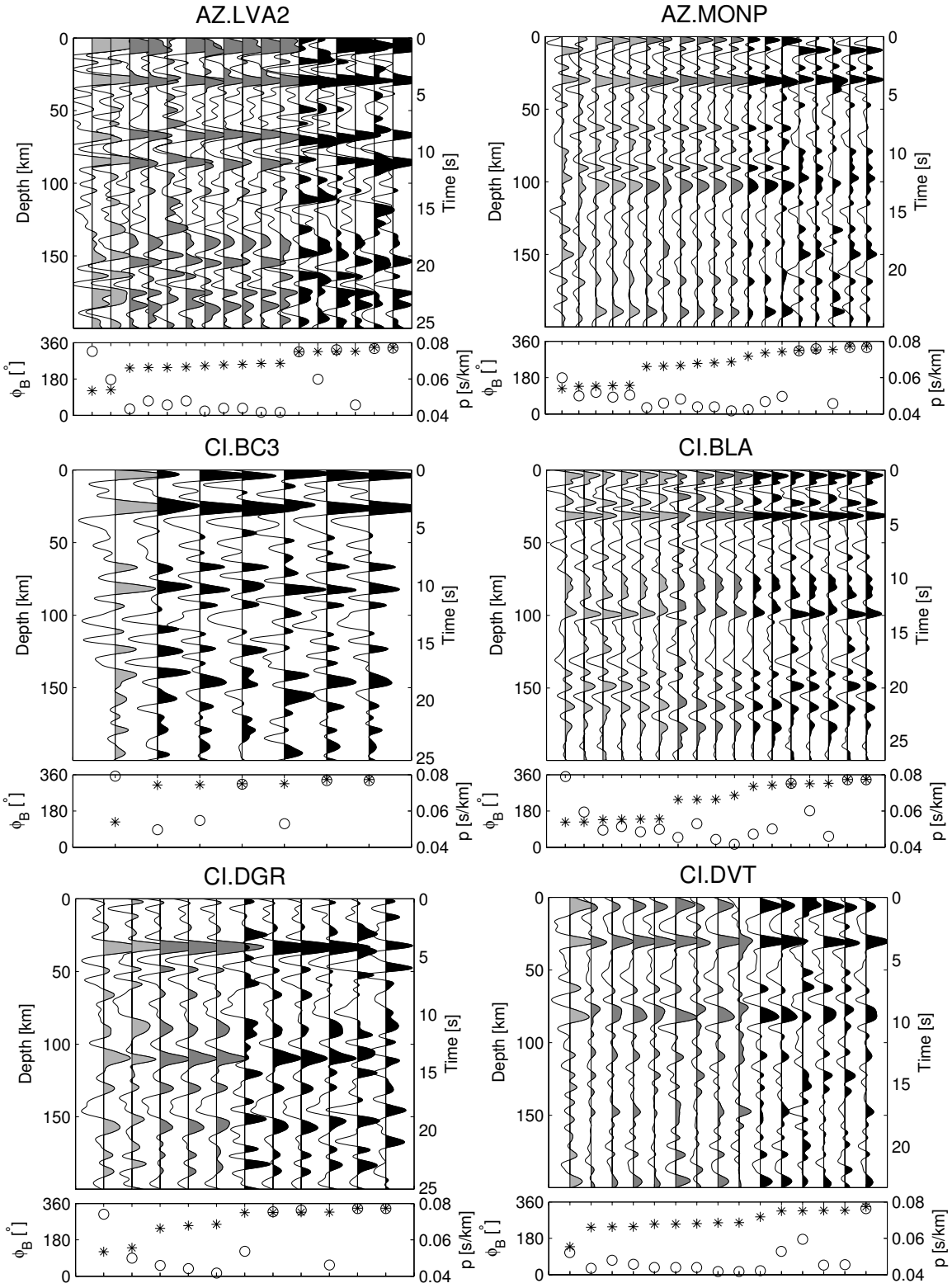
AZ.LVA2
AZ.MONP
CI.BC3
CI.BLA
CI.DGR
CI.DVT
Depth [km]
Time [s]
ϕ_B [°]
p [s/km]

Figure C.1:

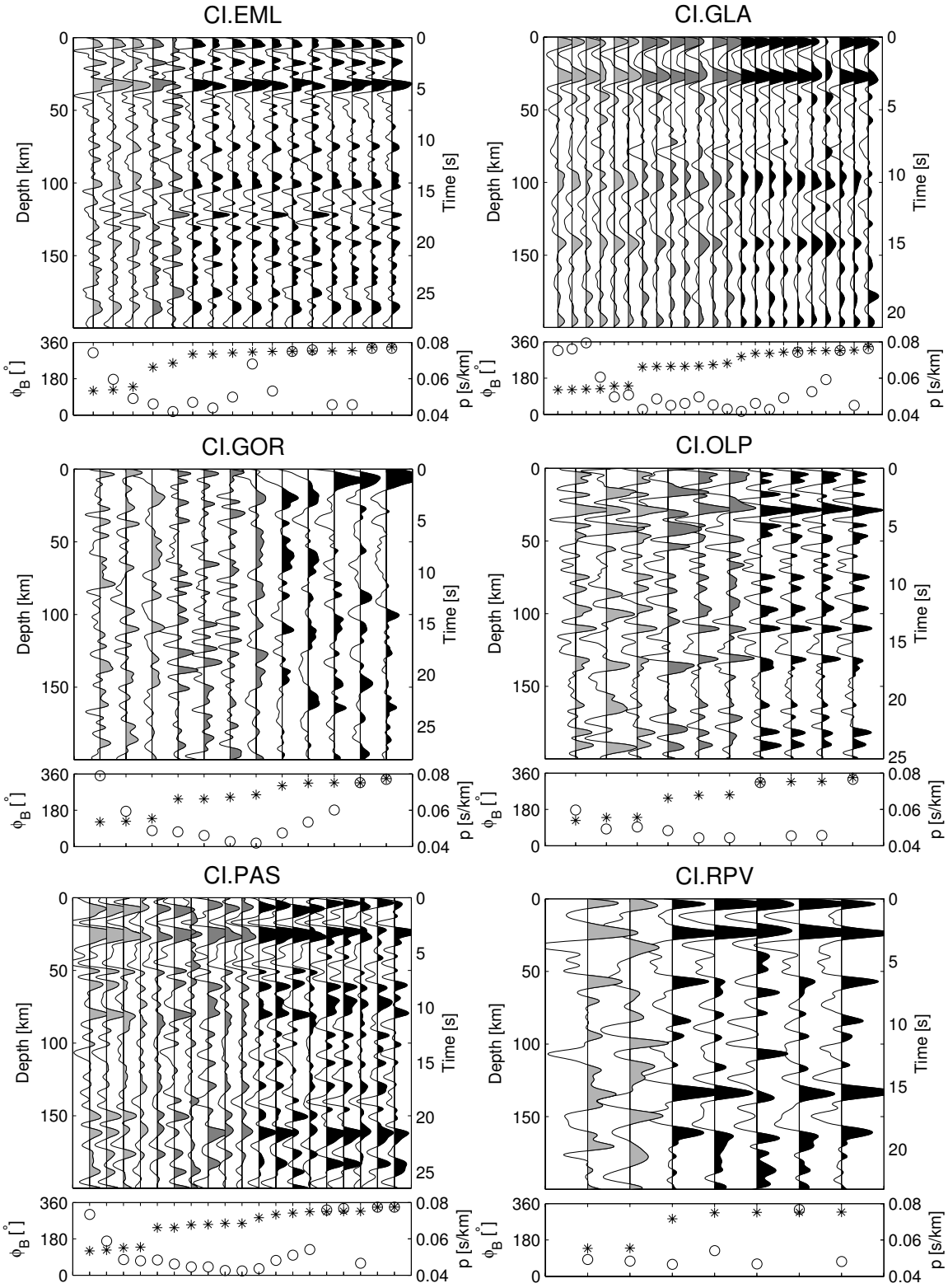
CI.EML
CI.GLA
CI.GOR
CI.OLP
CI.PAS
CI.RPV
Depth [km]
Time [s]
ϕ_B [°]
p [s/km]

Figure C.2:

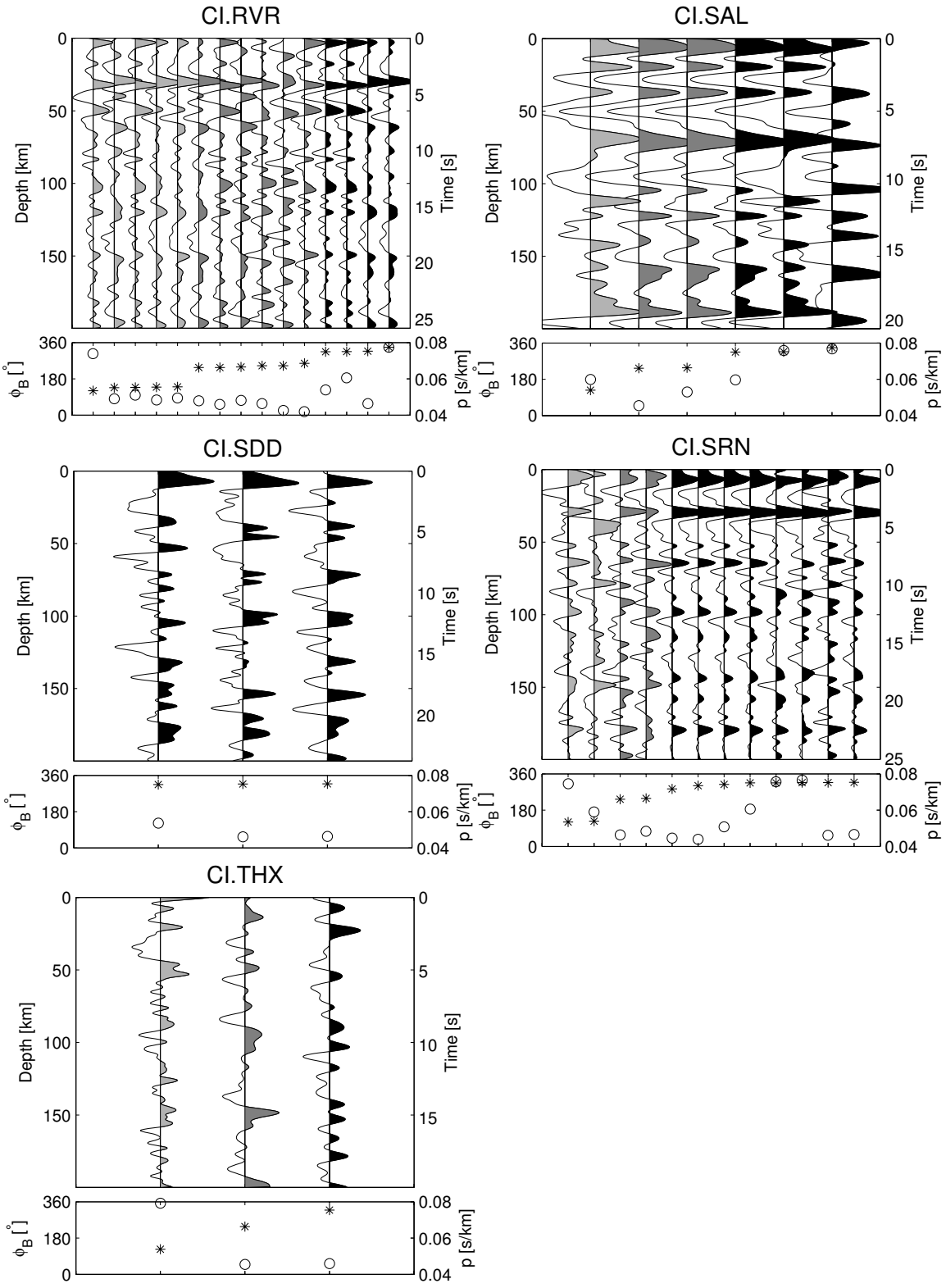

Figure C.3:

References

Geoffrey A. Abers, Aaron Ferris, Mitchell Craig, Hugh Davies, Arthur L. Lerner-Lam, John C. Mutter, and Brian Taylor. Mantle compensation of active metamorphic core complexes at Woodlark Rift in Papua New Guinea. *Nature*, 418:862–865, 2002.

Abdallah Al-Zoubi and Uri ten Brink. Lower crustal flow and the role of shear in basin subsidence: an example from the Dead Sea basin. *Earth and Planetary Science Letters*, 199:67–79, 2002.

Charles J. Ammon. The Isolation of Receiver Effects from Teleseismic P Waveforms. *Bulletin of the Seismological Society of America*, 81(6):2504–2510, 1991.

Tanya Atwater and Joann Stock. Pacific-North America Plate Tectonics of the Neogene Southwestern United States: An Update. *International Geology Review*, 40: 375–402, 1998.

Lisa Block and Leigh H. Royden. Core Complex Geometries and Regional Scale Flow in the Lower Crust. *Tectonics*, 9(4):557–567, 1990.

M. G. Bostock. Anisotropic upper-mantle stratigraphy and architecture of the Slave craton. *Nature*, 390:392–395, 1997.

W. R. Buck. Modes of continental lithospheric extension. *Journal of Geophysical Research*, 96:20,161–20,178, 1991.

J. F. Cassidy. Numerical Experiments in Broadband Receiver Function Analysis. *Bulletin of the Seismological Society of America*, 82(3):1453–1474, 1992.

Sebastien Chevrot and Nicole Girardin. On the detection and identification of converted and reflected phases from receiver functions. *Geophysical Journal International*, 141:801–808, 2000.

Rob W. Clayton and Ralph A. Wiggins. Source shape estimation and deconvolution of teleseismic bodywaves. *Geophysical Journal of the Royal Astronomical Society*, 47:151–177, 1976.

Trine Dahl-Jensen, Tine B. Larsen, Ingo Woelbern, Torben Bach, Winfried Hanka, Rainer Kind, Soren Gregersen, Klaus Mosegaard, Peter Voss, and Olafur Gudmundsson. Depth to Moho in Greenland: receiver-function analysis suggests two Proterozoic blocks in Greenland. *Earth and Planetary Science Letters*, 205:379–393, 2003.

Scott S. Fenby and R. Gordon Gastil. Geologic-Tectonic Map of the Gulf of California and Surrounding Areas. In J. P. Dauphin and B. R. T. Simoneit, editors, *The Gulf and Peninsular Provinces of the Californias*, American Association of Petroleum Geologists Memoir 47, pages 79–83. 1991.

John M. Fletcher and Luis Munguía. Active continental rifting in southern Baja California, Mexico: Implications for plate motion partitioning and the transition to seafloor spreading in the Gulf of California. *Tectonics*, 19(6):1107–1123, 2000.

Gordon Gastil, Judith Diamond, Charles Knaack, Michael Walawender, Monte Marshall, Carolyn Boyles, and Burton Chadwick. The problem of the magnetite/ilmenite boundary in southern and Baja California. *Geological Society of America Memoir*, 174:19–32, 1990.

R. G. Gastil, D. Krummenacher, and J. Minch. The record of Cenozoic volcanism around the Gulf of California. *Geological Society of America Bulletin*, 90:839–857, 1979.

R. Gordon Gastil. Plutonic zones in the Peninsular Ranges of southern California and northern Baja California. *Geology*, 3:361–363, 1975.

T. M. Hearn and R. W. Clayton. Lateral velocity variations in southern California I, Results from the upper crust from *Pg* waves. *Bulletin of the Seismological Society of America*, 76:495–509, 1986.

Christopher D. Henry and J. Jorge Aranda-Gómez. Plate interactions control middle-late Miocene, proto-Gulf and Basin and Range extension in the southern Basin and Range. *Tectonophysics*, 318:1–26, 2000.

E. S. Husebye, A. Christoffersson, and C. W. Frasier. Orthogonal representations of array-recorded short period P-waves. *NATO ASI Series, Series E: Applied Sciences, no. 11, Exploitation of Seismograph Networks, Nordhoff, Leiden*, pages 297–309, 1975.

Gene Ichinose, Steven Day, Harold Magistrale, and Ted Prush. Crustal thickness variations beneath the Peninsular Ranges, southern California. *Geophysical Research Letters*, 23(22):3095–3098, 1996.

C. W. Jennings. Fault activity map of California and adjacent areas. *California Division of Mines and Geology, California Geologic Data Map Series, Map No. 6, scale 1:750,000*, 1994.

E. R. Kanasewich. *Time Sequence Analysis in Geophysics*. The University of Alberta Press, 1973.

R. Kind, G. L. Kosarev, and N. V. Petersen. Receiver functions at the stations of the German Regional Seismic Network GRSN. *Geophysical Journal International*, 121:191–202, 1995.

Sarah Kruse, Marcia McNutt, Jason Phipps-Morgan, and Leigh Royden. Lithospheric Extension Near Lake Mead, Nevada: A Model for Ductile Flow in the Lower Crust. *Journal of Geophysical Research*, 96(B3):4435–4456, 1991.

V. E. Langenheim and R. C. Jachens. Crustal structure of the Peninsular Ranges batholith from magnetic data: Implications for Gulf of California rifting. *Geophysical Research Letters*, 30(11):1597, doi:10.1029/2003GL017159, 2003.

Charles A. Langston. Structure Under Mount Rainier, Washington, Inferred From Teleseismic Body Waves. *Journal of Geophysical Research*, 84(B9):4749–4762, 1979.

Charles A. Langston. Scattering of Teleseismic Body Waves Under Pasadena, California. *Journal of Geophysical Research*, 94(B2):1935–1951, 1989.

Vadim Levin, Lucia Margheriti, Jeffrey Park, and Alessandro Amato. Anisotropic seismic structure of the lithosphere beneath the Adriatic coast of Italy constrained with mode-converted body waves. *Geophysical Research Letters*, 29(22):2058, 2002.

Vadim Levin and Jeffrey Park. Shear zones in the Proterozoic lithosphere of the Arabian Shield and the nature of the Hales discontinuity. *Tectonophysics*, 323: 131–148, 2000.

Jennifer L. Lewis, Steven M. Day, Harold Magistrale, Raul R. Castro, Luciana Astiz, Cecilio Rebollar, Jennifer Eakins, Frank L. Vernon, and James N. Brune. Crustal thickness of the Peninsular Ranges and Gulf Extensional Province in the Californias. *Journal of Geophysical Research*, 106(B7):13,599–13,611, 2001.

Jennifer L. Lewis, Steven M. Day, Harold Magistrale, Jennifer Eakins, and Frank Vernon. Regional crustal thickness variations of the Peninsular Ranges, southern California. *Geology*, 28(4):303–306, 2000.

Peter Lonsdale. Geology and tectonic history of the Gulf of California. In D. Hussong, E. L. Winterer, and R. W. Decker, editors, *The Eastern Pacific Ocean and Hawaii*, volume N of *The Geology of North America*, pages 499–522. Geological Society of America Boulder, Colo., 1989.

Dan McKenzie, Francis Nimmo, James A. Jackson, P. B. Gans, and E. L. Miller. Characteristics and consequences of flow in the lower crust. *Journal of Geophysical Research*, 105(B5):11029–11046, 2000.

H. W. Oliver. Peninsular ranges. In *Interpretation of the gravity map of California and its continental margin*, volume 205, pages 17–19. 1980.

M. Oskin, J. Stock, and A. Martin-Barajas. Rapid localization of Pacific-North America plate motion in the Gulf of California. *Geology*, 29(5):459–462, 2001.

Thomas J. Owens, Geroge Zandt, and Steven R. Taylor. Seismic Evidence for an Ancient Rift Beneath the Cumberland Plateau, Tennessee: A Detailed Analysis of Broadband Teleseismic P Waveforms. *Journal of Geophysical Research*, 89(B9): 7783–7795, 1984.

M. Pérez-Gussinyé, T. J. Reston, and J. Phipps Morgan. Serpentinization and magmatism during extension at non-volcanic margins: the effect of initial lithospheric structure. In R. C. L. Wilson, R. B. Whitmarsh, B. Taylor, and N. Froitzheim, editors, *Non-Volcanic Rifting of Continental Margins: A Comparision of Evidence from Land and Sea*, volume 187 of *Geological Society Special Publications*, pages 551–576. 2001.

P. Persaud, J. M. Stock, M. S. Steckler, A. Martin-Barajas, J. B. Diebold, A. Gonzalez-Fernandez, and G. S. Mountain. Active deformation and shallow structure of the Wagner, Consag and Delfín Basins, Northern Gulf of California, Mexico. *Journal of Geophysical Research*, 108(B7):2355, doi:10.1029/2002JB001937, 2003.

Robert A. Phinney. Structure of the Earth's Crust from Spectral Behavior of Long-Period Body Waves. *Journal of Geophysical Research*, 69(14):2997–3017, 1964.

Jeroen Ritsema and Hendrik van Heijst. New seismic model of the upper mantle beneath Africa. *Geology*, 28(1):63–66, 2000.

Bruse R. Rosendahl, Jayson Meyers, Henrike Groschel, and Deborah Scott. Nature of the transition from continental to oceanic crust and the meaning of reflection Moho. *Geology*, 20:721–724, 1992.

Martha Kane Savage. Lower crustal anisotropy or dipping boundaries? Effects on receiver functions and a case study in New Zealand. *Journal of Geophysical Research*, 103(B7):15069–15087, 1998.

Keegan Schmidt. *Investigation of Arc Processes: Relationships among deformation, magmatism, mountain building, and the role of crustal anisotropy in the evolution of the Peninsular Ranges batholith, Baja California.* Phd, University of Southern California, 2000.

J. M. Stock and K. V. Hodges. Pre-Pliocene extension around the Gulf of California and the transfer of Baja California to the Pacific plate. *Tectonics*, 8:99–115, 1989.

Wayne Thatcher and James N. Brune. Seismic Study of an Oceanic Ridge Earthquake Swarm in the Gulf of California. *Geophys. J. R. Astr. Soc.*, 22:473–489, 1971.

J. Urrutia-Fucugauchi. Crustal Thickness, Heat Flow, Arc Magmatism, and Tectonics of Mexico - preliminary report. *Geofisica International*, 25(4):559–573, 1986.

L. P. Vinnik. Detection of waves converted from P to SV in the mantle. *Physics of Earth and Planetary Interior*, 15:39–45, 1977.

Brian Wernicke, Robert Clayton, Mihai Ducea, Craig Jones, Stephen Park, Stan Ruppert, Jason Saleeby, J. Kent Snow, Livia Squires, Moritz Fliedner, George Jirace, Randy Keller, Simon Klemperer, James Luetgert, Peter Malin, Kate Miller, Walter Mooney, Howard Oliver, and Robert Phinney. Origin of High Mountains in the Continents: The Southern Sierra Nevada. *Science*, 271:190–193, 1996.

J. Tuzo Wilson. A new class of faults and their bearing on continental drift. *Nature*, 207:343–347, 1965.

Lupei Zhu and Hiroo Kanamori. Moho depth variation in southern California from teleseismic receiver functions. *Journal of Geophysical Research*, 105(B2):2969–2980, 2000.